OPTICAL PRESSURE SENSORS USING INTERFEROMETRIC TECHNIQUES

By

P. V. P. Yupapin

A thesis

submitted to City University for

the Degree of Doctor of Philosophy in

Electrical and Electronic Engineering

City University

Measurement and Instrumentation Centre

Department of Electrical, Electronic and Information Engineering

Northampton Square, London EC1V 0HB

March 1993

to

my wife Nick
and
our families

TABLE OF CONTENTS

Chapter 1

Introduction

Chapter 2

Pressure Sensor Using An All Fibre Optic Michelson Interferometer

Chapter 3

Photoelastic Pressure Sensor Using A Low-Coherence Light Source

Chapter 4

A White Light Interferometry Based Pressure Sensor : A Further Study Of Photoelastic Sensing Material Characteristics

Chapter 5

A Study Of Polarisation Maintaining Fibre Characteristics Using Interferometric Technique For Pressure Sensor Applications

Chapter 6

Conclusions

Appendices

List of Tables

List of Figures

Acknowledgements

Declaration

xi

I grant powers of discretion to the University Librarian to allow this thesis to be copied in whole or in part without further reference to the author. This permission covers only single copies made for study purposes, subject to normal conditions of acknowledgements.

Abstract

An investigation of methods of optical pressure sensors using a novel polarimetric interferometric approach are presented. The use of several techniques and their experimental arrangements are demonstrated and discussed, for which results have indicated possible applications in pressure measurement. A comparison of their sensitivities to applied force has been made, using coated and uncoated standard single mode fibre as the sensing medium, and the stability of the output to temperature variations over the range 20 ^{0}C to 95 ^{0}C also demonstrated. This scheme has been discussed as a possible element for a differential pressure flow sensor.

An optical pressure sensor, using a low-coherence technique and a photoelastic material as the sensing element, is also presented. A change in the optical path of light propagating in the stressed sensing element has been observed by monitoring a corresponding change in that optical path in a "recovery" optical interferometer. Results have shown a linear relationship between this change in path difference and applied pressure.

Further, the measurement of force/pressure-induced birefringence has been investigated using a photoelastic technique, and in this case, the light source employed was a "quasi-white light", short coherence light source, a light emitting diode (LED). Its output was coupled into a multimode fibre before entering the processing interferometer. With the use of the processing interferometer, the sensing element birefringence was observed when a force was applied. The sensing material properties such as elastic limit, stress-relaxation and thermal effects were also investigated and are discussed, in light of the applications of the technique.

The characteristics of three individual types of polarisation maintaining fibres (Hi-Bi), for pressure sensing applications using a quasi-distributed sensing technique are presented. The output light from a low-coherence source was coupled into the fibre via one of the two polarisation modes, where the location of the coupling point was located by using a basic Michelson interferometer. The theoretical aspects of the sensor system and its experimental arrangement are discussed and demonstrated. A number of sensor applications such as a pressure/force sensor, or a position sensor, in addition to an investigation of fibre characteristics such as beat length and birefringence measurements are demonstrated. The device sensitivity to variations in temperature for these measurement is investigated.

Chapter 1

Introduction

1.1 General Introduction

1.1.1 General

The purpose of measurement today is usually to present an observer with a numerical value corresponding to the variable being measured. A number of important parameters relating to the science of measurement are discussed in Appendix A [1]. Pressure is one of the most important variables in many scientific and industrial applications. It is a quantity which cannot be measured directly but is derived from the basic unit definition of force acting upon an area. Generally, pressure measuring instruments can be divided into two main groups, labelled "direct" and "indirect". The first determines the value of applied pressure directly by calculating the force applied upon a known area, i.e. a pressure sensor, whereas the instruments of the second group are based on transforming pressure to some other variable which is then finally measured, i.e. a pressure transducer.

There are a number of methods of pressure measurement [2], one of the modern approaches for which is the application of optical techniques, which have been a rapidly growing area of research in the last decade [3-6]. Basically, such a system can be reduced to its basic mode of operation, as shown in Figure 1.1, utilising a light source, a transmission medium, a sensing unit, an optical processing unit and a detector. The scope of the system applications depends upon the characteristics of the light source, the efficiency of the transmission medium, the properties of the detector, and also the nature of the

1

signal processing unit. They are investigated in this work, and the results are reported herein.
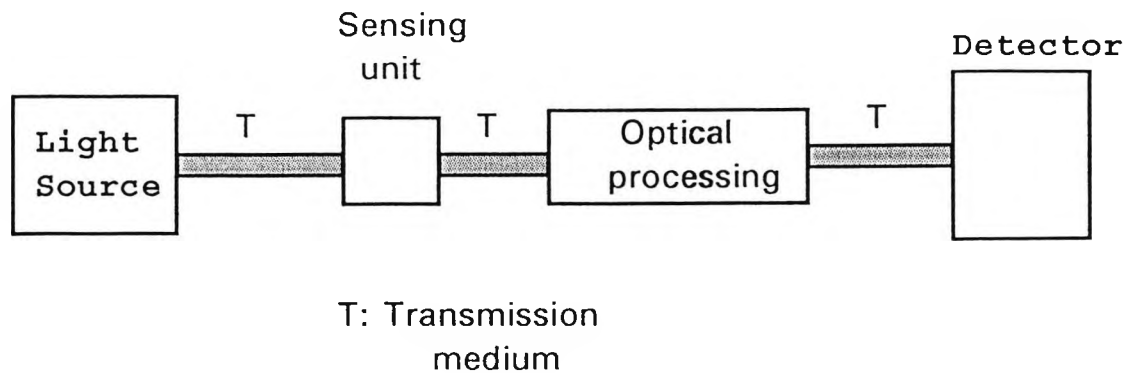
Figure 1.1 Schematic of an optical system arrangement for pressure sensor applications.

1.1.2 Aims of This Work

The aims and objectives of this work were:

(a) To demonstrate the use of a novel polarimetric interferometer as a prototype pressure/force sensor, where a comparison of the sensitivity to applied force is considered, using coated and uncoated standard single mode fibre as the sensing fibre. The stability of the output to temperature variations will also be discussed.

(b) To develop a prototype optical pressure sensor, using a low-coherence technique with a photoelastic material as the sensing element.

(c) To investigate the properties (elastic limit, stress-relaxation and thermal effects) of photoelastic materials, and their implication for pressure sensor applications.

(d) The consideration of the characterisation of three individual types of polarisation maintaining fibres (Hi-Bi), for use in quasi-distributed sensing systems, where a number of sensor applications such as in pressure/force measurement, position sensing, beat length and birefringence determination will be investigated. The sensor sensitivity to variations in temperatures for these measurement devices will also be considered.

(e) The reporting of the results of such investigations at major international conferences and in the learned Journals (see Appendix B).

1.1.3 Structure of the Thesis

The structure of the thesis is as follows.

Chapter One provides a brief overview of some relevant basic theory used in the optical pressure sensor systems. The general theory of the system used is presented to underpin the understanding of the subsequent experimental investigation. The applications involving the specific systems developed will be the concern of the rest of this work.

In Chapter Two preliminary experimental work on pressure sensing using an "all fibre optic Michelson interferometer" is described, where a temperature compensation technique is discussed. A comparison of the sensitivity of coated and uncoated sensing fibre schemes using a standard single mode fibre are reported. The linearity and stability of sensor sensitivity of the output to temperature variations over the range 20^0 C to 95^0 C is investigated. The principle of force/pressure induced birefringence in an ordinary single mode fibre is discussed, where a possible element of pressure sensor application for a differential pressure flow sensor is also discussed.

Chapter Three presents the results of an investigation of an optical pressure sensor, using a low-coherence light source and a photoelastic material as the sensing element. A change in the optical path difference between light propagating in the two eigenmodes of the stressed sensing element has been observed by monitoring a corresponding change in the optical path in a linked "recovery" optical interferometer. The pressure to be measured was applied by placing a calibrated mass on the sensing element. The sensing element used has a capability of stress-induced brefringence i.e. it is photoelastic, and was produced from the commercial products "Araldite" and "Perspex". Three optical arrangements using the sensing element in reflection, transmission, and optically biassed (with an initial phase change) are described. In these cases a recovery Michelson interferometer was employed to obtain the optical path difference of the light in the sensing element.

In Chapter Four, further measurements of force/pressure-induced birefringence have been investigated using a photoelastic technique as discussed earlier in Chapter Three. To improve the sensor sensitivity, a short coherence length source, a light emitting diode (LED), is used in this arrangement. The sensing material properties such as stress relaxation, the elastic limit, and its temperature dependence are also investigated. The results obtained have shown the possibility of using different sensing materials which are suitable for different ranges of measurement and possess differing material limits.

In Chapter Five, the characteristics of three individual types of polarisation maintaining fibres are investigated using an interferometric technique. One of the two optical eigenmodes is excited in the sampling fibre, then the coupling power between the orthogonal eigenmodes is observed when force is applied to it. The location of the output signal position is monitored using a detector and

a basic Michelson interferometer. For comparison purposes, each fibre type is considered in terms of a force-induced coupling power, and thermal effects are studied. Theoretical aspects of the sensor system and its arrangement are discussed and demonstrated. A number of applications, such as pressure and position sensing, beat length and birefringence measurement have been demonstrated. Device sensitivity and variations with temperature for these measurement devices are also examined.

A discussion, cross-comparison and evaluation of this work and consideration of further applications are the main features of Chapter Six. Some relevant basic background information used is also given in the Appendices, which include a list of work published in the refereeed external literature on this study.

1.2 Pressure Measurement

1.2.1 History

The first true pressure measurements were made by Torricelli in 1643 [1], during which he inverted a column of mercury at atmospheric pressure. In 1647 Pascal invented a similar device, known as barometer, and a decade later, in 1660 Boyle discovered the foundation relationship :

$$PV = \text{Constant} \tag{1.1}$$

where P is pressure, V is gas or fluid volume and the temperature is held constant.

Bernoulli in 1738 developed the impact theory of gases, and Avogadro declared in 1811 that equal volumes of gases contained the same number of molecules.

From this, the kinetic theory of gases developed in the mid-nineteen century. Thus, as an aspect of the subject of measurement, there is a long history of quantitative pressure determination.

Pressure can be defined in several different ways, which are based on the definition of pressure, P, being a force per unit area i.e.

$$P = F/A \tag{1.2}$$

where F is an applied force and A is a cross-sectional area over which it is applied.

From equation (1.2), i.e. pressure = force/unit area, where force in the SI system is given in Newtons (N) and area in square meters, the common unit of pressure used is the Pascal (Pa), that is $1 Nm^{-2} = 1 Pa$.

1.2.2 Optical Pressure Sensor

All pressure measuring devices operate by determining a change of differential pressure between the measurand and reference. The methods and operations of such devices, for example, deadweight gauges, force balance systems, vacuum systems and elastic transducers etc. are found in references [1, 2]. An optical method (elastic transducers) is one such method that it has been recognized as an important research technique for pressure determination [4, 7, 8]. For years, various optical techniques have been used as methods of stress analysis [4, 9, 10], where a photoelastic material is subjected to a load, (i.e. F/A) or stress in one direction, and then viewed with polarised light. The resulting fringe patterns the nature of which are directly proportional to the stress in or pressure applied to the material, are seen using a screen.

The use of optical fibres as sensors is currently the subject of a great deal of research and rapidly increasing product development. This growing interest in optical fibre sensors is justified by the advantages that such sensors are able to offer, in terms of high accuracy and measurement bandwidth, small size and immunity from radio frequency interference, even over long transmission paths, together with complete dielectric isolation. The basic momentum for the development of optical fibre sensors has been the desire for inexpensive, compact equipment for use in a wide variety of industrial applications.

Fibre optic sensors can be divided into two groups; often termed "intrinsic" and "extrinsic" sensors. The intrinsic sensors use the fibre itself or small fibre sections as the sensing element. The measurand directly or indirectly interacts with the fibre, resulting in a change of intensity, of polarisation or birefringence, or in the phase or optical path or another measurable feature of the guided light. The characteristic of the intrinsic sensor is directly coupled to the properties of the fibre. In extrinsic sensors the fibre is used only to guide the light to and from the sensing transducer. The sensor interaction (ideally) acts outside the fibre. The characteristic of extrinsic sensors are therefore that they are much less dependent on the properties of the fibre. This approach has been discussed extensively in the literature [8, 11, 12].

From this information and the known advantages of the optical technique, the possibility of its use for pressure sensing, i.e. the new development of a new optical pressure sensor, will be investigated and discussed.

1.2.3 Photoelastic Effects

The photoelastic effect arises from the change in refractive index distribution within a sensitive or photoelastic material when it is stressed. By using a general coordinate system, the state of stress distribution in any sensing element may be described by three normal stress components and three shear stress components [4]. A coordinate system can be chosen in which the shear stress components vanish and the whole stress state is described by the remaining three orthogonal normal components, as shown in Figure 1.2. These directions are called principal axes and their stress components the principal stresses, σ_x, σ_y, and σ_z. In this configuration a coordinate system which is parallel to the principal axes is considered.

A transparent sensing element under stress may be birefringent. In such a material, its optical properties are those of a rhombic crystal with three orthogonal axes of symmetry [13]. The principal axes correspond to these symmetry axes, and the three principal refractive indices n_x, n_y and n_z are related to these axes. They set up a so-called index ellipsoid [10] which may be used to describe the propagation of light in any volume element of the body. The relation to the principal stresses is described by [4]:

$$n_x = n_0 + C_1\sigma_x + C_2(\sigma_y + \sigma_z) \tag{1.3}$$

$$n_y = n_0 + C_1\sigma_y + C_2(\sigma_z + \sigma_x) \tag{1.4}$$

$$n_z = n_0 + C_1\sigma_z + C_2(\sigma_x + \sigma_y) \tag{1.5}$$

where n_0 is the refractive index in the unstressed state, and C_1 and C_2 are the photoelastic constants, which are material constants.
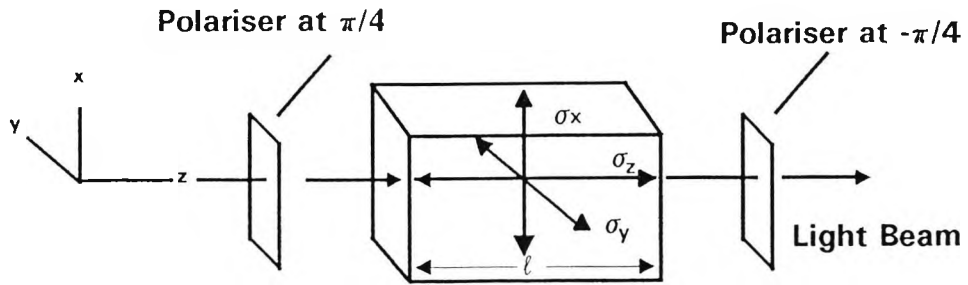
Figure 1.2 Illustration of stress distribution in photoelastic sensing element.

A plane wave (**E**) propagating in the **z**-direction, polarised at 45^0 to **x** in a medium of refractive index, n, is given by [14]

$$\mathbf{E} = (\mathbf{x} + \mathbf{y}) \, A \, e^{-i[\omega t - (2\pi n/\lambda)z + \phi_0]} \tag{1.6}$$

where $(2\pi n/\lambda) = k$ is the medium wave number, ϕ_0 is an initial phase change, and ω is the angular frequency. If this light wave of wavelength, λ, is incident on a photoelastic material with a two-dimensional stress, given by σ_x and σ_y (σ_z = 0), then the two orthogonal components in the **x** and **y** directions experience a difference in transit time or phase change, $\Delta\phi$, in travelling through a distance z = l (time t = l/c, c is the speed of light in the material), of the photoelastic material given by

$$\Delta\phi = (2\pi/\lambda)(n_x - n_y) \, l \tag{1.7}$$

When radiation from a monochromatic light source of intensity I_0 and wavelength λ is propagated through the system comprising the optical

9

elements, shown in Figure 1.2, then the output intensity, I, can be expressed as [14]

$$I=(I_0/4)\{1\text{-}\cos[(2\pi l/\lambda)(C_1\text{-}C_2)(\sigma_x\text{-}\sigma_y)]\} \tag{1.8}$$

where

$$(C_1\text{-}C_2)(\sigma_x\text{-}\sigma_y) = n_x\text{-}n_y \tag{1.9}$$

Equation (1.8) indicates that a single element of photoelastic material acts like a differential stress sensor (for orthogonal axes at $\pi/4$ to the crossed polariser transmission axes).

1.2.3.1 *Photoelastic pressure sensor*

In a simplified arrangement, it may be arranged that the light propagation is parallel to one of the axes, the principal axis, the **z**-axis, as shown in Figures 1.2 and 1.3. In the case of uniaxial stress, σ_x is applied to the **x**-axis of the photoelastic material.

When pressure P is applied to induce the stress, the photoelastic material acts as a stress-dependent wave plate with its fast axis parallel to the **x**-axis and the induced retardation, $\Delta\phi$, is given by

$$\Delta\phi = (2\pi/\lambda)\; C\; l\; (F/A) \tag{1.10}$$

where $C=C_1\text{-}C_2$ is a combination of photoelastic material parameters, the so-called stress-optic coefficient, $F/A = P = \sigma_x$ (i.e. uniaxial stress), A is the sample cross-sectional area, l is the thickness of the material, and λ is the wavelength of the light source.
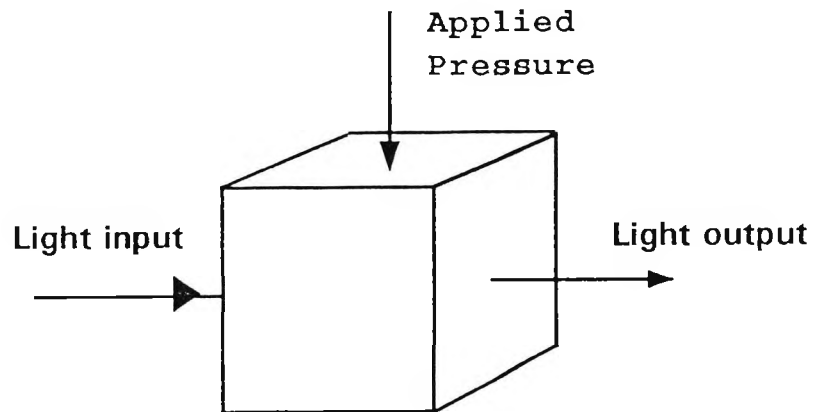
Figure 1.3 Illustrates one-axis pressure applied on the sensing element.

1.2.3.2 *Photoelastic fibre-optic pressure sensor*

An optical fibre may be considered as an elastic and mechanically homogeneous material as shown in Figure 1.4. When it is pressed between two parallel plates, a transverse force, F, induces a phase difference given by [15]
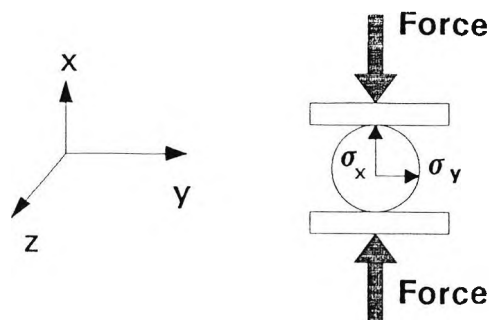
Figure 1.4 Illustrates a sensing fibre sandwiched between parallel plates.

$$\Delta\phi = 8(C_1 - C_2)\ (F/\lambda\ r) \tag{1.11}$$

where F is the applied force, λ is the wavelength, r is the fibre radius. Again this phase difference is proportional to applied force/pressure.

1.3 Sensor Systems and Devices

In this section, it is necessary to introduce the basic components and devices used in this work, to develop the above theoretical concepts into a pressure sensor. The use of these devices as exploited in this research will be reviewed in the following chapters. Important optical components such as beamsplitters, directional couplers, mirrors, polarisers, and retarders, which may be used for some particular applications, will be discussed and details are included within the experimental description, on their use.

1.3.1 Specific Light Sources

The most basic types of light sources to be employed successfully in an optical sensor must satisfy requirements in terms of power consumption, reliability, size and cost, and of course be suitable for the specific sensing purpose. Furthermore, the light source used should satisfy the requirement of the overall optical system, in terms of being of single mode, a low-coherence, or a short coherence length light depending on the application. In this section, a review of some of the most commonly used light sources and their properties for sensor applications is presented, in light of their potential subsequent application in the work described, where more details and their specific purposes will be discussed later.

1.3.1.1 *He-Ne laser*

The single mode He-Ne laser is one of the standard sources used in narrow band long-coherence interferometry. Its output wavelength is normally 632.8 nm, but it can operate at infrared or at shorter wavelengths [16]. Its linewidth can be as low as 10 kHz, i.e. a coherence length of 30 km (see Appendix C). For applications in long coherence techniques, the He-Ne laser is still widely used as a convenient light source.

1.3.1.2 *Laser diodes (LDs)*

Laser diodes are available with a wide range of emission wavelength in the visible or red and also the near infrared, typically 660 nm, 780 nm, 800 nm, 850 nm, 1.3 μm and 1.5 μm. The laser diode has a relatively short coherence length compared with that of the He-Ne laser. Laser diodes, of single mode and multimode output are widely available comercially. During laser oscillation, constructive interference allows the creation of a standing wave within the laser resonator. The laser resonator may support just a single longitudinal mode (i.e. single mode), or a single transverse mode and multi-longitudinal modes (i.e. multimode) [17]. The output power spectra (P_o) dependence on wavelength (λ_p) of a typical single mode laser diode (Sharp LT022 Series) and a representative multimode laser diode (Sharp LT023 Series) are shown in Figures 1.5(a) and 1.5(b) [18] respectively. Figure 1.6 shows the relation between the output power of a laser diode, changing with the forward driving currents and temperatures [18]. The complex spectra mean that the coherence properties of LD is also complex [19].
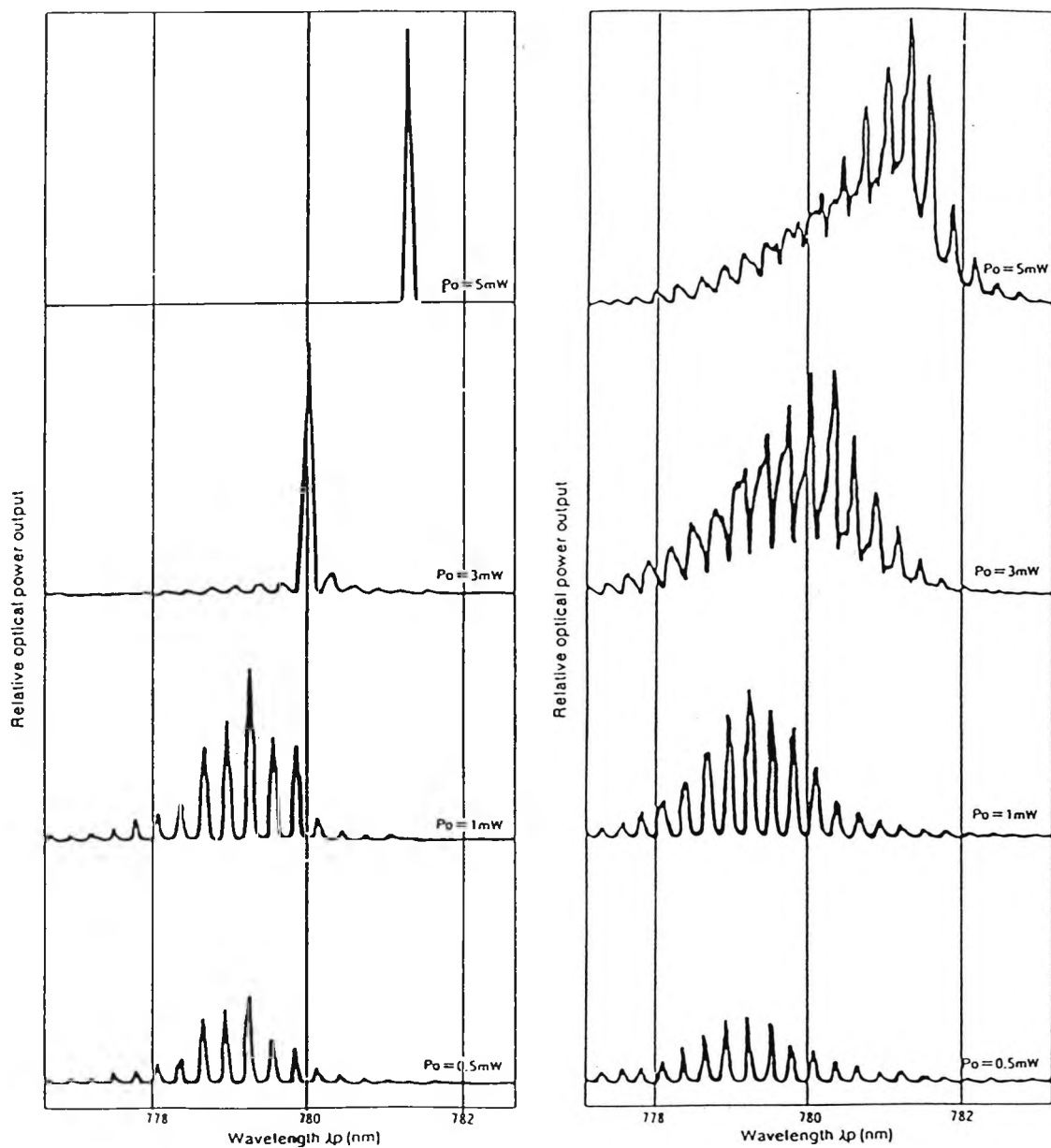
(a)   (b)

Figure 1.5 Spectral output characteristic of laser diodes: (a) Single mode, (b) Multimode.

As shown in Figure 1.5(a) a single mode LD has a single dominant frequency mode when it is in operation at near maximum current (i.e. P_0=5mW). As the driving current is reduced, other frequency modes start lasing simultaneously and the laser output becomes multimode (P_0=1mW). Its coherence length starts to decrease sharply as the forward current (I_f) approaches threshold (see Figure 1.5(a), top). When I_f is reduced, the spectrum becomes a broad "fluorescent peak" (see Figure 1.5(a), bottom).
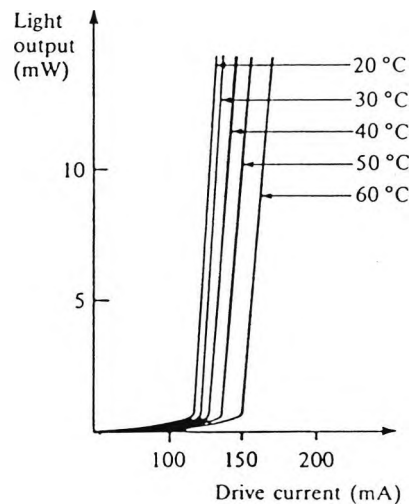
Figure 1.6 Laser diode output power versus drive current for a series of temperatures.

The multimode laser diode considered has a relatively short coherence length and a high level of coherence side peaks e.g. the laser output at the centre wavelength is not totally dominant with respect to the side peaks sub-order, (see Figure 1.5(b) (top), more details will be discussed in Section 1.3.2.) when it is normally driven. When I_f is reduced from the normal operating value, the multimode laser diode remains multimode but the overall spectral profile broadens as shown in Figure 1.5(b) (bottom).

In practice, variations in temperatures of these devices mean that the output wavelengths can change at a rate of up to 0.2 nm/^{0}C [18]. A single mode and multimode laser diodes with a spectral width of 0.03 nm and 6 nm operating at 780 nm would have a coherence length of about 2 cm and 100 µm respectively.

1.3.1.3 *Light emitting diodes (LEDs)*

There are two basic types of light-emitting diode that are frequently used in fibre optic sensor applications: the surface-emitting diode (SLED) and the edge-emitting diode (ELED). Some of the features of light-emitting diodes that are of interest to fibre optic sensors include a very short coherence length (with no side peaks), a result of a very broad spectral output, very low sensitivity to back reflection from elements of the fibre sensor (since emission is dominated by spontaneous emission) and high reliability. A light emitting diode with a spectral width of 60 nm operating at 780 nm would have a coherence length of about 10 µm.

Typically, SLEDs are now available at low cost and are frequently used in fibre optic sensing systems, where the light intensity requirements are modest and multimode fibre is the transmission medium. For high power applications requiring single mode fibre, an ELED is more efficient than a SLED, as the waveguide structure of the ELED (with a maximum output power of ~ 3 mW) allows significant power to be coupled into a single mode fibre, while retaining the advantages of low coherence length, high reliability, and the immunity to feedback characteristic of light emitting diodes.

1.3.1.4 *Superluminescent diode (SLD)*

The superluminescent diode, which has recently been developed, is manufactured by deliberately polishing both ends of a laser cavity at an angle to the normal parallelism of the laser cavity [14] to reduce the finesse. As a result, the SLD provides an output having a shorter coherence length and a lower level of side-peaks than that of a multimode laser diode. Its spectrum is shown in Figure 1.7. The SLD also has a much higher launching efficiency into a single mode fibre than that of an LED [14].

Relative Intensity

Wavelength(nm)
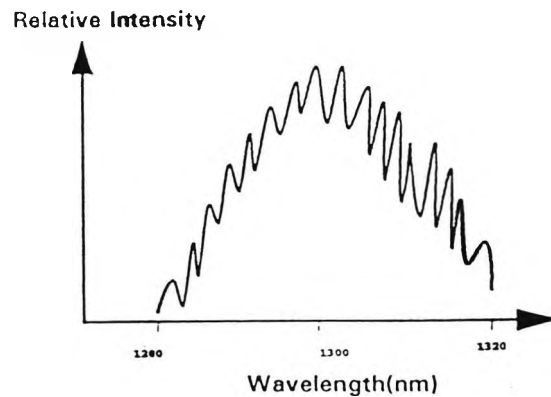
Figure 1.7 Spectral output of a superluminescent diode.

1.3.2 Specific Interferometry

There are many ways to make two or more beams of light interfere, and instruments for such a purpose are called "interferometers". In general, optical interferometers are used either to determine the fundamental parameters of an optical source such as its wavelength, coherence length or optical path difference (OPD) in an optical system. A change in the OPD may occur because of a physical displacement, or a change in the optical constants of the light transporting medium (e.g. its refractive index), in the interferometer.

The main advantage of using the interferometric technique for measurement is that it offers both a large dynamic range and incorporates a potential for very high resolution when applied to the measurement of varying optical path length. There are several possible interferometers of which, only a very few need be discussed in the context of this work [20]. The best known, and the most important are the Michelson, Mach-Zehnder and Fabry-Perot interferometers [13]. These are discussed in both free-space and fibre optic configurations. Since the objective of this work is that the use of such a scheme should also provide a temperature compensation technique, polarimetric interferometry, i.e. using the combination of the polarisation property of light and interferometric techniques, is discussed. Finally, to improve the measurement resolution, a further technique was required and low-coherence interferometry using a low-coherence light source offering a short coherence length was employed and is also discussed.

1.3.2.1 *Free-space interferometry*

(a) *Michelson interferometer*

A classic bulk-optic Michelson interferometer [20] is shown in Figure 1.8(a). A coherent optical beam from a laser source is split into two by a beamsplitter (BS) at P. Part A of the beam strikes a stationary mirror M_1, is reflected back to P, and forms the "reference" arm of the device. The other part of the incident beam is transmitted by the beamsplitter at P, and is reflected back to P by mirror M_2. Parts of the reflected beams are recombined at P and are detected by an optical detector. Mirror M_2 is scanned along the optical axis, thus changing the path length of the reflected beam. A change in the path difference, ΔL, leads to a change in the interference signal intensity, I, observed at the detector. This relationship can be expressed as

$$I = I_0[1 + Q \cos\varphi(t)] \tag{1.12}$$

where I_0 is related to the input optical power, $\varphi(t)$, the time dependent phase difference between the arms of the interferometer, is equal to $2k\Delta L$, where $k = (2\pi n/\lambda)$ is the propagation constant, n is the refractive index of the air path, λ is the light source wavelength in vacuum, and Q is the fringe visibility defined as

$$Q = [I_{max} - I_{min}]/[I_{max} + I_{min}] \tag{1.13}$$

Where, I_{max} and I_{min} are the maximum and minimum intensities of light in the interference pattern respectively. The signal intensity, I, plotted as a function of φ is shown in Figure 1.8(b). For an initial setting of $\varphi = (2n+1)(\pi/4)$, $n = 0,1,2..$, the sensitivity is maximum. This is called the "quadrature point" of operation of the interferometric sensor.

(b) *Mach-Zehnder interferometer*

A classic Mach-Zehnder interferometer [21] is shown in Figure 1.8(c). Basically the interferometer is used to compare the differences in path length of light over the optical paths BS_1-M_2-BS_2 and BS_1-M_1-BS_2. In this case, a multiple wavelength optical input can easily be employed (e.g. defined by wavelengths λ_1 and λ_2). In a practical sensor scheme, the path length over the path M_1-BS_2 experiences an environmental perturbation, following which the paths of light from those directions are compared. Any change in OPD of the perturbed medium represents a change of the output intensity, I, given by

$$I = I_0[1 + Q \cos(2\pi n\Delta L/\lambda)] \tag{1.14}$$
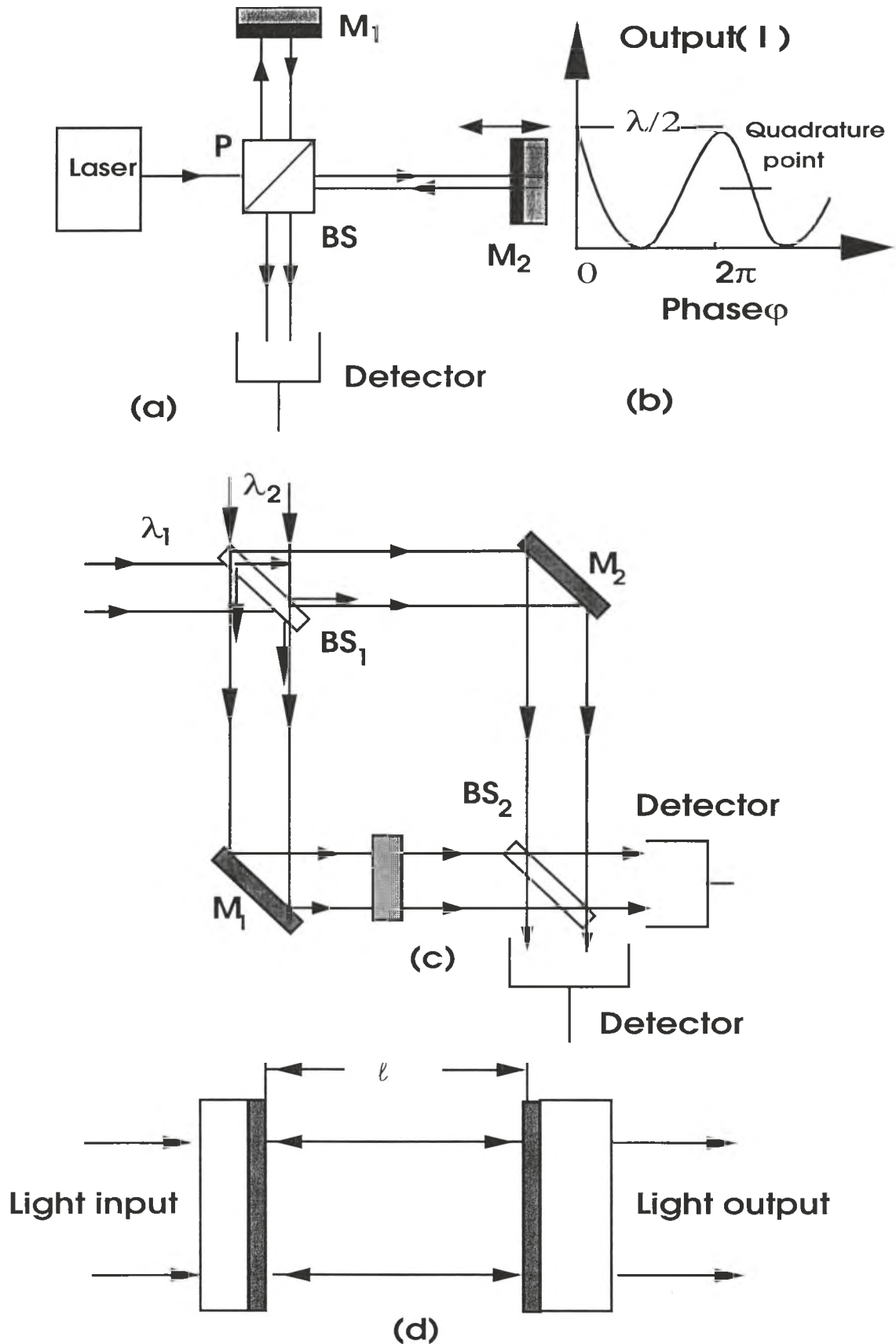
Figure 1.8 (a) Schematic representation of Michelson interferometer, (b) Plot of the Michelson interferometer output intensity as a function of phase φ, (c) Mach-Zehnder and (d) Fabry-Perot interferometers.

where I_0 is the input optical power, Q is the fringe visibility, n is the refractive index of the perturbed medium, ΔL is the path difference of the two wavefronts, and λ is the light source wavelength in free space.

(c) *Fabry-Perot interferometer*

The Fabry-Perot interferometer as shown in Figure 1.8(d) and consists of a plane-parallel plate of thickness ℓ and index n which is immersed in a medium of index n_M. The inner surfaces are coated with films that produce very high reflectivities. The intensities of the light transmitted, I_t, and reflected, I_r, of a Fabry-Perot etalon with no absorption are given by [21,22]

$$I_r = I_0 \, (4R\sin^2\delta)[(1-R)^2 + 4R\sin^2(\delta/2)]^{-1} \tag{1.15}$$

$$I_t = I_0 \, [\, 1 + \{4R/(1-R)^2\}\sin^2(\delta/2)]^{-1} \tag{1.16}$$

and

$$4R/(1-R)^2 = (2F'/\pi)^2 \tag{1.17}$$

where

$$I_r + I_t = I_0, \tag{1.18}$$

I_0 is the input intensity, δ is the double pass phase shift, and F' is the finesse.

From an analysis of equation (1.16) it is clear that the transmitted intensity reaches a maximum value equal to the incident intensity when $\delta = 2m\pi$, and a minimum when $\delta = (2m + 1)\pi$, where $m = 0,1,2,3.....$ The degree of phase change required to move from a maximum to a minimum in the optical signal is a π shift in the value of δ (see Figure 1.9 [23]).
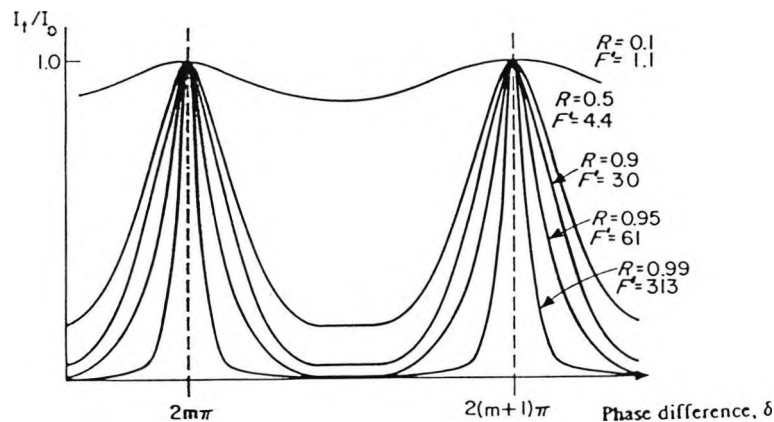
Figure 1.9 Schematic diagram showing the output intensities as a function of

mirror reflectance R.

1.3.2.2 *Fibre-optic interferometry*

The all single-mode fibre optic equivalent of both the Michelson and Mach-Zehnder interferometers are shown in Figures 1.10(a) and 1.10(b) respectively. In the case of the Michelson, the conventional beamsplitter is replaced with a single mode fibre directional coupler and the mirrors are formed by sputtering the normally cleaved ends of the fibre with an appropriate mirror coating. In the all fibre Mach-Zehnder the directional couplers replace both the conventional beamsplitters and mirrors. The advantage of these configurations of interferometers is that they can eliminate many effects of the mechanical disturbances which normally induce misalignment of the optical components in a conventional interferometer. However, in the single mode fibre optic sensor reported by Jackson [20], the reference and sensing arms, (i.e. without and with an applied force respectively) are physically positioned at different locations and, hence, a different change in temperature between these arms may affect

the phase difference detected at the interferometer output. This leads to a misinterpretation of the observed change in phase, due to temperature drifts being attributed to the deliberate external perturbation to be measured.
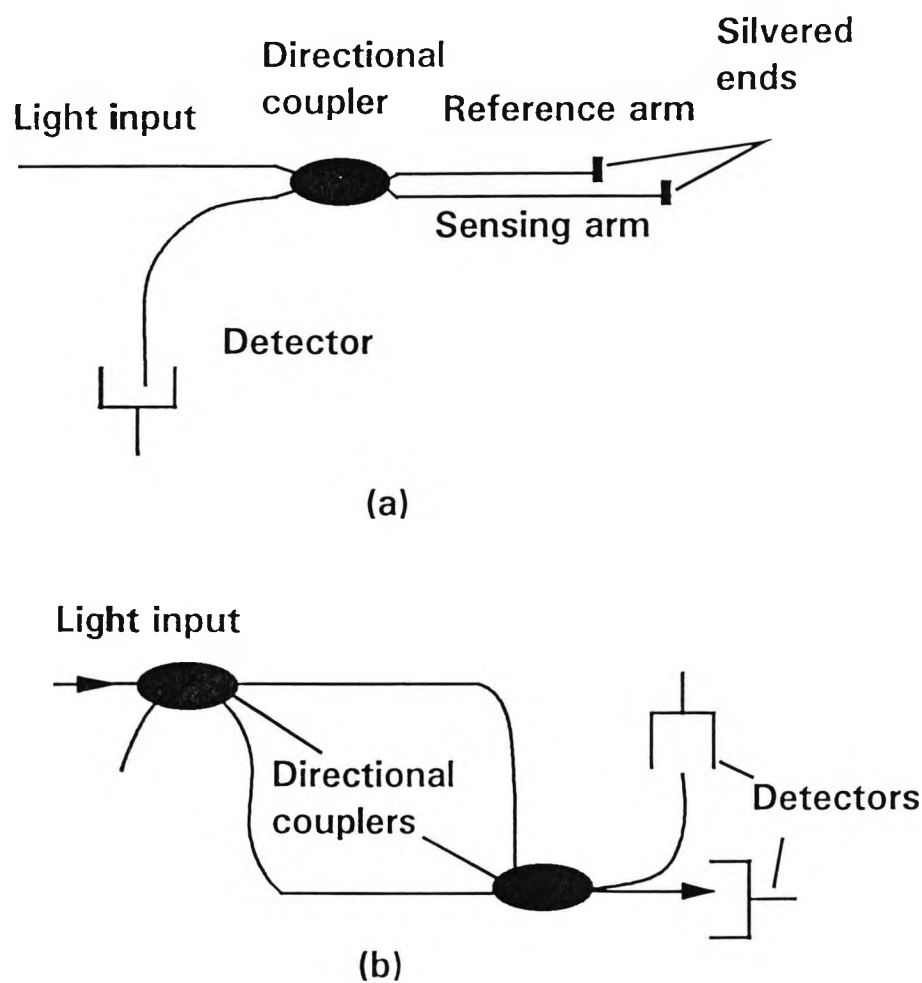
Figure 1.10 Fibre-optic interferometric types :
(a) Michelson, (b) Mach-Zehnder.
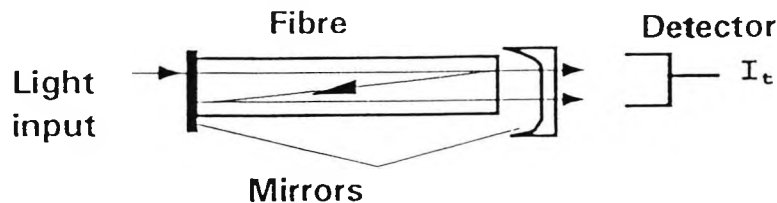
(a)
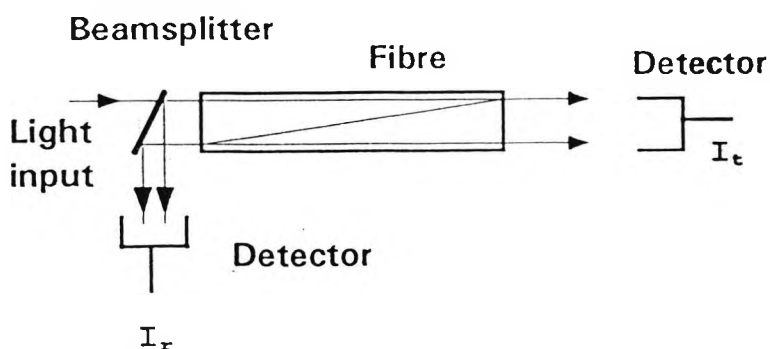
(b)
Figure 1.11 Fibre-optic Fabry-Perot interferometer: (a) Fibre ends-attached type, (b) Cleaving fibre-ends type.

Fibre optic equivalents of the Fabry-Perot interferometer are shown in Figures 1.11(a) and 1.11(b). In Figure 1.11(a) the instrument is used in the conventional transmission mode, where the mirrors have been attached to the fibre ends to enhance the finesse [22]. Figure 1.11(b), shows a single section of single mode fibre with normally cleaved uncoated ends, where 4% of transmitted light is reflected in the Fabry-Perot cavity, i.e R=4 %. From equations (1.15) to (1.17), in this case, the finesse will be low, and so the finesse can be increased by coating the cleaved fibre ends. In the back reflection case (see equation 1.15), the transfer function is very similar to that of the Michelson interferometer [20].

1.3.2.3 *Polarimetric interferometry*

In a polarimetric interferometer as shown in Figure 1.12, light entering the sensing element has its polarisation set at 45^0 to the fast and slow axes. Components from these two beams represent orthogonally polarised modes which propagate along different optical paths. The emerging light is processed by passing through a processing polariser also set at 45^0. These two modes are then superimposed, and fall onto a detector. By using this technique, the birefringence can be measured. Birefringence measurement has been used for many years to make models which are stressed, in both static and dynamically induced stresses in structures [4, 24]; for example, stressed photoelastic materials are usually examined between crossed polarisers. Polarimetric interferometers are based upon the same fundamental principle of these systems, and have been implemented, using as the sensing units, a photoelastic crystal [25], an ordinary single mode fibre [26], and a single mode birefringent fibre [27] where linear or circular birefringence was introduced and these have been used for sensor applications. In this work, the case of induced linear birefringence is used in the interferometer, and will be considered.
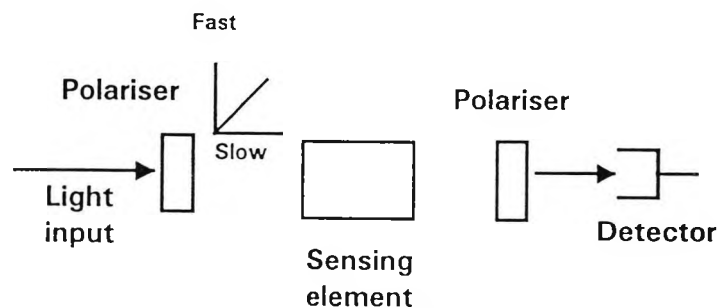
Figure 1.12 Illustration of polarimetric interferometry.

1.3.2.4 *Low-coherence interferometry*
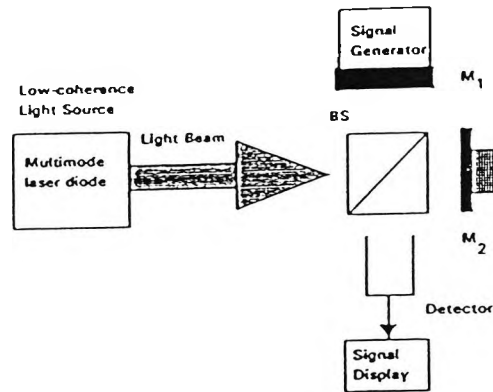
(a)
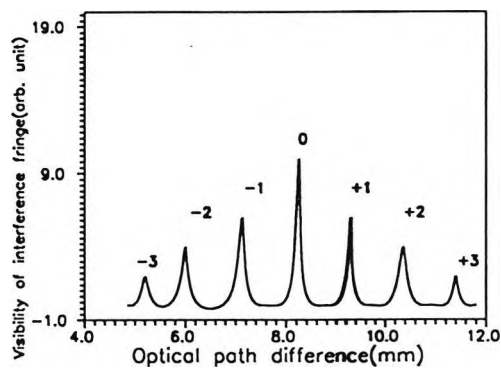
(b)

Figure 1.13 Schematic of low-coherence technique using a basic Michelson
interferometer: Ms Mirrors, BS Beamsplitter; (a) System arrangement, (b)
Visibility of the interference fringes, where the number denotes the fringe's
order.

Single mode, long-coherence light sources used in an interferometric system
offer only a limited operating range equivalent to an optical retardation of 2π
rad. It is in the nature of the interferometer output that its signal will be repeated
with a period of 2π. A number of studies [19, 28, 29] have demonstrated that

this limitation of unambiguous operating range can be overcome by using low-coherence techniques. Furthermore, this arrangement can be achieved using a relatively simple signal processing scheme.

A multimode laser diode is employed as the low coherence light source as shown in Figure 1.13(a). If this is used in a Michelson interferometer a maximum in fringe visibility is observed at zero path length difference as shown in Figure 1.13(b). This visibility plot shows the position of the maxima of fringe visibility. A series of equally space sub-orders of interference of the same width also occur (labelled +/-1, +/-2, +/-3, side peaks). Care must be taken in using a multimode laser diode in such low-coherence interferometry system that these sub-orders do not influence the measurements.

An analysis of such low-coherence interferometry has been described by Ning et al [19], where the light source used was a multimode laser diode from which light was launched into a basic Michelson interferometer, with the imbalance in one arm provided by an oscillator-driven vibrator attached one of the mirrors, as shown in Figure 1.13(a). The other arm of the interferometer is adjusted by scanning it along the optical axis. The pattern of the interference fringes produced is shown in Figure 1.13(b), and these fringes occur when the path difference between the two interferometric arms was at a balanced position (0 position) and when moving away from that position in both directions (i.e. left and right from the balanced position are denoted by the minus and plus signs respectively).

The basic system for the measuring interferometer consists of a low-coherence light source, a sensing unit and a recovery interferometer, as shown in Figure 1.14(a). The sensing interferometer which is sensitive to the parameter of interest (such as in the photoelastic sensor) is positioned before the light enters

the Michelson interferometer. If the optical path difference, ΔL, of the sensing interferometer is greater than the width of the peak of the zero order interference fringe, for an optical path difference of zero in the Michelson interferometer, no difference in fringe pattern will be observed. This corresponds to the position ΔL shown in the visibility plot, see Figure 1.14(b). Adjustment of the optical path difference in the Michelson, will then re-establish interference with maximum fringe visibility when the path difference in the Michelson interferometer matches that in the first. Thus the path difference ΔL can be read directly from the position of measurement interferometer.
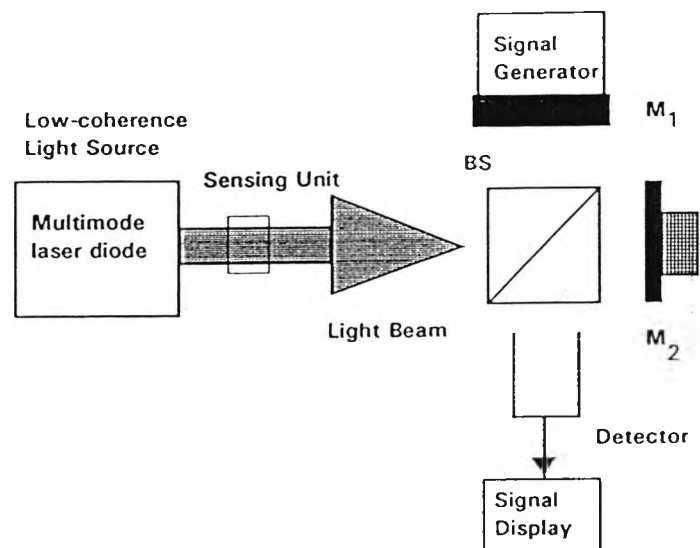
(a)
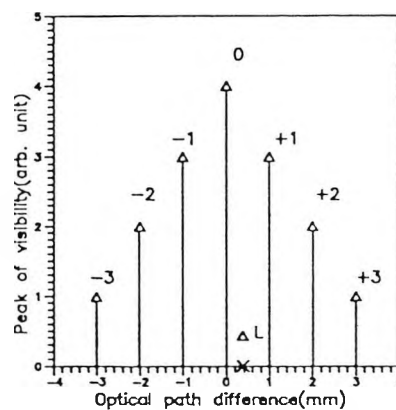
(b)

Figure 1.14 Schematic of low-coherence technique using a basic Michelson interferometer: Ms Mirrors, BS Beamsplitter; (a) System arrangement, (b) Position of the maximum amplitude of the interference fringes when a sensing unit is disturbed. Only zero order fringe position shown for clarity.

The same system and operation of the low-coherence interferometer can also be used when a light emitting diode (LED) is employed as a light source. In this case, a single peak (there is no side peak i.e. it has a continuous broadband spectrum) of fringe visibility is observed. The change in path difference in the sensing unit is measured in the recovery interferometer when its OPD is greater than the light source coherence length (typically 10 μm to 100 μm away from the balanced position [30]).

1.3.3 Fibre-optic

Light transmission through a fibre optic may be treated as radiation guided along the dielectric waveguide fibre by reflections at the core-cladding interface. For guidance of the wave to occur, the incident angle θ at which the ray of light strikes the interface must exceed the critical angle, θ_c at which total internal reflection of the ray will occur, see Figure 1.15. This is expressed as [17]

$$\theta > \theta_c = \sin^{-1}(n_{clad}/n_{core}) \tag{1.19}$$

where n_{core} and n_{clad} are the refractive indices of the fibre core and the surrounding medium respectively and $n_{core} > n_{clad}$. The relationship of these two refractive indices in terms of the numerical aperture (NA) of the fibre is given by

$$NA = (n_{core}{}^2 - n_{clad}{}^2)^{1/2} \tag{1.20}$$

In term of the incident angle on the end of the fibre, α, where the maximum value that α can take, α_{max}, is determined by the minimum value that θ can take i.e. critical angle θ_c, is given by

$$\alpha_{max} = \sin^{-1}(NA/n_o) \tag{1.21}$$

where n_o is the medium refractive index.

The greater the numerical aperture, the more light can be accepted and the better the coupling of the light to the fibre. There are two different types of fibre where in one there exists an abrupt change in refractive index between core and cladding, known as "step index fibre", and in the other where there is a gradually change in refractive index from a maximum at the centre of the core to its minimum at the interface-this is called a "graded-index fibre".

A fiber optic waveguide can only support a finite number of propagation paths. These modes occur due to the two dimensional confinement of the light beam [23]. In most practical waveguides, the refractive indices of core and cladding differ from each other by only a few percent and in this case the full set of modes (i.e. EH, HE and TE) can be approximated by a single set called linearly polarised (LP_{lm}) modes. The condition to determine which modes of propagation will be supported and maintained in the fibre is given by [23]

$$V = (2\pi a/\lambda)\ NA \tag{1.22}$$

V is called the V-number, or the normalized wavenumber (where the relation between the V-number and propagation modes can be found in reference [17]), a is the core radius of the fibre, and λ the wavelength of operation. The fibre operates in this single mode propagation regime when V is less than 2.405. For 2.405< V < 3.823, two linearly polarised modes can propagate through the fibre.
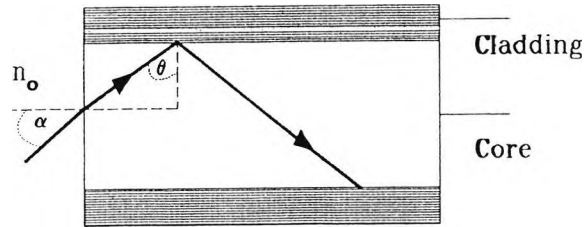
Figure 1.15 Illustration of light coupling into optical fibre.

Single-mode fibre   (a)

Multimode step-index fibre   (b)

Multimode graded-index fibre   (c)
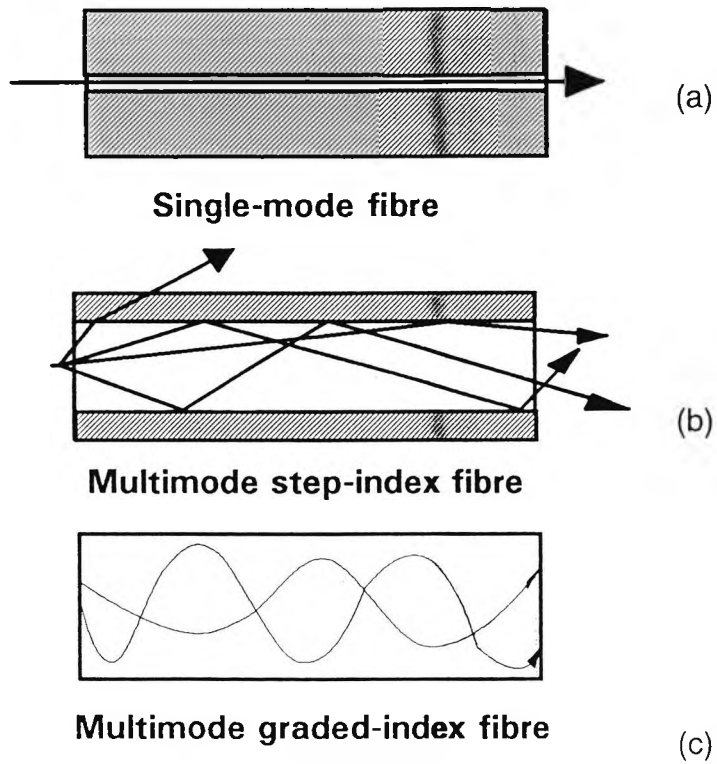
Figure 1.16 Characteristic of light propergation in optical fibres: (a) Single mode fibre, (b) Step-index fibre with multimode propagation, (c) Graded-index fibre with multimode propagation.

1.3.3.1 *Ordinary single mode fibre*

From equation (1.22), to limit the mode of propagation by reducing the diameter of the fibre until only one mode can enter and propagate along the fibre (see Figure 1.16) gives a type of fibre known as a single mode fibre. The core diameter of such a single mode fibre is usually about 2 to 10 μm. It may be shown [17] that when V is less than 2.405 only the LP_{01} mode can propagate. In theory, the LP_{01} mode will propagated no matter how small the V value (i.e. no matter how small the core radius). As V decreases, however, the mode field will extend increasingly into the cladding. If the field becomes significantly large at the edge of the cladding, most of energy may be radiated away from the fibre causing the mode to be highly attenuated (this is loss process).

1.3.3.2 *Birefringence single mode fibre*

In a circularly symmetrical fibre, (such as an ordinary single mode fibre), the two orthogonally polarised modes will have identical propagation velocities. However, real fibres will not be perfectly symmetrical; there are some slight anisotropies in both shape and refractive index. The result of this is that the two modes will have slightly differing velocities. In other words, the fibre experiences birefringence. The birefringence may result either from the intrinsic properties of the fibre (intrinsic birefringence) or from external perturbations (extrinsic birefringence).

There are some special fibres used in particular and individual applications, such polarisation preserving fibre (Hi-Bi), which is discussed and used in this work. The polarisation maintaining fibres are intrinsically birefringent and several different techniques have been used to produce them, as shown in Figure 1.17 [31, 32]. All rely on producing a fibre cross section which is in some

way asymmetric about two perpendicular axes. Usually, this asymmetry is built into the fibre preform before the fibre is drawn, causing birefringence in the fibre core.
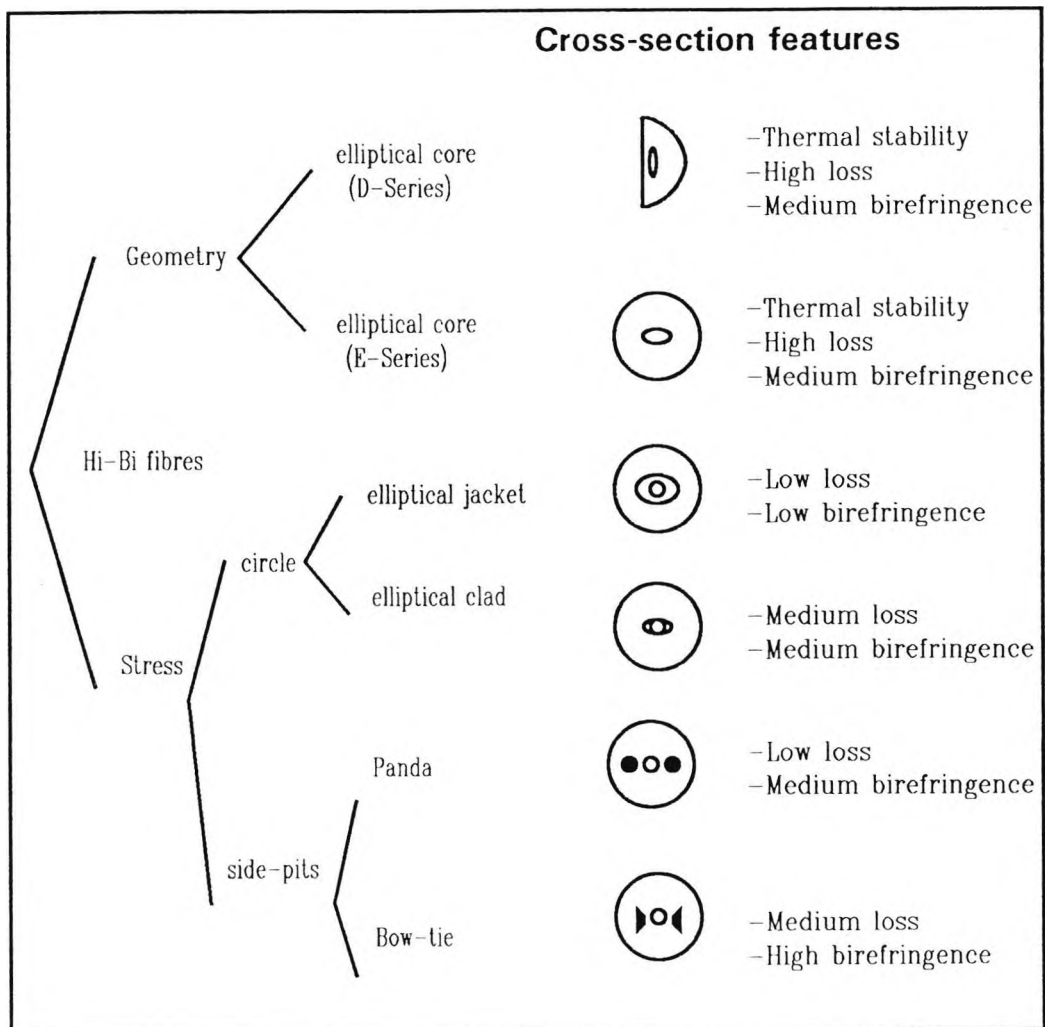
Figure 1.17 Types of single mode polarisation maintaining fibres (Hi-Bi).

Another single mode optical fibre with very low linear birefringence (Lo-Bi) has been developed for exploitation in particular applications, such as where a low-birefringence fibre is needed and these include Faraday-effect current sensors, magnetic field sensors, and fibre isolators [33]. Lo-Bi fibre is circularly symmetric in both internal and external structures (cladding or protective coating). In principle this particular fibre would be useful for interferometric sensors where the birefringence effects induced externally in the fibre can be calculated directly from the change in the polarisation state of the output light. However, its high susceptibility to externally induced birefringence has generally restricted its use in such applications.

1.3.3.3 *Multimode fibre*

Consider a fibre in which its core diameter is large enough to allow the propagation of several modes where rays strike the core/cladding interface at angle greater than the critical angle to propagate into the fibre independently of each other, i.e. V>2.405. In other words, the fibre can support many different modes: the fibre is known as multimode fibre [17]. The overall diameter of such multimode fibres is typically 125 to 200 μm with a core around 50 μm diameter. Generally, a multimode fibre does not maintain the phase information, however, with careful design the required information can be delivered into the sensor system using a multimode fibre link (more details of this approach are found in Chapter 4).

1.4 Signal Processing

A signal processor is a basic requirement in the field of measurement and instrumentation, where such a device used in this work is the interferometer itself. In general terms the effect of a measurand applied to the interferometer

will be [20] (i) to increase continuously the relative phase between the two arms, (ii) to modulate periodically the relative phase, (iii) to impose a phase modulation which is a combination of (i) and (ii). To understand this, when the optical path length of one arm of the interferometer is modulated by a signal Φ_s = $\phi_s(t)\sin(\omega_s t)$ of frequency ω_s, then the optical phase difference between the optical beams $\phi(t)$ is given by

$$\phi(t) = \phi_d + \Phi_s \tag{1.23}$$

where ϕ_d is the static phase difference and ϕ_s is the amplitude of the phase change induced in the interferometer by the perturbing signal. The output current, I, of the detector then has the following form:

$$I \propto [\ 1+ Q\cos(\phi_d + \Phi_s(t))] \tag{1.24}$$

The argument of the cosine term can be written as:

$$\cos(\phi_d + \phi_s \sin\omega_s t) = [\cos\phi_d\{J_o(\phi_s) \tag{1.25}$$

$$+ 2\Sigma J_{2n}(\phi_s)\cos(2n\omega_s t)\}$$
$$s=1$$

$$- \sin\phi_d\{2\Sigma J_{2n+1}(\phi_s)\sin(2n+1)\omega_s t\}]$$
$$s=0$$

where J_n is the Bessel function of order n.

The output from an interferometer, I (equation (1.24)), with varying induced optical phase change is not constant, due to the fluctuation of ϕ_d which may arise from temperature changes. In sensor applications, this variable sensitivity

is not acceptable as it causes signal fading, therefore interferometric sensors are usually operated such that the output is linearly related to the induced optical phase change. Linearisation of the interferometer sensor transfer function has been achieved by a variety of different approaches which may be classified as : active homodyne, passive homodyne, and heterodyne (heterodyne and pseudo-heterodyne). Some relevant techniques are discussed briefly in the following sections.

1.4.1 Active Homodyne

The basic needs of the interferometric technique is such that the device is maintained at constant sensitivity (over a limited range) by either physically controlling the length of the reference arm of the interferometer, or by varying the frequency of the modulation of the light source such that $\cos\phi_d = 0$ (the so called quadrature point). This is usually achieved by some form of servo arrangement. If the servo system used to lock the interferometer at quadrature had an infinite gain bandwidth product, then I would remain constant and contain no spectral information. In practice, the servo will have a finite gain bandwidth product and spectrum of intensity, I, for a frequency ω_s above the servo cut-off frequency is

$$I \propto J_1(\phi_s)\sin\omega_s t + J_3(\phi_s)\sin 3\omega_s t + \ldots\ldots \qquad (1.26)$$

provided ϕ_s is relatively small.

1.4.2 Heterodyne

One of the classical methods of signal recovery for conventional interferometers is to include some form of frequency shifter in one of the arms of the interferometer, typically via a Bragg cell, such that the interferometer output signal is centred about the offset frequency generated by the Bragg cell. Conventional electronic signal processing can then be used to demodulate the signal, typically a phase locked loop or frequency tracker. The output signal of the interferometer is then given by

$$I \propto \cos(\omega_b t + \phi_d + \Phi_s) \tag{1.27}$$

where ω_b is the offset frequency. This signal represents a carrier at frequency ω_b which is phase modulated by $(\phi_d + \Phi_s)$.

1.4.3 Pseudo-Heterodyne

Bragg cell frequency shifters are not particular suited to intrinsic fibre optic sensor systems as they are expensive and difficult to configure into the sensor. Generally, it is possible to change the relative optical phase difference between the arms of an unbalanced interferometer by varying the absolute frequency of the injected laser light. By using a pseudo-heterodyne technique, linear modulation of the laser source frequency will also produce a moving fringe pattern at the optical output of the interferometer. The details of this technique will be described in Chapter 2.

1.5 Conclusion

In this chapter, some of the prior background to the work undertaken in this thesis has been reviewed. The basic introductory material for the subsequent chapters has been presented. The concepts of the sensor system used including pressure measurement methods, optical fibres and interferometers, signal detection and processing, and some specific light sources were described.

As discussed, one of the aims of this work is to investigate and develop a prototype of a simple pressure sensor using an optical technique. Therefore, an ideal light source used should be a very small size, e.g. LD or LED, which is suitable for a compact device. However, the He-Ne laser can also be used for such a demonstration or for alignment. A simple Michelson interferometer is suggested to employ in this work whereas a large dynamic range with high precision of measurement can be obtained. The more details of the related systems used will be found in the following chapters, which discuss several approaches to the problem of pressure measurement.

References

[1] BARNLEY, G. C. (1988). Intelligent instrumentation:microprocessor applications in measurement and control. 2 nd edit. (London : Prentice Hall).

[2] DOEBELIN, E.O. (1983). Measurement system: application and design. 3rd edit. (Singapore: McGraw-Hill).

[3] YUPAPIN, P.V.P. WEIR, K. GRATTAN, K.T.V. and PALMER, A.W. (1993). An optical pressure sensor using a low-coherence light source with a photoelastic sensing element. Sensors and Actuators 36(2):105-111.

[4] MARTENS, G. (1992). Fibre optic photoelastic sensors. International Journal of Optoelectronics 17(3):385-407.

[5] BOIS, E. SPOONCER, R.C. and JONES, B.E. (1989). A hybrid resonant differential pressure transmitter with wavelength multiplexed power and data channels. In: Springer Proceedings in Physics 44, Ed. by H.J Arditty, J.P. Dakin and R. Th. Kersten. (Berlin:Springer-Verlag).

[6] ZHANG, L.M. UTTAMCHANDANI, D. and CULSHAW, B. (1989). Optically powered silicon microresonator pressure sensor. In: Springer Proceedings in Physics 44, Ed. by H.J Arditty, J.P. Dakin and R. Th. Kersten. (Berlin:Springer-Verlag).

[7] WANG, A. HE, S. FANG, X. JIN, X. and LIN, J. (1992). Optical fibre pressure sensor based on photoelasticity and its application. Journal of Lightwave Technology 10(10):1466-1472.

[8] MEDLOCK, R.S. (1986). Review of modulating techniques for fibre optic sensors. Ed. by A.J. Rogers, R.J. Weiss and S. Chomet. International Journal of Optical Sensors 1 1) : 43-68.

[9] DALLY, J. W. and RILEY, W. F. (1991). Experimental stress analysis. 3rd edit. (New York:McGraw-Hill).

[10] HETENYI, M. (1950). Handbook of stress analysis. (New York: John Wiley & Sons).

[11] GIALLORENZI, T.G. BUCARO, J.A. DANDRIDGE, A. SIGEL, JR., G.H. COLE, J.H. RASHLEIGH, S.C. and PRIEST, R.G. (1982). Optical fibre sensor technology. Journal of Quantum Electronics 18(4):629-665.

[12] GRATTAN, K.T.V. (1991). Sensors-technology, system and applications. Ed. by K.T.V. Grattan. (Bristol:Adam Hilger).

[13] HECHT, E. and ZAJAC, A. (1974). Optics. 4th edit. (Manila: Addison-Wesley).

[14] UDD, E. (1991). Fibre optic sensors : an introduction for engineers and scientists. (Canada:John Wiley & Sons).

[15] NAMIHIRA, Y. KUDO, M. and MUSHIKAKE, Y. (1977). Effect of mechanical stress on the transmission characteristics of optical fibres. The Transactions of IECE of Japan 60 (7):375-376.

[16] YARIV, A. (1988). Quantum electronics. 3rd edit. (Canada : John Wiley & Sons).

[17] Projects in fibre optics : applications handbook. (1988). Newport Corporation, U.S.A.

[18] SHARP laser diodes. (1988). Laser diodes user's manual, Available from Access Pacific Ltd., Kymbrook School House, Kimbolton Road, Keysoe, Bedford MK44 2HH, U.K.

[19] NING, Y. GRATTAN, K.T.V. MEGGITT, B. T. and PALMER, A.W.(1989). Characteristics of laser diodes for interferometric use. Applied Optics 28 (17):3657-3661.

[20] JACKSON, D. A. (1985). Monomode optical fibre interferometers for precision measurement. Journal of Physics E:Scientific Instruments 18 : 981-1001.

[21] FRANCON, M. (1966). Optical Interferometry. (New York: Academic Press).

[22] CRAIG, D. W. and STAROMLYNSKA, J. (1990). Comparison of variable birefringence devices and Fabry-Perot etalons for use as tunable filters. Journal of Quantum Electronics 26 (8) : 1440-1446.

[23] WILSON, J. and HAWKES, J.F.B. (1989). Optoelectronics : an introduction. 2nd edit. (Englewood Cliffs:Prentice Hall).

[24] GAUTHIER, R. C. and DHLIWAYO J. (1992). Birefringent fibre-optic pressure sensor. Optic & Laser Technology 24 (3):139-143.

[25] YUPAPIN, P. V. P. WEIR, K. GRATTAN, K. T. V. and PALMER, A. W. (1992). A Photoelastic interferometric technique using a low-coherence light source for pressure sensor application. In: INTERNATIONAL CONFERENCE ON ELECTRONIC MEASUREMENT & INSTRUMENTS. Tainjin. 1992. Proceedings. Pub. ICMI'92.

[26] YUPAPIN, P. V. P. WEIR, K. GRATTAN, K. T. V. and PALMER, A. W. (1993). A polarimetric interferometry based pressure sensor for qualitative measurements. Journal of Flow Measurement and Instrumentation, in press.

[27] PICHERIT, F. and MINEAU, J. L. (1990). Interferometric-polarimetric force and temperature sensor using high and low birefringence fibres with a short coherence length source. Optics Communications 79 (5):295-299.

[28] GERGES, A.S. FARAHI, F. NEWSON T.P. JONES, J.D.C. and JACKSON, D.A. (1988). Fibre-optc interferometric sensor utilising low coherence length source : resolution enhancement. Electronics Letters 24 (8):472-474.

[29] GERGES, A.S. FARAHI, F. NEWSON, T.P. JONES, J.D.C. and JACKSON, D.A. (1987). Interferometric fibre-optc sensor using a short-coherence-length source. Electronics Letters 23 (21):1110-1111.

[30] JONES, R. (1992). White light interferometry-a road to low cost, high performance optical fibre sensors. Paper presented at IEE Colloquim on fibre optic sensor technology, London, 1992.

[31] NODA, J. OKAMOTO, K. and SASAKI, Y. (1986). Polarisation-maintaining fibres and their applications. Journal of Lightwave Technology 4 (8): 1071-1089.

[32] Polarisation maintaining optical fibres, The Andrew Corporation, Bulletin 1259D, Available from Andrew Attenna, Weybridge, Surrey, U.K.

[33] Ultra-low birefringence fibre, York V.S.O.P. Product specification data sheet no. 9/86, Available from York V.S.O.P., York House, School Lane, Chandler's Ford, Hampshire SO5 3DG, U.K.

Chapter 2

Pressure Sensor Using An All Fibre Optic
Michelson Interferometer

2.1 Introduction

The work reported in this chapter presents the experimental results on fibre optic pressure/force sensor measurements obtained using a polarimetric interferometric technique. A comparison of the sensitivity of uncoated and UV-curable acrylate coated (the coating applied by the manufacturer coating) standard single mode fibre to applied force and the stability of the output to temperature variations are investigated. The sensitivity of an uncoated sensing fibre was found to be 18% greater than that of the coated fibre. Results are also presented showing good linearity and an acceptable stability of force measurements over the temperature range 20 ^{0}C to 95 ^{0}C. The force/pressure induced birefringence in an ordinary single mode fibre has been described as a possible element for a differential pressure flow sensor.

2.2 Review of Previous Work

The field of optical fibre sensors has been the subject of a great deal of research and now increasing product development. These devices have been applied successfully to the measurement of parameters such as pressure [1], temperature [2], and strain [3], amongst many other parameters. However, the measurement of such parameters shows several problems in many such fibre sensors due to the cross-sensitivity of the device to other influences. In particular, reduction or elimination of the thermal effect on the measurement of

non-thermal parameters is an important area of work in the development of fibre optic sensors, which have prospects for commercial development.

Ordinary single mode optical fibres have been widely used in the development of fibre optic sensors [4, 5, 6]. A fibre optic polarimetric interferometer, using such a single mode fibre, has also been applied successfully to pressure measurement [7]. Reduction in intrinsic errors in a polarimetric sensor using a low intrinsic birefringence fibre has been reported [8], while a novel polarimetric fibre optical sensor with high sensitivity using a Fabry-Perot structure has been applied to measure a static force using stress induced birefringence in an optical fibre [9]. Farahi et al [10] have demonstrated an interferometric technique which allows the simultaneous measurement of strain and temperature applied to a high- birefringence sensing fibre. It has been shown that the cross-sensitivity (i.e. the sensor responsivity when a temperature change and strain are applied simultaneously) is dependent on the fibre sensing length and the applied strain or temperature change. Herzog and Meyreis [11] have also shown that a pressure/strain sensor, incorporating temperature compensation, could be developed using this technique with standard single mode fibre, and these authors have shown successfully the feasibility of flow-rate measurements via the differential pressure principle.

As discussed in Chapter 1, a single mode Lo-Bi fibre has a very high susceptibility to externally induced birefringence. However, the birefringence of a single mode Hi-Bi fibre may be changed by the changing of local temperatures [12]. Therefore, ordinary single mode fibre may still be implemented in a sensor for a qualitative measurement. In practice, however, an improvement in the experimental sensitivity is still needed. One problem of sensor sensitivity shown in previous work, using single mode fibre, is the uneven force distribution experienced through the protective sheath of the fibre

and the cladding to the core when it is sandwiched between two parallel plates. Smith [13] has shown that this problem could be reduced by using an uncoated sensing fibre as the sensing element. The effect of coating of the fibre is to increase the surface area of contact; however, deformation of the soft coating of the fibre will reduce the force induced birefringence in the fibre core [14].

| Laser diode | → | Launching optics | → | Fibre optic sensor | → | Detection electronics |
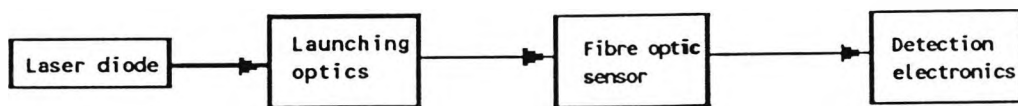
Figure 2.1 Block diagram description of a basic fibre optic sensing scheme.

2.3 Operating System

This section provides basic background information on the sensor design system, and its operation. The sensor system configurations used and the signal processing employed in this scheme are presented. As an introduction, the basic decomposition of an optical fibre sensor system is shown in Figure 2.1. In an interferometric fibre optic sensor, an optical fibre coupler may be used to provide a fibre equivalent to the Michelson interferometer.

2.3.1 Interferometric Arrangement

The operation of a classical Michelson interferometer was described in Chapter 1. A fibre optic equivalent to the Michelson interferometer is shown in Figure 2.2. This system uses a fibre optic to guide the light and a 2x2 coupler instead of the beamsplitter employed in free space approach. In this arrangement, light is at all times confined inside the fibre, which removes alignment problems associated with the bulk optics. To increase the output signal level, the endfaces of the two arms can be coated with a reflective material. However, the light reflected by the uncoated fibre end itself is about 4% of its input, which is sufficient for this operation. The path difference provided between the arms gives the same output dependence as in the classic interferometer.
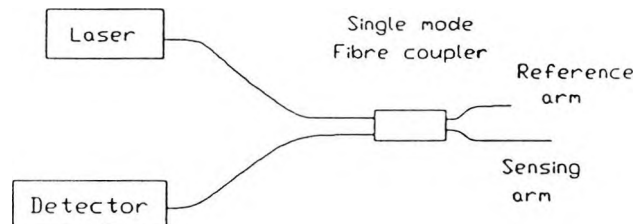
Figure 2.2 Schematic representation of an equivalent fibre-optic Michelson interferometer.

The 2x2 bi-directional fused single mode fibre coupler is a device which allows a percentage (a nominal 50%) of light travelling in one fibre to be transferred to a second fibre. The cladding of the two fibres is removed and they are placed side by side over a certain distance known as the "*interaction length* " [15]. The two fibres are then fused together over the

interaction length to form a single device. The amount of light that is transferred (the coupling ratio) depends on the wavelength used and the value of the interaction length. The coupling ratio can thus be varied, but a 50% coupler is of most use in fibre interferometers. Such devices are commercially available with reliable and reproducible characteristics.

2.3.2 Sensor Configurations

The pressure sensing devices presented are based on the use of an ordinary, single mode, 2x2 fibre coupler, using light from a single mode laser diode. A sensing unit is provided by using the two "arms" of the coupler, termed the "sensing" and "reference" arms, i.e. the arm to which pressure is applied, and the arm which is kept isolated from the pressure, as shown in Figure 2.2. The principle of operation is described as follow.

2.3.2.1 *Preliminary system*

As shown in Figure 2.3, if light is coupled into the sensor system, the difference in phase of the reflected light, $\Delta\phi$, between the "reference" and "sensing" arms, in term of the output intensity, I, can be written as [4]

$$I = I_0[1 + Q\cos(\Delta\phi)] \qquad (2.1)$$

where

$$\Delta\phi = 4\pi n\Delta L/\lambda \qquad (2.2)$$

I_0 and Q is the input optical power and fringe visibility as discussed in

46

Chapter 1 respectively, and ΔL is the path length difference of the interferometer, n is the fibre refractive index, and λ is the light source wavelength. The intensity change for a given change in path length between the arms is a function of the initial phase difference Δφ of equation (2.1). The pseudo-heterodyne arrangement used is as shown in Figure 2.3, (and was described in Chapter 1).

Thus, if any of the parameters such as ΔL, n or λ change due to some external influence, the detected intensity will change (due to the changing of phase Δφ) and may be related back to the external effect (i.e. measurand). For example this may be used for the measurement of strain (stretching of the fibre-change in ΔL), temperature or pressure (change in refractive index, n).
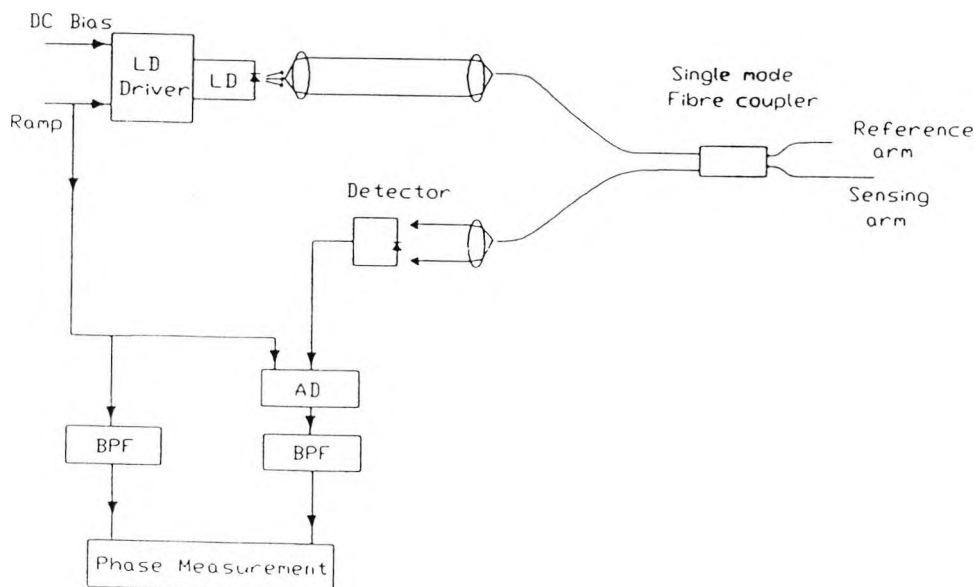
Figure 2.3 Schematic of the optoelectronic arrangement. LD Single-mode laser diode, BPFs Bandpass filters, AD Amplitude demodulator.

As described in Chapter 1, a stress distribution may be introduced when a sensing fibre is sandwiched between two parallel plates, i.e. birefringence is introduced in the fibre because its circular symmetry is broken, producing an anisotropic refractive index distribution in the fibre core. The two eigenmodes of the birefringence are parallel and perpendicular to the direction of the applied force, and these are characterised by refractive indices n_1 and n_2. In an ideal, unstressed fibre, with perfect rotational symmetry, the two modes are degenerate with $n_1=n_2$, and the input polarisation state would propagate unchanged along the length of the fibre. The force-induced birefringence, Δn, is given by [16]

$$\Delta n = n_1 - n_2 = n_o^3(p_{11}- p_{12}) (1+\alpha)(4F/\pi Ed\ell) \tag{2.3}$$

and

$$C = n_o^3(p_{11} - p_{12})(1 + \alpha)/2E \tag{2.4}$$

where n_1 and n_2 are the refractive indices of the two induced eigenmodes, n_o is an average refractive index, p_{11} and p_{12} are components of the strain-optic tensor of the fibre material, α is Poisson's ratio, E is Young's modulus, F is the applied force, and d and ℓ are the outer diameter and the length of sensing fibre respectively.

Polarised light propagating in a birefringent fibre may be considered to consist of two independent, linearly polarised states propagating in the two eigenmodes. Due to the difference of refractive indices in these two modes, on traversing a length ℓ, each mode will experience a phase change. The difference in phase, $\Delta\phi$, between the light propagating in the two eigenmodes is related to the change of phase in each mode $\Delta\phi_j$ (j =1,2), and the birefringence by

$$\Delta\phi = \Delta\phi_1 - \Delta\phi_2 = (2\pi/\lambda)(n_1 - n_2) \, l \tag{2.5}$$

The phase changes $\Delta\phi_j$, in each mode, can be detected independently, using an interferometric technique. This is shown in Figure 2.4, the changes in phase of the light propagating in the eigenmodes of the sensing fibre can be recovered independently using polarisation control and a polarisation beamsplitter. Each of these two signals may be detected by a photodetector. The phase difference can be obtained by use of simple signal processing, and the relative phase changes of the two eigenmodes (i.e. $\Delta\phi$, equation (2.5)) will yield the the force-induced birefringence (Δn) and applied force (F), respectively, as shown in equation (2.3).

2.3.2.2 *Thermal effects*

When the sensing fibre is subjected to a temperature variation, the change in phase, $\Delta\phi_t$, due to unwanted thermal effects arises from induced changes in the optical refractive index, n, and geometrical length, l, of the sensing fibre. This can be expressed as

$$\Delta\phi_t = (2\pi/\lambda)[n \, (dl/dT) + l \, (dn/dT)] \, \Delta T, \tag{2.6}$$

where ΔT is the temperature change. It is important to examine how temperature effects modify the optical phase change in each of the eigenmodes of a polarimetric interferometer. From equation (2.6), for the case of a uniform temperature across a length l of the unstressed sensing, fibre, the phase change will be the same for both eigenmodes. For a small force applied to the sensing element, dn/dT and dl/dT may be taken to be the same for each mode. As the final observed output from the signal processing is the difference in phase between these two components, this measurement will be immune to a

small ambient temperature variation. However, as was discussed by Farahi et al [10] this technique is not valid for large temperature variations, high birefringence (large force) and long lengths of sensing fibre where, the cross-sensitivity effects of both modes needs to be considered. However in the work reported herein, care has been taken to avoid situations where these extremes were experienced in the design of the sensor system.

2.3.2.3 *Sensor Sensitivity*

Using equations (2.3), (2.4) and (2.5), the theoretical sensitivity, S, of the experimental scheme can be expressed in terms of the change of the phase difference of the light propagating with applied force,

$$S = \frac{d\Delta\phi}{dF} = \frac{16C}{\lambda d} \tag{2.7}$$

Therefore, this important factor S depends on the outer diameter of the sensing fibre, the wavelength stability of the light source and the stress-optic coefficient, C. As an example, for an outer diameter d = 125 μm, a value of C = 3.7×10^{-12} $m^2 N^{-1}$ (for a fused silica fibre) [8], and λ = 780 nm, the sensor sensitivity is 0.6 radN^{-1} (or ~ $34^0 N^{-1}$).

2.3.3 Signal Processing

Heterodyne detection of the interferometer output (as discussed in Chapter 1) is one of the most successful methods of signal processing used, due to its advantage is that it has an infinite range as no signal fading occurs [17]. Unfortunately conventional heterodyne detection requires additional bulky expensive optical components such as a Bragg cell [4] to produce the carrier

signal in the interferometer output, while the other heterodyne schemes need a phase shifter to provide an offset frequency. Therefore, a pseudo-heteroyne system was used to overcome this problem [17,18], which does not require any additional optical components to produce the heterodyne offset frequency.

The principle of operation of the scheme is to change the relative optical phase difference between the arms of an unbalanced interferometer, and this is achieved by varying the absolute frequency of the laser light. The phase change, $\Delta\phi$, induced in the interferometer for an absolute optical frequency shift, Δv, of the laser is given by

$$\Delta\phi = (2\pi\Delta L/c)\Delta v \tag{2.8}$$

where ΔL is the optical path imbalance in the interferometer.

In the scheme presented in this section, the laser frequency is modulated with an applied current ramp. Linear frequency modulation of the laser diode emission is achieved by injecting a sawtooth current ramp of periodicity T=1ms (1kHz) into the DC current supply of the laser. By changing the DC drive current (e.g. 1 mA), the absolute frequency of the laser diode changes, and if the emission frequency increases linearly in time, then time dependent interference fringes will be created at the optical output of the interferometer, where from equation (2.8), the frequency of the fringe pattern is given by

$$(\Delta\phi/\Delta t) = (2\pi\Delta L/c)(\Delta v/\Delta \iota)(\Delta \iota/\Delta t) \tag{2.9}$$

The frequency spectrum of the detector current is complex and contains components at the fundamental harmonics of the ramp frequency. The distribution of energy in each of these frequency components depends on the

fringe pattern during the ramp period T. A ramp drive current, $\Delta\iota$, is provided for the laser diode which causes a small change in output wavelength, $\Delta v/\Delta\iota$. If the path length difference, ΔL, is not zero, this then causes a change in the phase $\Delta\phi$. Careful control of the ramp amplitude (see equation 2.9) allows the phase change of the output signal to be controlled to be $(\Delta\phi/\Delta t)T = 2\pi$. Any external influence on the phase is then observed as a change of the initial phase of this signal. This allows the measurement to be made in the time domain rather than by measuring absolute intensities and thus compensates for any changing losses within the fibre.

2.4 Experimental Arrangement

This experimental arrangement used for pressure measurement is shown in Figure 2.4. The light source employed was a single mode laser diode (Sharp LT022MCO) [19] with an output of 3 mW at the nominal source wavelength of 786 nm. It was driven by a sawtooth ramp of 1 kHz, above the threshold current, to allow pseudo-heterodyne detection of the phase changes. The detector output shows a complex spectral pattern, composed of components depending on the phase excursion of the fringe pattern during the ramp period. The peak amplitude of the ramp was adjusted to satisfy the condition $(\Delta\phi/\Delta t)T = 2\pi$ rad, where the OPD of the interferometric arms used was about 5 cm. Light was collimated by a x10 microscope objective with NA = 0.25 and then passed through a polarising prism and half-wave plate to allow control of the polarisation azimuth, before entering the fibre. The fibre formed the input to a 2x2 coupler (manufactured by SIFAM, U.K.) [20], with a splitting ratio of 50/50, which is the optimum for this purpose. The fibre was single mode at the operating wavelength, had a mode field diameter of 6 mm, a cladding diameter of 125 $\pm$ 2 μm, a coating (of a UV curable acrylate) diameter of 250 $\pm$ 15 μm, and a maximum cladding non-circularity 2%.
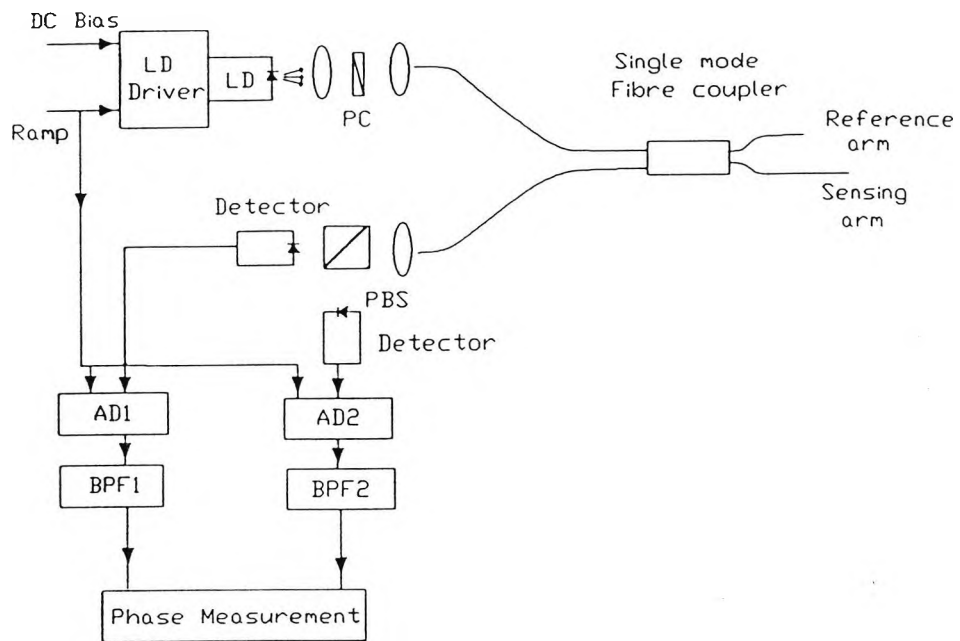
Figure 2.4 Schematic of the optoelectronic arrangement. LD Single-mode laser diode, PC Polarisation control element, PBS Polarising beamsplitter, BPFs Bandpass filters, ADs Amplitude demodulators.

The signal encoding the information was derived from the interference of light reflected from the ends of the sensing and reference arms of the fibre coupler. The output light was collimated, then split to fall on the two detectors by using a polarising beamsplitter. A half-wave plate was used to ensure the polarisation axes of the fibre and beamsplitter were coincident. The signals from these detectors were processed by amplitude demodulation to remove the effect of intensity modulation cause by ramping the diode drive current. Bandpass filtering around 1kHz was used to remove the distortion caused by the ramp flyback and final demodulation of the carrier ramp signal was performed before the phase difference between the signals was measured.
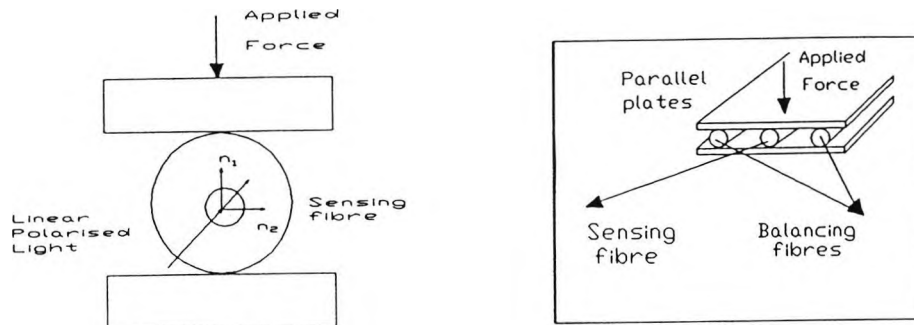
Figure 2.5 Illustration of the fibre optic pressure sensing unit.

The polarisation state of the light entering the fibre was adjusted to give equal intensities of light in each eigenmode of the sensing fibre. The sensing arm is subjected to the measurand of interest, i.e. in this case pressure. In this arrangement, it is the pressure applied via a bridge formed from the plates of mass 220 g sandwiching the fibre. Thus, one arm of the coupler formed a sensing arm (using coated or uncoated fibre) whereas the other fibre was unstressed and acted as the reference arm. The sensing unit used was as shown in Figure 2.5. The sensing and reference arms, were placed in a temperature controlled environment, one arm of which was longer than the other, by about 5 cm ($\pm$ 2mm) to form the unbalanced interferometer (i.e. optical path difference of the interferometer). Two other lengths of fibre were also placed between the two plates to provide a balanced force and prevent the fibre twisting and the top plate rocking. The bias due to the mass of the top plate does not change the sensitivity to the applied force, shown in equation (2.5). The sensing length was 90 mm, as a short sensing length produces smaller thermal effects. The applied force was varied by placing several calibrated masses on the top plate. By varying the temperature in a thermally controlled test chamber, the device temperature stability could be investigated. In this

work a range from room temperature (~20^{0}C) up to 95 ^{0}C could be achieved, and was used in the study.

Relative Amplitude

(a)
Ramp signal

Detected signal

(b)
Demodulated signal

Filtered
ramp signal(reference)

(c)
Filtered
demodulated signal

Filtered ramp
signal(reference)

10   20   30   40   50   60

Time(arbitary unit)
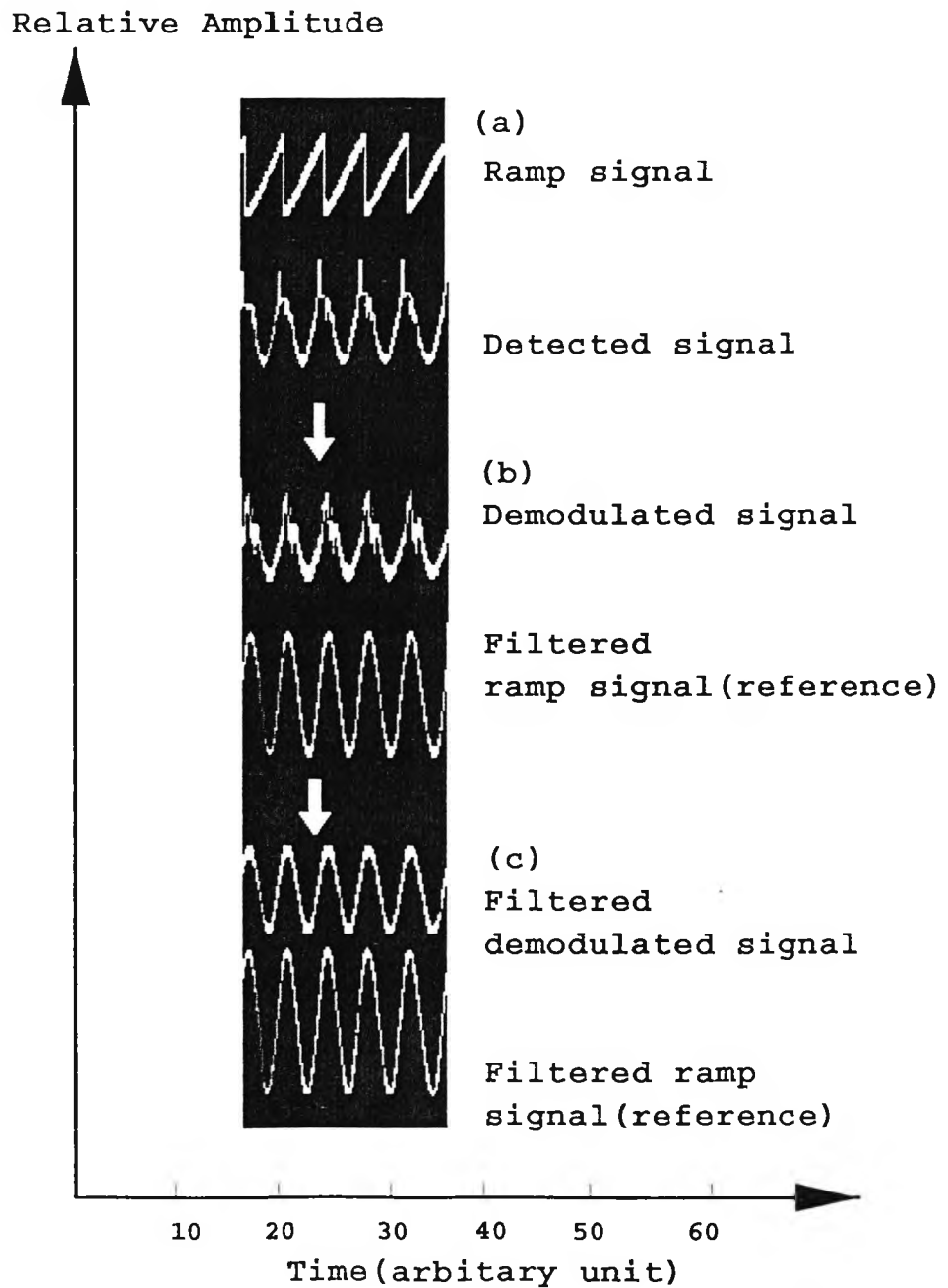
Figure 2.6 Illustration of interferometer output signals obtained from oscilloscope.

2.5 Results

The traces, shown in Figures 2.6 of the interferometer output signals, were observed on the oscilloscope. Trace (a) shows the ramp signal applied to the laser diode and the output signal obtained from the detector, (b) shows the detected signal derived from amplitude demodulation and a filtered reference signal, with bandpass filtering around 1 kHz being used to remove the distortion caused by the ramp flyback, and (c) shows the filtered detected and reference signals from (b).

These signals show that, in practice, there are some problems encountered in the use of this kind of sensor configuration. Firstly, there is the well-known 2π ambiguity in the output signal, i.e. once $\Delta\phi$ has exceeded 2π, the phase information becomes uncertain [17], which also implies there will be a problem with initialisation (i.e. no change in phase when there was no applied force on the sensing arm). Secondly, ambiguity also exists in the determination of the direction of the phase shift. After initialisation, the change in phase $\Delta\phi$ was measured when force was applied to the sensing arm. By "squaring up" the filtered demodulated and ramp signals as shown in Figure 2.6(c), the difference in time of these signals (i.e. phase) was obtained using simple digital timing techniques.

Figures 2.7 (a) to (c) illustrate the measured change in phase difference plotted against applied force at room temperature ($\sim 20\ ^0$C), and also at 80 ^{0}C and 95 ^{0}C for both the "coated" and "uncoated" (i.e. by removing a UV curable acrylate from the fibre) fibre respectively in the sensing arms. The solid lines were obtained by applying a linear curve fitting scheme to the data points. The measured sensitivities at each temperature for the coated

and uncoated fibres respectively were 9.3 $^0N^{-1}$ and 11.1$^0N^{-1}$ (20^{0}C), 9.6 $^0N^{-1}$ and 11.5 $^0N^{-1}$ (80^{0}C) and 9.9 $^0N^{-1}$ and 11.7 $^0N^{-1}$ (95^{0}C). Figure 2.8 shows the plot of phase difference against applied force, up to 60 N, in which the sensor sensitivity of 9.3$^0N^{-1}$ is noted at room temperature. Here the pressure was measured across the **2π** ambiguity of the interferometer output. However, the measurement uncertainty still remains when the system is switched off, or if the laser fails, clearly an unsatisfactory situation.

(a)

(b)

(c)
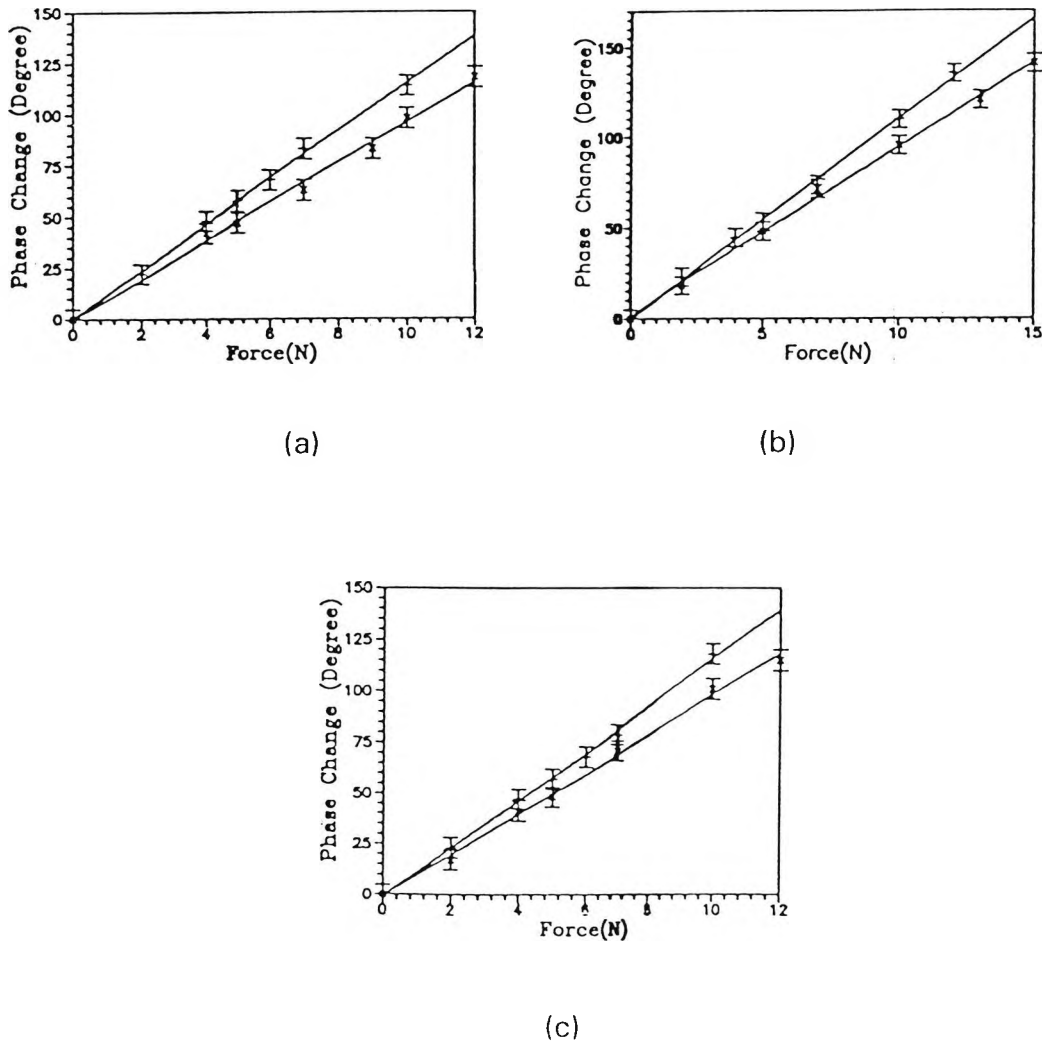
Figure 2.7 Plot of changes in phase between the signals against applied force for coated (x) and uncoated (+) sensing fibres at temperatures: (a) 20 ^{0}C, (b) 80 ^{0}C, (c) 95 ^{0}C.

57
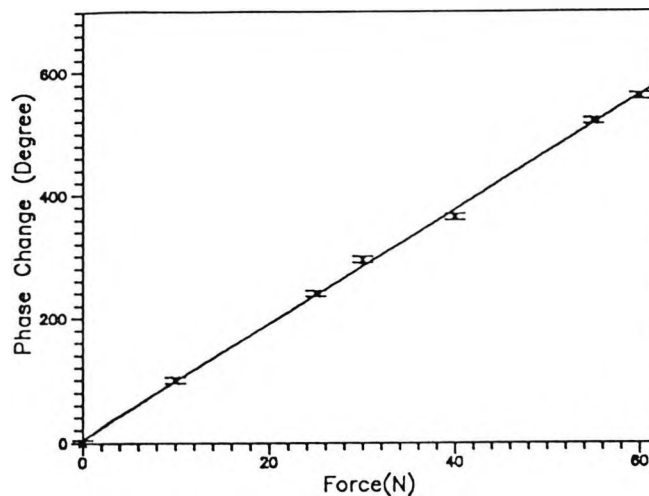
Figure 2.8 Plot of change in phase between the signal against applied force up to 60 N at room temperature (~ 20 ^{0}C), for coated fibre.

2.6 Application of The Sensor Principle

There are a number of potential applications of the principles discussed. For example, this system may be used as a flowrate sensor whereas the sensing arm will be submerged in fluid flow. Pressure sensing elements form an essential part of a range of flowmeters which generate a differential pressure which is a function of density and flowrate where [21]:

$$\Delta h = (1/2) \ K\rho\omega^2 \tag{2.10}$$

and ω is the volume flowrate, K is a geometrical factor, Δh, the differential pressure and ρ the fluid density. A differential pressure may be produced by fluid flow in a sensing arm of the interferometer. Optical fibre devices, being inert and non-electrical in operation at the sensor head are potentially well suited to the measurement of flow of inflammable fluids.

2.7 Measurement Limitations

The results obtained compare well with the results obtained by Weir et al [22], but they differ (~50 %) from theoretical values discussed in Section 2.3.2.3. This discrepancy may arise from errors in the calculation of the applied force loading geometry, changes in the light source wavelength, stress-optic coefficient temperature variation and imperfections in the contact between the plates and fibre. The main error is that of the problem of force distribution, and it is possible that other hard coatings may enhance further the sensitivity. The change in sensitivity over the temperature range was 5.6 % and 5.1% for the coated and uncoated sensor elements respectively.

However, there are unavoidable errors in the measurement due to the nature of the force distribution on the sensing element, fibre bending and the intrinsic birefringence in the fibre. These problems could be avoided using a different arrangement of the sensing element itself, where the applied force would be directly contacted to the sensing element, producing a more uniform force distribution and by the use of highly birefringent polarisation preserving fibre to carry the light to and from the sensing element [23]. In this work a simultaneous measurement of the pressure and temperature is possible, in theory. However in any real system this would be difficult to implement due to the high sensitivity of the fibre to temperature (sensitivity ~100 $radK^{-1}m^{-1}$[12] without a compensation technique) and a dedicated signal processing system involving fringe counting would be required to be developed. There may will be instances where this is deriveable, as a system, but alternatively temperature measurements by other fibre optic sensor schemes are possible.

2.8 Discussion

The use of an all fibre optic device as a polarimetric interferometer for pressure sensor development, including a discussion of sensitivity considerations, has been presented. The principle of force-induced birefringence and the theoretical sensitivity in the fibre based device has been included. Results are presented, based on the application of the principle of force-induced birefringence showing the stability over a range of temperatures with both coated and uncoated sensing fibres. Device sensitivities were measured in the temperature range from room temperature to 95^0C. The variation of sensitivity over this temperature range is relatively small at 5% (for both coated and uncoated fibre). However, these results represent measured sensitivities of the relative difference between coated and uncoated fibres. This increase in sensitivity for the uncoated fibre sensing element is due to a better distribution of the force through the fibre to the core, in the absence of the soft coating which is easily deformed. An increase in sensitivity for the use of uncoated sensing fibre over coated fibre of about 18% has been observed. It also is linear in response and stable within a small temperature variation ($\sim 1^0$C). However, this technique offers a potentially practical implementation of a pressure sensor for use in making isotropic static pressure measurement, which may form the essential element of a flow sensor device. Other mechanical differential pressure devices form the essential core of some flow meters, and the optical device has potential advantages for use in inflammable or hazardous environments. The device sensitivity improvement using a further development of signal processing and a new sensing element arrangement is an area for possible future work.

References

[1] GAUTHIER, R. C. and DHLIWAYO, J. (1992). Birefringent fibre-optic pressure sensor. Optics & Laser Technology 24: 139-143.

[2] CHARDON, D. and HUARD, S. J. (1986). A new interferometric and polarimetric temperature optical fibre sensor. Journal of Lightwave Technology 9 (7): 720-725.

[3] BOCK, W. J. WISNIEWSKI, R. and WOLINSKI, T. R. (1992). Fibre-optic strain-gauge manometer up to 100 MPa. Instrumentation and Measurement 41 (1):72-75.

[4] JACKSON, D. A. (1985). Monomode optical fibre interferometers for precision measurement. Journal of Physics E: Scientific Instruments 18: 981- 1001.

[5] LEE, C. E. and TAYLOR, H. F. (1988). Interferometric optical fibre sensors using internal mirrors. Electronics Letters 24(4):193-194.

[6] YOSHINO, T. KUROSAWA, K. ITOH, K. and OSE, T. (1982). Fibre-optic Fabry-Perot interferometer and its sensor application. Journal of Quantum Electronics 18(10): 1624-1633.

[7] YUPAPIN, P. V. P. WEIR, K. GRATTAN, K. T. V. and PALMER, A. W. (1991). Static force measurement incorporating a reduction in thermal effects reduction. In: SENSORS AND THEIR APPLICATIONS V CONFERENCE, Edinburgh 1991. Proceedings. Pub. in: Sensors -Technology, Systems and Applications, Ed. by K.T.V. Grattan. (Bristol : Adam Hilger).

[8] BERTHOLDS, A. and DANDLIKER, R. (1986). High-resolution photoelastic pressure sensor using low-birefringence fibre. Applied Optics 25(3):340-343.

[9] MAYSTRE, F. and DANDLIKER, R. (1989). Polarimetric fibre optical sensor with high sensitivity using a Fabry-Perot structure. Applied Optics 28(11):1995-2000.

[10] FARAHI, F. WEBB, D. J. JONES, J. D. C. and JACKSON, D. A. (1990). Simultaneous measurement of temperature and strain: Cross-sensitvity considerations. Journal of Lightwave Technology 8 (2): 138-142.

[11] HERZOG, J. P. and MEYREIS, P. (1990). Interferometric optical fibre pressure sensor with temperature compensation. In: FIBRE OPTIC SENSORS CONFERENCE 4th, 1990. Proceedings. SPIE 1267, pp. 134-141.

[12] CHEN, S. (1990). Optical interferometry for novel optical fibre sensor systems. Ph.D. thesis: King's College, University of London, Department of Electrical and Electronic Engineering.

[13] SMITH, A. M. (1980). Single-mode fibre pressure sensitivity. Electronics Letters 16(20):773-774.

[14] TIMOSHENKO, S. and GOODIER, J. N. (1951). Theory of elasticity. 2 nd edit. (New York: McGraw-Hill).

[15] HUNGSPERGER, R. G. (1984). Integrated optics: theory and technology. 2nd edit. (Heidelberg: Springer-Verlag).

[16] RASHLEIGH, S. C. (1983). Origins and control of polarisation effects in single-mode fibre. Journal of Lightwave Technology 1 (2): 312-331.

[17] JACKSON, D. A. KERSEY, A. D. CORKE, M. and JONES, J. D. C. (1982). Pseudoheterodyne detection scheme for optical interferometers. Electronics Letters 18(25):1081-1083.

[18] MEGGITT, B. T. PALMER, A. W. and GRATTAN, K. T. V. (1988). Fibre-optic sensors using coherence properties : signal processing aspects. International Journal of Optoelectronics 3(6):451-464.

[19] SHARP laser diodes. (1988). Laser diode user's manual, Available from Access Pacific Ltd., Kymbrook School House, Kimbolton Road, Keysoe, Bedford MK44 2HH, U.K.

[20] Sifam fibre optics. Product specification of Single-mode fused couplers and splitters, Available from SIFAM Limited, Woodland Road, Torquay, Devon TQ2 7AY, U.K.

[21] DOEBELIN, O.E. (1985). Measurement system : application and design. 3rd edit. (Singapore : McGraw-Hill).

[22] WEIR, K. GRATTAN, K. T. V. and PALMER, A. W. (1991). Static force measurement using a polarimetric interferometric technique. In: OPTICAL FIBRE SENSOR CONFERENCE. 7th. Sydney 1991. Proceedings. Pub: IREE, Australia, pp. 221-223.

[23] YOSHINO, T. HASHIMOTO, T. NARA, M. and KUROSAWA, K. (1992). Common path heterodyne optical fibre sensors. Journal of Lightwave Technology 10(4):503-513.

Chapter 3

Photoelastic Pressure Sensor
Using A Low-Coherence Light Source

3.1 Introduction

This chapter presents the results of an investigation of an optical pressure sensor, using a photoelastic material as the sensing element. A change in the optical path of the two rays of light (i.e. the two orthogonal eigenmodes) propagating in a stressed sensing element has been observed by monitoring a corresponding change in the optical path in a "recovery" optical interferometer. The pressure to be measured was simulated by placing a calibrated mass on the sensing element, over a constant area of application. Three optical arrangements using the sensing element in reflection and transmission (unbiassed) and a biassed system, (i.e. such a system where the initial change in phase of the two eigenmodes of light propagating into the sensing element could be introduced into the system), were used. In these cases, a recovery Michelson interferometer was employed to obtain the optical path difference of the light in the sensing element. For the biassed system, light was launched into a highly birefringent fibre to provide a reference bias signal. Results are presented showing the possibility of using such systems for pressure sensor applications. The basics of the photoelastic effect (the principle of force-induced birefringence in the sensing element), the technique used and the sensor configurations employed are also discussed in detail.

3.2 Review of Previous Work

Optical fibre sensors have been developed and reported in the literature, using stress-induced birefringence to modulate the light coupled between the input and output fibres [1, 2]. Birefringence is created in the stressed sensing element due to the asymmetric transverse stress distribution induced, and the light passing through it is split into two components polarised at right angles, which travel at difference speeds. By measuring the change in phase of these components of polarised light propagated through the sensing element, it is possible to determine the applied force or pressure causing the stress-induced effects [2].

A polarimetric optical sensor, using a single mode laser diode as a light source and an all-fibre optical interferometer has been demonstrated for force or pressure sensing applications [3, 4]. Results have shown that the device sensitivity was independent of small ambient temperature changes. However, the ambiguity of the interferometric output signal limits the useful dynamic range of the sensor. The use of a low-coherence light source, e.g. a multimode laser diode, is suggested to overcome this problem. In such a scheme, the range of the unambiguous output signal would be maximised [5-7]. Furthermore, a simplification of the signal processing scheme is possible in such an arrangement and is widely used in the area of optical sensors [5, 8].

3.3 Sensor Configurations

One of the most important factors in a photoelastic sensor is the selection of the most suitable material for the photoelastic element. Unfortunately, as an ideal photoelastic material does not exist, one must be selected from the

available materials which most closely fits the particular application. The ideal photoelastic material should exhibit the following properties [9], in that it should

- be transparent to the wavelength of light employed in the polarimeter,

- be sensitive to stress/pressure,

- have a linear characteristic with respect to stress/pressure,

- have a high elastic limit and

- exhibit a small variation of photoelastic constant with temperature.

The sensing element subjected to the pressure to be used in this work is a small piece of photoelastic material, Araldite resin or Perspex being chosen as these materials having large photoelastic constant and are widely used in stress analysis [9,10]. Table D.1 is a summary of the optical and mechanical properties of several photoelastic materials, reported in Appendix D.

Photoelastic sensor elements employed make use of the induced stress distribution in the material. A simple element for sensing force or pressure is a rectangular solid or cube-like element [11-13]. As illustrated in Figure 3.1, a force F or a pressure P is applied in the vertical direction (x-direction) on the upper surface of the cube. When a distributed load is applied homogeneously on the sensing element, the stressed component σ_x, as discussed earlier in Chapter 1, can be expressed as

$$\sigma_x = P \tag{3.1}$$

where $\qquad P = F/(L_z L_y) \tag{3.2}$
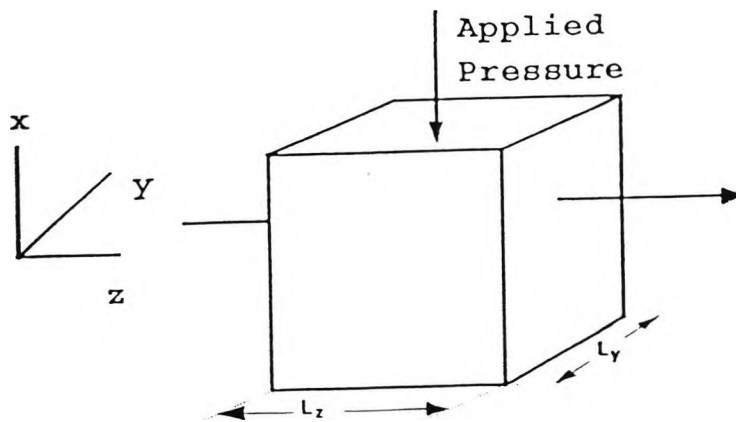
Figure 3.1 Geometric arrangement of the stress optic sensor element.

3.3.1 Unbiassed System

When polarised light propagates in the sensing element, the fast axis of the two eigenmodes is parallel to the applied force as shown in Figure 3.1. Using equations (1.7), (1.9) and (3.2), the birefringence Δn, may be given by

$$\Delta n = n_1 - n_2 = CF/A \tag{3.3}$$

where C is the stress optic coefficient as discussed earlier, F is the applied force, and A is the sensing element cross-sectional area, (i.e. F/A is the applied pressure).

The sensing element consists of a small piece of the photoelastic material where the front and back surfaces are arranged to be parallel to each other.

Polarised light propagating in a birefringent material may be considered to consist of two independent linearly polarised states in the two eigenmodes. The difference in the refractive indices of these two modes means each mode will experience a phase change $\Delta\phi_j$ (j=1,2) on traversing a sensing element of thickness, l. The net difference in phase, $\Delta\phi$, between each of the modes can then be related to the birefringence by

$$\Delta\phi = \Delta\phi_1 - \Delta\phi_2 = (2\pi/\lambda)(n_1 - n_2)\, l \qquad (3.4)$$

where λ is the wavelength of the light source.

As described in Section 1.3.2.4, due to a very broad spectral width (i.e. short coherence length) of a low-coherence source, the phase difference induced by the birefringence in the sensing element can be recovered using low-coherence interferometer [14]. If the applied force induces a path difference between the two eigenmodes which is greater than the coherence length of the light source used, a recovery Michelson interferometer can then be used to re-establish interference between the light in the two eigenmodes by placing a polariser, at 45^0 to the birefringence axis, before the detector. The optical path difference (OPD) of the Michelson interferometer is adjusted away from the zero position and when it coincides with the path difference of the sensing element, the path difference, ΔL, of the recovery interferometer can then be related to the phase difference as

$$\Delta L = (\lambda/2\pi)\, \Delta\phi \qquad (3.5)$$

A multimode laser diode can be used in low-coherence interferometry, giving a narrow region of interference and a series of equally spaced sub-orders of interference, as discussed in Section 1.3.2.4. Scanning the path difference of

the recovery interferometer then requires the central order of the interference to be located. The path difference due to the sensing element can then be read from a micrometer adjustment of the path difference.

In the two configurations of sensing element used in this work, the path difference is obtained from the analysis as $\Delta L = 2l$ CF/A for reflection and $\Delta L = Cl$ F/A for transmission. Clearly, in reflection (with double the optical path in the sensing element) the measurement is more sensitive, but, experimentally, the amplitude of the signal was observed to be considerably smaller. The details of this will be discussed later.

3.3.2 Biassed System

One problem of the use of the unbiassed system, as discussed in the last section, is that if the change in OPD (equation (3.5)) of the two paths of light is less than the coherence length of the light source. Then the interference signal cannot be observed, thus, the minimum measurement of OPD is limited by the light source coherence length. Additionally the use of a low-coherence light source (a multimode laser diode) overcomes the uncertainty in phase of the periodic output. In practice, the change in OPD (or the associated phase difference), when no force is applied to the sensing element, between the two eigenmodes can be arranged to be greater than that of the coherence length of the light source. In this work, a bias in phase is provided by introducing a high birefringence (Hi-Bi) fibre to enable the light to be guided into the sensing element.

In this scheme, a length of high birefringence (Hi-Bi) fibre, is used to introduce further birefringence into the system. The eigenaxes of the Hi-Bi fibre are arranged to coincide with the axes of the induced birefringence in the sensing

element, and the birefringence of each eigenmode thus add. If the birefringence of the Hi-Bi fibre is given by Δn_B, the induced differential optical phase shift, $\Delta\phi$, between light in each eigenmode is then given by

$$\Delta\phi = (2\pi/\lambda)[(n_1 - n_2)l + \Delta n_B L_F] \tag{3.6}$$

where L_F is the length of the fibre.

To apply this low-coherence technique, the length of the fibre is chosen to take the two modes emerging from the fibre outside the "coherence region" (of the laser diode used as source). A recovery Michelson interferometer will then give a bias "reference" interference signal when the path length difference coincides with that between the modes of the fibre. The path difference of the recovery Michelson, ΔL_m is then given by

$$\Delta L_m = \Delta n_B L_F \tag{3.7}$$

Any birefringence arising from a pressure applied to the sensing element will produce a change in its optical path difference of the two eigenmodes. The change in its OPD can be observed by matching the optical path difference in the recovery interferometer to give a maximum interference signal. This change in path difference from the reference position ΔL_m is the required measurand signal, ΔL_s, due to the applied pressure, given by

$$\Delta L_s = (n_1 - n_2)\,l \tag{3.8}$$

Comparison of equations (3.3) and (3.8) show this measurement to be linear with applied pressure, which can thus be determined.

Using this technique, the two eigenmodes of the force induced birefringence are observed, and the phase change between the light propagating in each of the two eigenmodes is obtained using an interferometric technique. This difference in phase between the light propagating in each eigenmode is the required measurand signal in the sensor arrangement. When a multimode laser dode is used in low-coherence interferometry it gives rise to a narrow region of interference and a series of equally spaced sub-orders of interference, as discussed in Section 1.3.2.4. Scanning the path difference of the recovery interferometer then requires the central order to be located. The path difference due to the sensing element can then be read from the micrometer adjustment of the path length difference.

3.4 Experimental Arrangement

Three optical arrangements, investigated using a low-coherence technique and utilising a photoelastic sensor are,

   (a) Unbiassed system-reflection scheme
   (b) Unbiassed system-transmission scheme
   (c) Biassed system

These schemes each use a multimode laser diode as a light source, and the output inteference signal was matched by using a recovery Michelson interferometer. Both unbiassed and biassed techniques are presented. The temperature effects of the sensing device is also investigated.
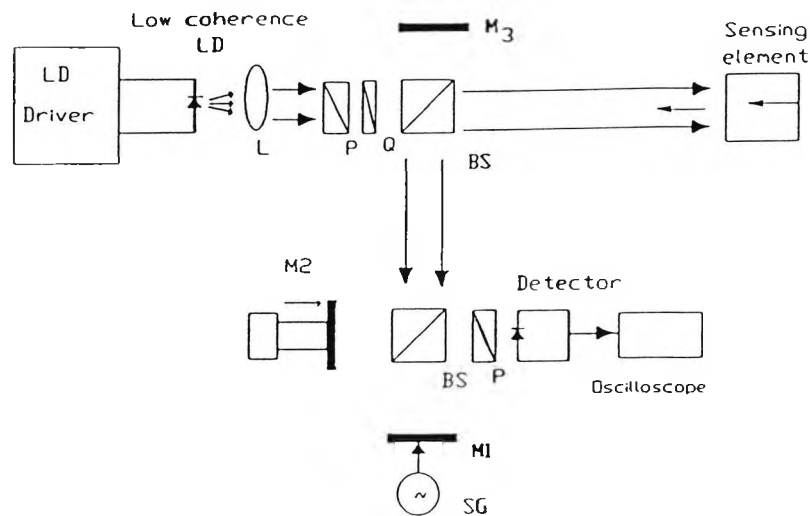
Figure 3.2 Schematic diagram of the experimental arrangement used in reflection: LD Laser diode, Q Half-wave plate, BS Beamsplitter, Ms mirrors, Ls Lenses, SG Signal generator, Ps Polarisers.

3.4.1 Unbiassed System

Two arrangements of the experimental configuration used for pressure sensing investigations using a low-coherence light source were investigated and are discussed in this section. The force inducing the pressure to be measured is applied directly to the sensing element. The difference in the range of measurement and the signal reliability of these two schemes was also examined.

Figure 3.2 shows the experimental system when using the sensing element in reflection. The light source used was a multimode laser diode manufactured by Sharp (type LT023MDO) [15] with an output power of 3 mW, operating at a wavelength of 780 nm. Light from it was launched into the optical system, after collimation by a x10 microscope objective, with numerical aperture (NA) of 0.25. The light passed through a polariser and a half-wave plate to produce a linear polarisation state at 45^0 to the axis of the sensing element (e.g. x-axis as shown in Figure 3.1). The light beam

71

the applied force to be measured was varied by placing various calibrated masses on the sensing element, the changes in path difference were determined by scanning one arm of the interferometer along the optical axis.
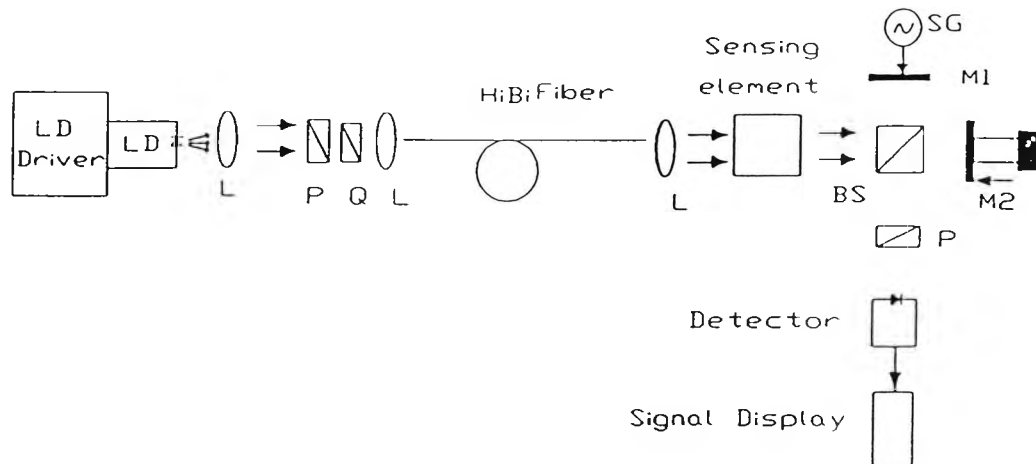
Figure 3.5 Experimental arrangement: LD Laser diode, Ls Lenses, Q Half-wave plate, BS Beamsplitter, Ms Mirrors, Ps Polarisers.

3.5 Results and Discussion

Results are presented on the measurement of applied force via the monitoring of the induced birefringence in the sensing element. The interference signal was observed by adjusting the path difference of the Michelson interferometer. The conversion of the effect of a force or pressure change to a measurable change in path difference was thus achieved.

3.4.2 Biassed System

To overcome the problem of the overlapping between the required signal and the centre fringe of the interferometer output at the balanced position, an initial change in the OPD (reflected as a phase change) of the light propagating into the sensing element may be introduced by using a biassed birefringence scheme. The experimental arrangement for such a system is shown in Figure 3.5. Light was launched into an optical system, after collimation by a x10 microscope objective with NA = 0.25, after which the light beam passed through a polariser and a half-wave plate to produce a linear polarisation at 45^0 to the axis of the Hi-Bi fibre before entering a such a fibre (York HB 750 [16], beat length = 2 mm, length = 30 cm). The birefringence (Δn_B) of the fibre used was 4×10^{-4}, i.e. the OPD of the output interferometer of 120 µm away from the balanced position was noted. The orientation for the output end of the fibre was adjusted in order to align the birefringence axes of the fibre with those induced in the sensing element. The sensing element was placed on a micrometer movement to allow for a small positional adjustment when a force was applied, allowing further alignment of the axes of the sensing element so that they were coincident with those of the Hi-Bi fibre. The light transmitted through the sensing element entered the recovery Michelson interferometer. The interference signals thus obtained from the sensing element were detected by a photodetector with a polariser set at 45^0 to the direction of the birefringence axis before it, and were observed on an oscilloscope.

The changes in path difference in the sensing element were determined by scanning one arm of the interferometer along the optical axis and reading the change in position of the centre peak of interference fringe from the micrometer with respect to the reference signal due to the Hi-Bi fibre. As

The cross-sectional areas of the sensing elements were 72 mm^2 and 120 mm^2 for the Araldite resin and Perspex, with lengths of 6 mm and 8 mm, respectively. The applied force and thus the pressure was varied by placing a series of calibrated masses on the sensing element. The changes in path difference were determined by scanning one arm of the interferometer along the optical axis and reading the change in position from the micrometer. This procedure was repeated with the other sensor element incorporated into the optical system.

Figure 3.4 shows the experimental arrangement employed in the second case, using the sensing element in transmission. The arrangement is similar to that of Figure 3.2, the difference being that the light transmitted by the sensing element is introduced directly into the recovery Michelson interferometer. All the optical components were configured as described for the previous arrangement, and the changes in path difference were determined in the same manner.
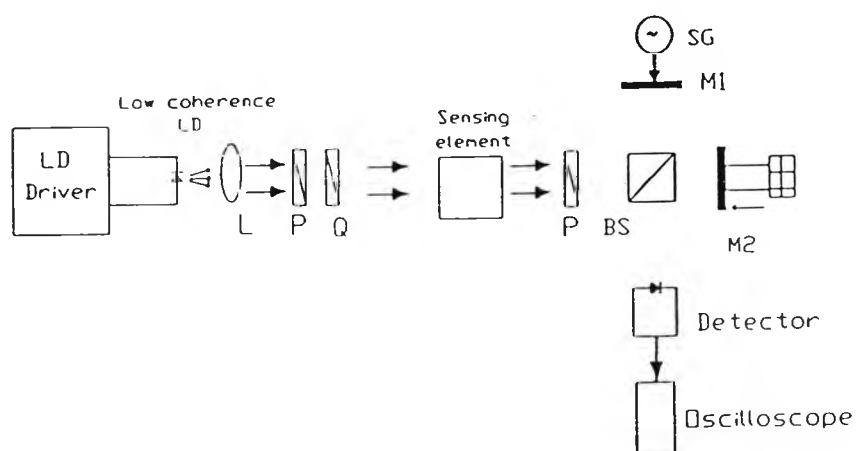
Figure 3.4 Schematic diagram of the experimental arrangement used in transmission : LD Laser diode, Q Half-wave plate, BS Beamsplitter, Ms mirrors, Ls Lenses, SG Signal generator, Ps Polarisers.

was divided by a beamsplitter to pass to the sensing element or to a mirror. Reflected light signals from the front and back surfaces of the sensing element were split by the same beamsplitter and the reflected light beam entered the recovery Michelson interferometer. An imbalance in one arm was provided by an oscillator-driven vibrator attached to mirror M_1, operating at a known frequency of 470 Hz. The mirror M_2 was adjustable in position along the optical axis by being capable of scanning with a micrometer drive. The interference signals obtained from the front and back surfaces were detected by a photodetector with a polariser set at 45^0 to the direction of the birefringence axis before it, and were observed on an oscilloscope, as shown in Figure 3.3. For ease of alignment, the light beam reflected from the mirror, M_3, passed through the same optical system; it was blocked when the measurements were made.
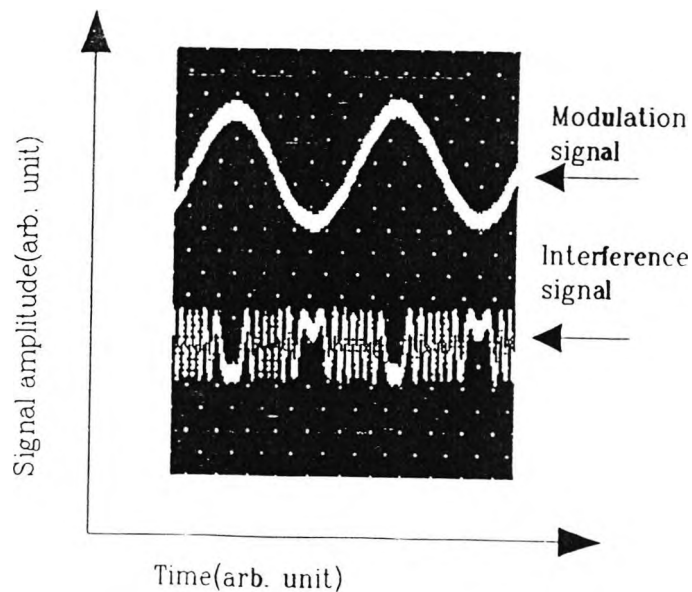
Figure 3.3 Illustration of the signal intensity of the interference signal recorded on the detector in the interferometer, and the modulation source.

3.5.1 Results Obtained

These results obtained are discussed in the first case, using the unbiassed system. As the mirror M_2 is scanned along the optical axis, the reference interference fringes, i.e. due to zero applied force, were determined. As the mirror M_2 was adjusted, constructive interference occurred in both directions on the optical axis, characteristic of a multimode laser source, as discussed in Chapter 1.

Figure 3.6(a) illustrates details of the maximum amplitude of interference fringes in the reflection mode in the zero order region from the front and back surfaces of the sensing element when a force was applied. Figure 3.6(b) shows the position of the interference fringes at zero order obtained with the sensing element used in transmission, and also when the force was applied on the sensing element.

Using the system in the reflection mode (as shown in Figure 3.2), the change in path difference was plotted against applied force, as shown in Figure 3.7(a). In practice, the Araldite was more sensitive to material deformation (i.e. the bending of material when it is stressed) than was the Perspex. Therefore, a force of not exceeding 15 N (0.21 MPa) was applied to the Araldite block, and a force sensitivity of 4.0 μmN^{-1} was noted. A preliminary result using a Perspex sensing element was noted, where a change of path difference (the position of M_2) of 30 μm was measured when a force of 30 N (0.25 MPa) was applied to the Perspex, giving a sensitivity of 1.0 μmN^{-1} of the measurement.

Figure 3.7(b) shows the measured change in postion of mirror M_2, using the system in transmission (as shown in Figure 3.4), plotted against an applied

76

force of up to 50 N (0.70 MPa) for the Araldite sensing element. The sensor force sensitivity of 0.99 μm N^{-1} was noted in this case. As a preliminary result, a change in path difference of 26 μm (i.e. sensitivity of 0.52 μm N^{-1}) was observed when a force of 50 N (0.42 MPa) was applied to the Perspex.
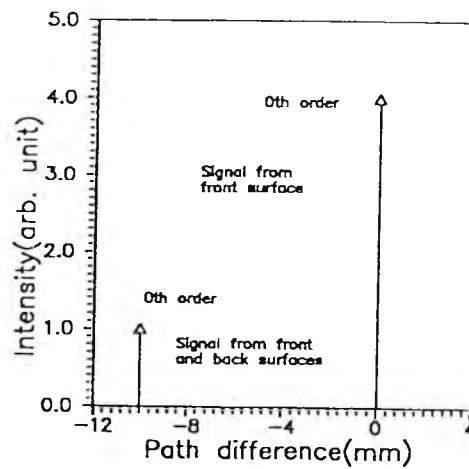
(a)
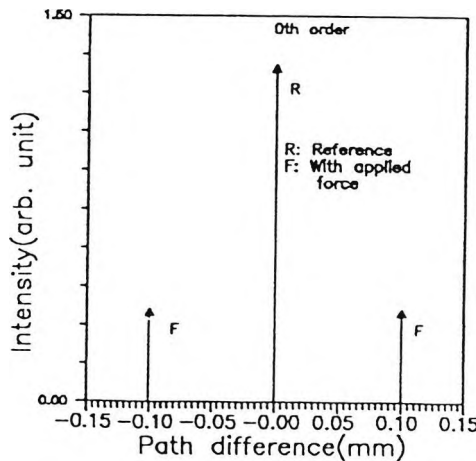
(b)

Figure 3.6 Position of the maximum amplitude of the interference fringes when a force is applied. Only zero order fringe position shown for clarity :

(a) in reflection, (b) in transmission.

The change in sensitivity from the reflection to transmission arrangements of a factor of 2 for perspex is an indication of the longer path length of the light, travelling in the sensing element. A factor of 4 in sensor sensitivity for the araldite is not as would be anticipated from path length consideration alone, as other considerations such as the distribution of strain within the softer material may give rise the induced-birefringence in the unloading sensing element. These factors are suggest to explain this discrepancy.
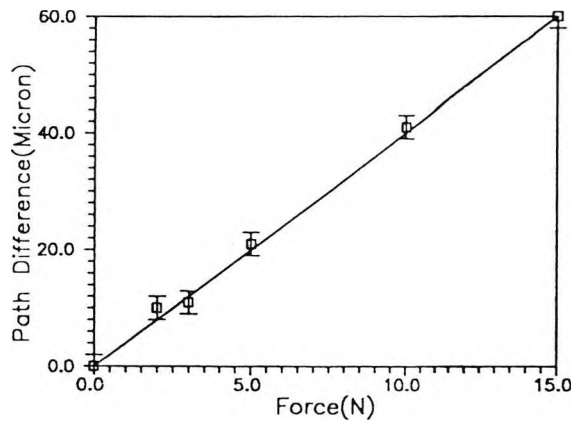
(a)
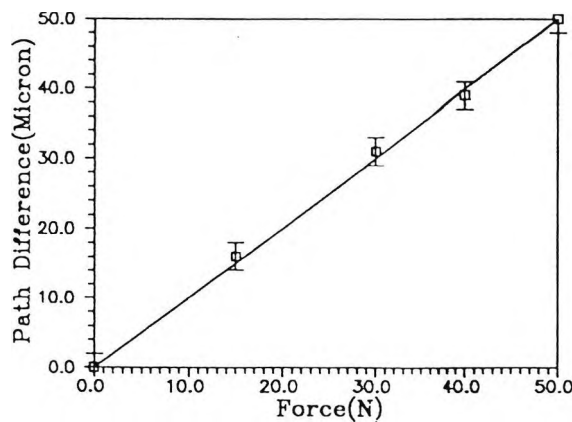
(b)

Figure 3.7 Calibration graph showing the changes in path difference of the interference signals against applied force:(a) in reflection, (b) in transmission, for the Araldite sample at a temperature of 20^0C.

One problem which arose in the reflection scheme was that the amplitude of the interference signal obtained in the recovery interferometer was much smaller than that from the transmission sensing element. This was due to the low surface reflectivity of the light beam and the distortion of the sensing element on loading which led to the reflected light from the back surface being non-colinear with that from the front surface.

The resulting uncertainty in the fringe-maxima measurement and the lower S/N ratio obtained thus gave rise to larger errors in the measurement. The signal to noise ratios (S/N) of the output signal were 26 dB and 46 dB for the reflection and transmission schemes, respectively.

The experiment was carried out at room temperature ($\sim 20^0$C) and, as discussed the results show good linearity and stability at this temperature. However, an investigation of the detailed response of the system to temperature variations is required and this is discussed later in this chapter.

This technique could be further improved by using a scheme that will overcome the limit observed in the work on the minimum measurement of force or pressure. A large unperturbed path difference using a bias for the reference signal (i.e. a path difference larger than the light source coherence length) could be employed in such a system. Such a technique may be used to improve the measurement resolution.
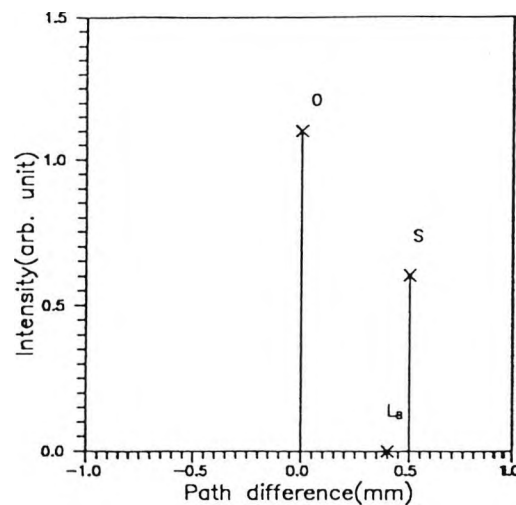
Figure 3.8 Visibility of interference fringes with an applied force, L_B denotes the reference, bias position due to Hi-Bi fibre, S the peak signal position and O the central order.

3.5.2 Biassed System

Figure 3.8 shows the positions of the interference fringes obtained with a pressure applied to the sensing element. Figure 3.9 shows the measured change in path difference, plotted against an applied force of up to 50 N (0.70 MPa) and 80 N (0.67 MPa) for the Araldite and Perspex. The sensor sensitivities of 0.96 μmN^{-1} and 0.51μmN^{-1} were noted, respectively. Figure 3.10 shows the measured change in path difference, using the system in transmission, plotted against an applied force of up to 50 N for the Araldite sensing element. The sensing element was placed in a temperature controlled environment to study the effect of temperature variation with the sensing device sensitivity. A value of 1.0 μmN^{-1} was noted at a temperature of 80 ^0C when Araldite was employed as the sensing elenent. A change of path difference of 26 μm (i.e. sensitivity of 0.52 μmN^{-1}) was observed when a force of 50 N was applied to the Perspex at the same temperature. Deviations in sensor sensitivities by 4% and 2 % for the Araldite and Perspex with respect to the full scale force

measurement of 50 N from that at a temperature of 20 ^{0}C were noted respectively. These results indicate good stability of the sensor over an extended temperature range, with a small change in sensitivity in agreement with previous work [17].

It can be seen from Figure 3.3 that the visibility of the fringe pattern is flat near the centre fringe. Therefore, it is difficult to distinguish the central fringe from its adjacent fringes. The resolution of the apparatus used in this work may be determined from the precision of the measurement of the position of the fringe-maxima on the micrometer where a resolution of 2 μm was noted. The resolution of this problem could be further enhanced by using a scheme that will give rise to a much smaller uncertainty in the fringe maxima (i.e. a very short coherence length light source such as a light emitting diode, LED) to provide a clearly distinguishing of the centre fringe in the interferometer output.
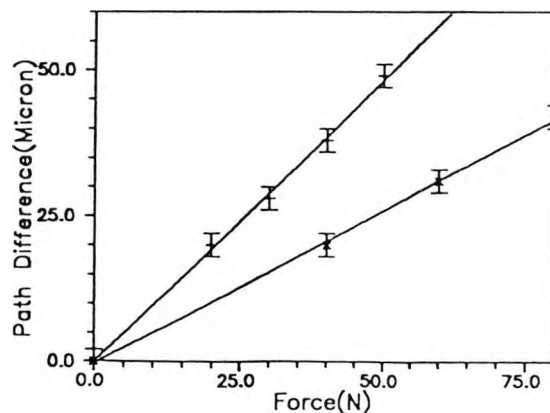
Figure 3.9 Calibration graph showing the changes in path difference of the interference signals against applied force in biassed scheme for the Araldite(+) and Perspex (x) samples at a temperature of 20^{0}C.

The required signal obtained from this low-coherence technique must lie between consecutive orders, which is equivalent to ~ 100 μm in terms of the scanning range (optical path difference) ; if not, measurement uncertainty becomes a problem, due to the effect of the overlapping of the signals with fringes from the adjacent orders. If a very short coherence length light source is used, an increase in device resolution is achieved, and there are no lower order fringes.

There is an small, unavoidable error due to the limited resolution of the mechanical movement on the optical axis, which in the present work was 2 μm. However, Kotrotsios and Parriaux [18] have shown that the mechanical resolution could be reduced to 0.1 μm by using a stepping motor driving the mechanical scanning device. To improve the measurement resolution, an imaging of the interference pattern, using optical means, using a charge-coupled device (CCD array) and electronic scanning may also be one possible solution to this problem [19, 20], as discussed in recent work undertaken.
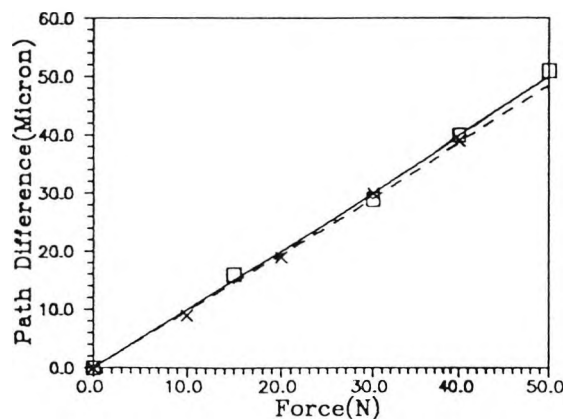
Figure 3.10 Calibration graph showing the changes in path difference of the interference signals against applied force using Araldite sample at temperatures of 20⁰C (Dashed line) and 80⁰C (Solid line).

A further property of these photoelastic materials which must be considered is the response time of the system as the material undergoes a relaxation process [17, 21]. Thus there is a "settling time" before any meaningful measurement can be made. This relaxation process is dependent on applied force and was investigated, the results being reported in the next chapter.

3.6 Conclusion

Results obtained gave force (pressure) sensitivities from 0.5 μmN^{-1}(58 μm/MPa) for the Perspex, to 4.0 μmN^{-1} (300 μm/MPa) for the Araldite. For these results the error in measurement of path difference of 2 μm gives a maximum error in the measurement of force of 2% for Perspex and 4% for the Araldite. As discussed earlier, these results show significant differences in device sensitivities in the use of both methods and materials. Firstly, the sensitivity obtained from the transmission scheme was lower than that obtained from the reflection scheme, as expected, due to path length consideration and to the material deformation effect. Secondly, the range of applied force that could be measured using the Araldite was smaller than that obtained using the Perspex, i.e. a material property, such as elastic limit, has limited the range of the applied force.

However, the extra sensitivity gain obtained using the apparatus in reflection mode has to be offset against the limitations imposed on the sensing element and the reduction in signal amplitude. Experimentally, the sensing element configured in transmission is to be preferred where a higher intensity and thus sufficient light output could be obtained. It has been shown that the Araldite resin has a larger photoelastic effect than that of the Perspex, and therefore this material may be chosen to fulfil a particular measurement range and sensitivity requirement. The next chapter will

concentrate on an investigation of these materials and their properties such as stress relaxation time, elastic limit, an extension of the range of measurement (i.e. for high pressure application), and temperature effects on sensor sensitivity. The scheme will also incorporate a fibre optic link between the sensor and recovery interferometer, to facilitate its use.

References

[1] BERTHOLDS, A. and DANDLIKER, R. (1986). High-resolution photoelastic pressure sensor using low-birefringence fibre. <u>Applied Optics</u> <u>25</u> (3):340-343.

[2] HOCKER, G.B. (1979). Fiber-optic sensing of pressure and temperature. <u>Applied Optics 18</u>(9): 1445-1448.

[3] WEIR, K. GRATTAN, K.T.V. and PALMER, A.W. (1991). Static force measurement using a polarimetric interferometric technique. <u>In: OPTICAL FIBRE SENSOR CONFERENCE. 7th. Svdnev 1991. Proceedings.</u> Pub: IREE, Australia, pp. 221-223.

[4] YUPAPIN, P. V. P. WEIR, K. GRATTAN, K. T. V. and PALMER, A.W. (1993). A polarimetric interferometry based pressure sensor for qualitative measurements. <u>Journal of Flow Measurement and Instrumentation,</u> inpress.

[5] NING, Y. GRATTAN, K.T.V. MEGGITT, B.T. and PALMER, A.W. (1989). Characteristics of laser diodes for interferometric use. <u>Applied Optics 28</u>:3657-3661.

[6] PICHERIT, F. and MINEAU, J.L. (1990). Interferometric-polarimetric force and temperature sensor using high and low birefringence fibers with a short coherence length source. <u>Optics Communications 79</u>(17):295-299.

[7] GERGES, A.S. FARAHI, F. NEWSON, T.P. JONES, J.D.C. and JACKSON, D.A. (1988). Fibre-optic interferometric sensor utilising low coherence length source: resolution enhancement. <u>Electronics Letters 24</u>(8):472-474.

[8] WEIR, K. BOYLE, W.J.O. PALMER, A.W. GRATTAN, K.T.V. and MEGGITT, B.T. (1991). Low coherence, interferometric fibre optic vibrometer using novel optical signal processing scheme. <u>Electronics Letters 27</u>(18):1658-1660.

[9] DALLY, J. W. and RILEY, W.F. (1991). Experimental stress analysis. 3 rd edit. (New York:McGraw-Hill).

[10] HETENYI, M. (1950). Handbook of stress analysis. (New York:John Wiley & Sons).

[11] SPILLMAN, Jr., W.B. and McMAHOND, H. (1983). Multimode fibre optic sensors based on photoelastic effect. <u>In: FIBRE OPTIC AND LASER SENSORS I. Proceedings.</u> SPIE <u>412,</u> pp. 110-115.

[12] WESSON, L. N. (1986). High-sensitivity photoelastic pressure sensor. <u>In: FIBRE OPTIC AND LASER SENSORS IV. Proceedings.</u> SPIE <u>718,</u> pp. 244-250.

[13] DARIO, P. FEMI, D. and VIVADI, F. (1987). Fibre-optic catheter-tip sensor based on photoelastic effects. Sensors and Actuators 12: 35-47.

[14] YUPAPIN, P. V. P. WEIR, K. GRATTAN, K. T. V. and PALMER, A.W. (1992). A photoelastic interferometric technique using a low-coherence light source for pressure sensor applications. In : INTERNATIONAL CONFERENCE ON ELECTRONIC MEASUREMENT & INSTRUMENTS, Tianjin 1992. Proceedings. Pub. (ICEMI'92).

[15] SHARP laser diodes. Laser dode user's manual, Available from Access Pacific Ltd., Kymbrook School House, Kimbolton Road, Keysoe, Bedford MK44 2HH, U.K.

[16] Polarisation preserving fibre, Data sheet, pp. 7/86, Available from York V.S.O.P., York Hourse, School Lane, Chandler's Ford, Hampshire SO5 3DG, U.K.

[17] AYUB, M. SPOONCER, R. C. and JONES, B. E. (1990). Measurement of the temperature dependence of the stress-optic coefficient of photoelastic materials. Paper presented at International Conference at New Materials and their Applications, University of Warwick, 1990.

[18] KOTROTSIOS, G. and PARRIAUX, O. (1989). White light interferometer for distributed sensing on dual mode fibres. In : Springer Proceedings in Physics 44, Ed. by H.J. Arditty J.P Dakin and R. Th. Kersten. (Berlin:Springer-Verlag).

[19] CHEN, S. ROGERS, A.J. and MEGGITT, B.T. (1990). A novel electronic scanner for coherence multiplexing a quasi-distributed pressure sensor. Electronics Letters 26(19): 1367-1368.

[20] DANDLIKER, R. ZIMMERMANN, E. and FROSIO, E. (1992). Noise resistant signal processing for electronically scanned white-light interferometry. In: OPTICAL FIBRE SENSOR CONFERENCE, 8th, Monterey 1992, Proceedings. New York: Institute of Electrical and Electronics Engineers, pp.53-57.

[21] BENHAM, P. P. and CRAWFORD, R. J. (1987). Mechanics of engineering materials. (London:Longman Scientific & Technical).

Chapter 4

White Light Interferometry Based Pressure Sensor : A Further Study Of Photoelastic Sensing Material Characteristics

4.1 Introduction

In this chapter the measurement of force/pressure induced birefringence has been investigated using a photoelastic technique in a similar way to that discussed earlier in Chapter 3. To produce a large scanning range of the recovery interferometer i.e. for high pressure measurement, the light source used was a short coherence light source, an LED. It is equivalent to a "white light" source in white light interferometry [1], or low-coherence interferometry, as discussed in Chapter 1.

A multimode fibre link was employed in this arrangement to provide efficient coupling of light from the LED. The output light from it was launched into a multimode fibre before propagating through the sensor system and into a second multimode fibre, in advance of entering another recovery interferometer. With this recovery interferometer, the path difference between the two eigenmodes of the stress induced birefringence was compensated. Thus the applied force was translated into an equivalent measurement of path difference in the recovery interferometer. The sensing element used was constructed from either of two photoelastic materials, based on "Araldite" as discussed in the previous chapter. With the technique described, the measurement of optical path difference (OPD) could be made when it was greater than the LED coherence length. The

87

sensor system design and the photoelastic sensing **device** construction and testing are described.

An investigation of the photoelastic sensing material properties using this interferometric technique are presented. The sensing material properties such as stress relaxation, elastic limit, and its temperature dependency are also discussed with a view to using such a material as a pressure sensing device.

4.2 Review of Previous Work

A white light source has been employed as a useful source in measurement systems [1-3]. It has been widely used in the field of optical sensors where physical parameters are the required measurand [4-6]. One of these techniques is termed "Babinet compensation" and has been a successful scheme for material birefringence measurement [7]. The principle of this technique is that when white light is used in transmission, through the stressed sample sandwiched between two polarisers, the interference fringes obtained can be recovered using a Babinet compensator.

However, with the rapid development of measurement and optical technology, such as light sources and other optoelectronic devices, a significant improvement in the technique is offered. For example, the use of a broadband source with either a sensitive detector or CCD array gives rise to a potential improvement of measurement resolution. An increase in resolution over the mechanical scanning arrangement of the Michelson interferometer could be achieved by using a CCD detection scheme [8], discussed in the literature.

Some recent work has shown the possibility of using such light sources with photoelastic materials for pressure sensor applications. Ayub **et** al [9] have indicated that different photoelastic materials could be suitable for a different ranges of specific pressure sensors. Other properties of the materials are also different, such as their thermal sensitivity which may be important in particular applications. The result of using pressure sensing devices as discussed in Chapter 3, has been that it would appear such a device could be achieved using a photoelastic material as a sensing element with a low-coherence light source (a multimode laser diode, MMLD) in an interferometer arrangement. However, its fringe pattern characteristics, as discussed in Chapters 1 and 3, introduce the problem of locating the fringe-maxima position, and this limits the use of this interferometric technique.

A true, "broadband" source (by comparison to the laser) such as an LED is capable of overcoming these problems. There is no signal detection ambiguity, with the further advantage that the shorter-coherence length of this light source could be used to increase the range of measurement.

4.3 Sensor System Configuration

The sensing unit uses the same principle as discussed earlier in Chapters 1 and 3. When a photoelastic sensing element is sandwiched between two crossed polarisers, with the axes of the polarisers at 45^0 to the direction of applied force (relative to the optical axes), the polarised light propagating in the photoelastic material can be resolved into two equal components polarised parallel and perpendicular to the direction of the applied force. When no force is applied to the sensing element, these two components travel through it with the same speed and combine upon exiting the sensing element to produce light which is linearly polarised. With an applied force

the refractive indices change (see equation (3.3)) and the two components experience a path difference.

If the optical path difference (i.e. one introduced by force/pressure), ΔL, of light propagating in the sensing element is greater than the light source coherence length, the measurement of optical path difference can be performed in a recovery interferometer. When an uniaxial stress is applied to the sensing device, the phase of the light propagating in each eigenmode will change due to the induced birefringence. The "fast axis" of the birefringence is parallel to the applied force.

This phase difference, $\Delta\phi$, introduced by the stress-induce birefringence can be related to the OPD and then determined in the recovery interferometer. The recovery Michelson interferometer can then be used to re-establish the interference pattern. The path difference of the Michelson is adjusted to be away from the "balanced" position i.e. when the path difference coincides with the path difference of the sensing element, the interference pattern can be observed. The optical path difference of the recovery interferometer can then be related to the phase difference of those eigenmodes, as $\Delta L = [\lambda/2\pi]\Delta\phi$, where λ is the wavelength of the source.

Since an LED can provide a very narrow region of interference, by scanning the path difference of the recovery interferometer, the required measurand signal can be seen to be located away from centre peak signal, i.e. the reference signal position. The path difference due to the applied force on the sensing element can then be read from the micrometer adjustment along the OPD in the second interferometer. The applied force(F)/pressure is obtained from the relation as $\Delta L = C l\ F/A$, where l and A are the thickness and cross-sectional area of the sensing element respectively and C is the

stress optic coefficient of the sensing material, when using the transmission scheme as discussed in Chapter 3.

4.4 Multimode Fibre Link

It is often assumed that fibre interferometers must be constructed from single-mode fibres [10]. However, for efficient coupling of light, the active diameter of the source should be less than the core diameter of the fibre to ensure maximum coupling with a good match to the core of light from the source. Even then, only some of the light will fall within the collection cone of the fibre. The greater the numerical aperture, the more light can be accepted and the better the coupling achieved. A multimode fibre link, as illustrated in Figure 4.1, overcomes this problem, where its advantages such as ease of alignment, high coupling efficiency, reliability, and tolerance to small changes of environment are attractive. However, in the core of the multimode fibre, in which a large number of modes can propagate, the group velocity of the modes are different. After propagating some distance into the fibre, mode conversion effects can cause energy to be scattered into other modes from those of the "launch" modes. This means that the different modes travel different distances along the fibre, with the result that they arrive at the end of the fibre at different times. This behaviour is known as "multipath dispersion" [11] and its consequence is that a pulse of light launched at one end will have spread out in time when it reaches the other. The longer the fibre, the more pronounced the effect. By using a short length of a step-index, multimode fibre, all the modes of propagation arrive at the end of the fibre with a much reduced temporal spread by comparison to what is achieved with a longer fibre. Therefore, the smaller the dispersion, the greater is the potential of the fibre to carry or delivery information encoded in the optical beam.
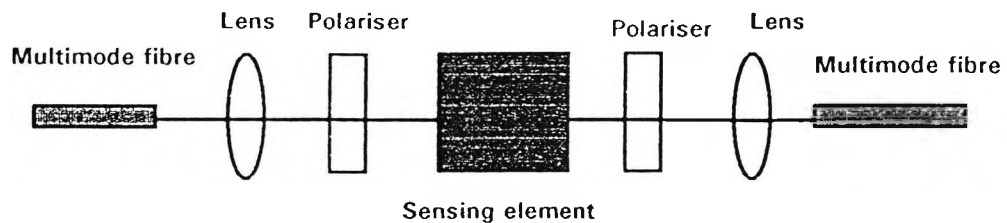
Figure 4.1 Illustration of multimode fibre link used in sensor system

arrangement.

The most important property of a multimode fibre linked sytem is that it has an advantage of having a large core diameter, where efficient coupling of power can be achieved, and that in conjunction with white light interferometry, it is suitable for use in sensor applications. Spillman et al [12] have successfully demonstrated that the use of a multimode fibre optic link, i.e. a beam delivery system, for sensors based on photoelastic effect. The short coherence light source, an LED, which can couple effectively into multimode fibre is suggested for use as the illumination [13].

4.5 Sensing Materials

When selecting the material for the photoelastic sensing element the magnitude of the photoelastic constant, C, (see equation (3.3)) is an essential, but not the only, criterion for a proper choice. The loss in sensitivity due to the choice of material with low photoelastic constant can be partly compensated by increasing the path length (and thus the sensing material thickness, i) of the light. Other essential properties for a proper choice of material are a consideration of the mechanical properties such as

stress relaxation, elastic limit, hysteresis, and also the thermal properties. Special attention has to be paid to the stress relaxation of the material, which may lead to a restricted range of applications. These aspects will be discussed in this chapter. However, data concerning the temperature dependence of the photoelastic constant are rare. For glasses an increase of 5% to 20% has been reported for the value of C in the temperature range from 20^0 to 400^0 C [14]. Ayub et al [9] observed that the change of C values of 0.38 %, 0.11% and 0% were noted in the range of 10^0 to 50^0C, using polyurethane, polycarbonate and fused quartz respectively.

Most photoelastic sensor elements make use of the induced stress distribution in the principle axis, as described. A simple element for sensing force or pressure is a rectangular solid or cube-like element as discussed earlier. Two types of Araldite resins are chosen in this work due to its large value of the coefficient, C, [15, 16] compared to the other materials suitable for the stress-induced effect. Their other properties such as stress relaxation, temperature and hysteresis are discussed in this chapter in relation to the application.

4.6 Experimental Arrangement

The experimental arrangement used is shown in Figure 4.2. This system employs a short-coherence light source in order to enhance in accuracy the determination of the fringe-maxima position and a scanning range of the interferometer output. The light source used was a high power IR emitter (LED), manufactured by RS (type RS 633-313) with an output of 10 µW, operating at a wavelength of 850 nm. Light from it was launched into the optical system through a fused silica step-index multimode fibre with core diameter of 50 µm and a length of 15 cm, and it was then collimated before

passing through a polariser to produce a linear polarisation state at 45^0 to the axes of the sensing element. After light passed through the output polariser, the interference signal contained within the beam was coupled to another multimode fibre of the same length as the previous one. The output from this fibre was collimated before entering the processing interferometer.
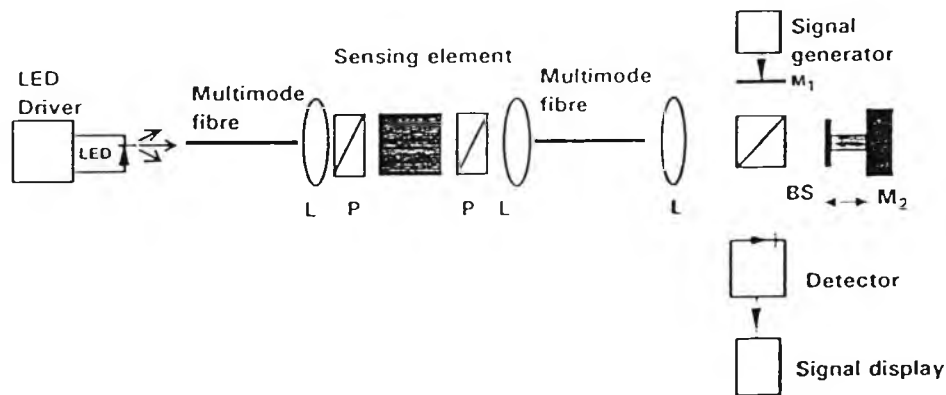
Figure 4.2 Schematic diagram of the experimental arrangement: LED Light emitting diode, BS Beamsplitter, Ms Mirrors, SG Signal generator, Ps Polarisers, Ls Lenses.

Light from the LED was launched into a multimode fibre by positioning it close, providing maximum coupling power. The optimum output was simply determined by observing the maximum power that could be coupled from the light source into the fibre. An unavoidable coupling loss of 2 dB obtained from the coupling light between the two multimode fibres, as shown in Figure 4.2, was noted.

The materials used were mixed Araldite, (CY 1311 + HY 1300), and Araldite resin, CY 1311 [17]. The cross-sectional area of both sensing elements was 72 mm^2, with a length of 6 mm. The applied force was varied by placing the series of calibrated masses on the sensing element. The changes in path differences were determined by scanning one mirror of the interferometer along the optical axis and reading the change in position of the micrometer to re-establish the interference position.

4.7 Results and Discussion

4.7.1 Force Sensitivity

When a force/pressure is applied to a sensing element, birefringence is induced. The applied force may then be related to the change in OPD. The first sensing element investigated was the mixed Araldite, and a plot of its sensitivity is shown in Figure 4.3(a). It shows the optical path differences measured at several values of applied forces. This result confirmed that a device sensitivity of 0.82 μmN^{-1} (solid line) was achieved before reaching the material elastic limit. These measurements were reproducible, provided that the applied force was less than 60 N (or 0.83 MPa pressure). A better material for sensor use was found to be the Araldite resin which has the advantage of a higher elastic limit (in addition to properties to be discussed below). It has a sensitivity of 0.57 μmN^{-1} with an applied force of up to 100 N (or 1.38 MPa), as shown in Figure 4.3(b). A comparison of the sensitivity of both materials is plotted in Figure 4.3(c).

These figures indicate that short-coherence techniques can be use to remove the phase ambiguities that occur in optical interferometry for discrete displacement measurements. A minimum OPD of ~10 μm could be

measured due to the use of a very short coherence source. However, some material properties limit the device performance and these will be discussed in the next section. The uncertainty of the measurement of OPD is of the order of 2 μm, arising from the micrometer resolution.
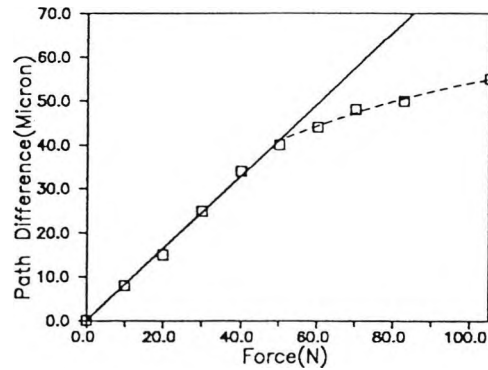
(a)
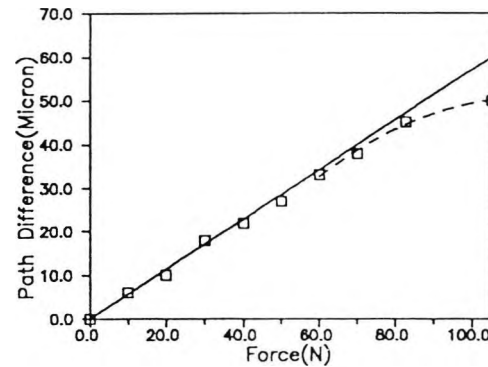
(b)
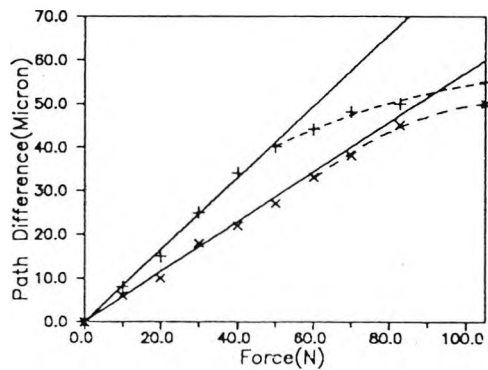
(c)

Figure 4.3 Calibration graphs, showing the changes in path difference of the interference signals against applied force:(a) using mixed Araldite, (b) using Araldite resin, (c) using mixed Araldite(+) and Araldite resin(x) : where solid line presents elastic limit of both materials.

4.7.2 Material Properties

A variety of sensitive materials has been used for dynamic photoelastic studies. A number of investigators [9, 14, 18] have studied the photoelastic technique including the mechanical and optical properties of photoelastic materials under dynamic conditions. Both materials discussed here, mixed Araldite and Araldite resin, indicate the possibility that they may be used for stressed birefringence measurement. However, the material properties, e.g. stress relaxation, elastic limit, hysteresis, and thermal dependence require certain specific conditions to be fulfilled. The most difficult situations for sensor design arise in the material properties that cause a variation in the photoelastic properties of the material. Some materials suffer from stress relaxation, elastic limit and temperature dependency of sensitivity. This is a serious problem, the change of stress-optic coefficient with temperature. By correct material selection, it is still possible to minimize (or eliminate) most of these problems.

4.7.2.1 *Mechanical stability*

To demonstrate the stress relaxation effect in a graphic fashion, Figure 4.4(a) shows a plot of the relationship between the applied force/stress and the relaxation time for the two different materials. This is the time taken for the stress-induced effect in the material to become stable. Figure 4.4(b) shows the relation between the change of output intensity and time which represents the temporal response of the stress-induced effect using mixed Araldite and Araldite. Times of about 40 s and 20 s passed before the measurand signal could be considered stable and read (for an applied force of 20 N). It should be note that in each material the relaxation time

becomes smaller when a larger force is applied to the sensing element. In order to reduce the stress relaxation effect, a bias force may be applied to the sensing system. However, this will reduce the range of the sensor, before the elastic limit is reached, and thus may not be appropriate for some applications.

4.7.2.2 *Thermal properties*

The sensing device was placed in temperature controlled environment system for testing and evaluation. It was left in there for a period of time to provide a uniform thermal environment before the measurement was taken. It was found that the temperature change of the device had only a small effect on device sensitivity for the Araldite resins studied. Ayub et al [19] have shown the properties of some photoelastic materials suffered slightly due to the thermal effect. Experimentally, the temperature sensitivity of the mixed Araldite, was estimated at 0.06 μm^0C^{-1}, while that for the Araldite resin was 0.05 μm^0C^{-1}, within the temperature range 20 ^0C to 80 ^0C.

4.7.3 Measurement Resolution

The resolution of the apparatus may be determined from the precision of the measurement of the fringe-maxima and the resolution of the micrometer. Device performance in terms of minimum detectable force/pressure was ~15 N (or 0.20 MPa) which is equivalent to ~10 μm in OPD, with respect to the device sensitivity. However, if a bias were provided, the minimum OPD would reduce. This can be done either by applying a constant bias force (whereby the relaxation time would also be reduced) or by introducing an additional permanent optical retardation in the system which is independent of the applied force. No evident of hysteresis

in device performance was observed, up to pressures of 0.70 MPa and 1.11 MPa for mixed Araldite and Araldite resin, respectively.
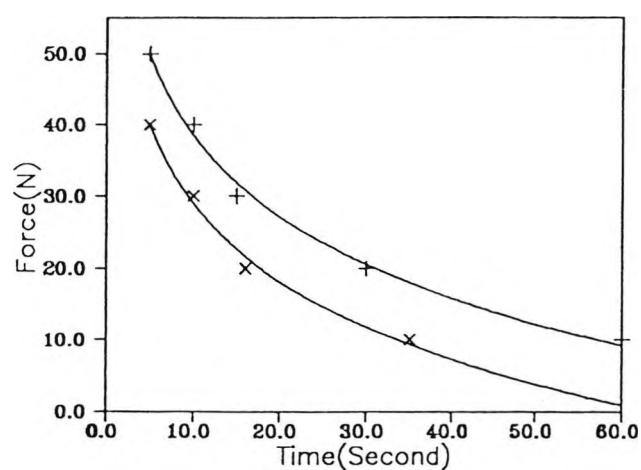
(a)
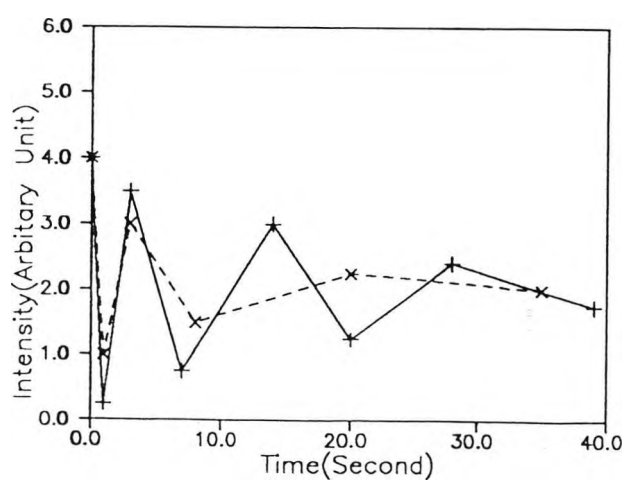
(b)

Figure 4.4 Illustration of the change in relaxation time with applied force on the sensing element, mixed Araldite (+) and Araldite resin (x): (a) varying force, (b) constant force (20N).

The errors seen arise mainly due to the limit of the scanning resolution. This is an unavoidable error due to the limited resolution of the mechanical movement on the optical axis of the recovery interferometer. An error in measurement due to a path difference of 2 μm gives a maximum error in the measurement of force of ~4% of the full scale force of 50 N. The change in sensing device properties due to hysteresis or temperature effects is negligible, in comparison to this error. By using an electronic scanning technique using a linear detector array (CCD array), offering a better resolution than of the mechanical system (e.g. a minimum OPD measurement of 45 nm may be achieved [1]) over a limited displacement range ~140 μm, then the resolution may be increased significantly, as discussed in recent work [8, 20].

4.8 Conclusion

The technique of using white light interferometer and its application to a pressure sensor has been described. Using this scheme with a multimode fibre link, and a photoelastic sensing element, the measurement accuracy achieved was evaluated. The device displayed a minimum detectable force of 15 N (0.2 MPa) in both materials, and the maximum range achieved was dependent on the sensing material properties. Here, the maximum pressures 0.70 and 1.11 MPa was applied to mixed Araldite and Araldite resin respectively, before reaching its elastic limit. The maximum recovery times of the devices of about 40 and 20 seconds for mixed Araldite and Araldite resin respectively were noted, although methods for reducing these times were discussed.

A strength of this scheme is that the LED can provide efficient optical coupling into multimode fibre, and it offers a short-coherence length to

enable the use of white light interferometry, as the basis for pressure measurement which may be achieved with a large dynamic range of the recovery interferometer. The birefringence, or optical path difference, of the sensing elements was found to vary linearly with applied force within a certain range of device performance. Since the scheme sensitivity is limited by the other material properties of elastic limit and relaxation time, careful choice of the material is required for a specific range of measurements. The effects of temperature on these devices was also discussed. However, the choice of sensing materials needs further investigation in order to optimize the sensor operation. By varying the sensing element cross-sectional areas and the thicknesses, the device can be adapted to difference ranges of pressure determination.

References

[1] KOCH, A. and ULRICH, R. (1991). Fibre-optic displacment sensor with 0.02 mm resolution by white light interferometry. <u>Sensors and Actuators A</u> <u>25-27</u>:202-207.

[2] JONES, R. (1992). White light interferometry - a road to low cost, high performance optical fibre sensors. Paper presented at IEE Colloquium on fibre optics sensor technology, London, 1992.

[3] GERGES, A.S. FARAHI, F. NEWSON, T.P. JONES, J.D.C. and JACKSON, D.A. (1987). Interferometric fibre-optic sensor using a short-coherence-length source. <u>Electronics Letters</u> <u>23</u>(21):1110-1111.

[4] KOTROTSIOS, G. and PARRIAUX, O. (1989). White light interferometry for distributed sensing on dual mode fibres. <u>In</u>: Springer Proceedings in Physics <u>44</u>, Ed. by H.J. Arditty, J.P. Dakin and R. Th. Kersten. (Berlin:Springer-Verlag).

[5] PICHERIT, F. and MINEAU, J. L. (1990). Interferometric-polarimetric force and temperature sensor using high and low birefringence fibres with a short coherence length source. <u>Optics Communications</u> <u>79</u>(5): 295-299.

[6] MARILLER, C. and LEQUIME, M. (1987). Fibre-optic white-light birefringent temperature sensor. <u>In</u>: <u>FIBRE OPTIC SENSOR 2. Proceedings</u>. SPIE <u>798</u> , pp.121-130.

[7] RIANDE, E. and GUZMAN, J. (1985). Stress-optical behaviour of poly (cis/tran-1,4-cyclohexane diamethanal-alt-formaldehyde) (PCDO) networks. <u>Journal of Polymer Science : Polymer Physics edit</u>. <u>23</u> : 1031-1041.

[8] CHEN, S. MEGGITT, B. T. and ROGERS, A. J. (1990). Novel electronic scanner for coherence multiplexing in a quasi-distributed pressure sensor. <u>Electronics Letters</u> <u>26</u>(19): 1367-1369.

[9] AYUB, M. SPOONCER, R. C. and JONES B. E. (1990). Measurement of the temperature dependency of the stress-optic coefficient of the photoelastic materials. Paper presented at Internatinal Conference on New materials and their applications, University of Warwick, 1990.

[10] FORMAN, P.R. JAHODA, F.C. and MASON, B.L. (1991). Multimode fibre interferometry with and without phase conjugation. <u>Applied Optics</u> <u>30</u>(13):1629-1632.

[11] WATSON, J. (1988). Optoelectronics. (Berkshire : Van Nostrand Reinhold (U.K.) Co.Ltd).

[12] SPILLMAN, Jr., W. B. and McMAHON, D. (1983). Multimode fibre optic sensors based on the photoelastic effect. In: FIBRE OPTIC AND LASER SENSORS. Proceedings. SPIE 110 , pp. 110-115.

[13] PETERMANN, K. (1991). Laser diode modulation and noise. (Dordrecht : Kluwer Academic Publishers).

[14] MARTENS, G. (1992). Fibre optic photoelastic sensor. International Journal of Optoelectronics 17(3):385-407.

[15] DALLY, J. W. and RILEY, W.F. (1991). Experimental stress analysis. 3 rd edit. (New York:McGraw-Hill).

[16] YUPAPIN, P. V. P. WEIR, K. GRATTAN, K. T. V. and PALMER, A. W. (1993). An optical pressure sensor using a low-coherence light source with a photoelastic sensing element. Sensors and Actuators 36 (2):105-111.

[17] Araldite Product Specification, Available from Ciba-Geigy Limited, Hinxton Road, Duxford, Cambridge, Cambs CB2 4QA, U.K.

[18] UDD, E. (1991). Fiber optic sensors: an introduction for engineers and scientists. (New York:John Wiley & Sons).

[19] AYUB, M. SPOONCER, R. C. and JONES B. E. (1988). Environmentally compensated photoelastic pressure sensors with optical fibre links. In: INTERNATIONAL CONGRESS ON OPTICAL SCIENCE AND ENGINEERING, Hamburg, Proceedings. SPIE 1011, pp. 130-135.

[20] SLESSOR, M. D. and GREEN, S. I. (1992). A simple and low- cost CCD-based imaging system. Measurement Science Technology 3 : 421-423.

Chapter 5

A Study Of Polarisation Maintaining Fibre Characteristics Using
An Interferometric Technique
For Pressure Sensor Applications

5.1 Introduction

An investigation of a fibre optic device configured as a "quasi-distributed" sensor (that is a fibre optic sensor which possesses a capability of sensing a measurand at a number of discrete points) is the subject of this chapter. In this work the characteristics of three individual types of polarisation maintaining, (High Birefringence or Hi-Bi) fibres, York Bow-tie, and Andrew E-series and D-series are considered. Using a low-coherence light source, the coupling of power between the two fibre eigenmodes allows the measured sensitive point to be located using a basic Michelson interferometer as a recovery interferometer. The theoretical aspects of the sensor system in this arrangement are discussed and demonstrated. A number of sensor applications such as force/pressure and position sensors are considered and fibre beat length and birefringence measurements made. The device sensitivity to temperature has been investigated and this is discussed.

5.2 Review of Previous Work

There are a number of sensor schemes which have been investigated, both theoretically and experimentally [1- 4], using Hi-Bi fibres. Properties such as the thermal stability has been investigated by Ourmazd et al [5], where the

temperature cycling of highly birefringent optical fibres has been used to investigate the thermal properties of bow-tie and elliptically clad fibre structures. Some recent studies, also using Hi-Bi fibre, reported an examination of their characteristics and potential for sensor applications [6-8] in particular, using them as distributed sensors [9,10].

The best known and most successful distributed fibre optic sensor is the optical time domain reflectometer (OTDR) which used Rayleigh back-scattered light in order to monitor the parameters of the optical fibre itself. As the OTDR is such a well-known instrument, details are not reproduced here. An introductory description can be found in the review by Dakin [11], and, in more detail, from Hartog [12]. The principles of distributed sensors have also been discussed elsewhere [13] and the work of Rogers [14] gives a more detailed introduction to the mathematical aspects of several types of distributed sensor. The work by Chen [15], on the application of a particular type of distributed fibre optic sensor (i.e a quasi-distributed sensor) provides a discussion of several aspects of this technique such as position, force and intensity sensors, and experimental results from measurements using bow-tie Hi-Bi fibre.

Other applications of the use of Hi-Bi fibres involve arranging for mode cross-coupling to occur, in response to the external influence. The methods of Franks et al [16] and Kurosawa et al [17] both use a frequency-swept source and, in each case, the beat frequency produced when signals are cross-coupled between the fibre eigenmodes are detected at the far end of the fibre. This signal provides information regarding the position of the cross-coupling. A further method is to use the two eigenmodes of the light propagating in the fibre and perform a phase comparison of light emerging from each mode. The phase change arising from a disturbance applied to a

length fibre has been found, by Dakin et al [18], to be dependent on the position at which the disturbance occurs, and the rate of change of that disturbance.

5.3 Operating Principles

In this section, the properties of three different Hi-Bi fibres such as (York) bow-tie, and (Andrew) E-series and D-series fibres and their relative advantages in sensor applications are investigated and discussed. The basic nature of the elements of the sensor system used, such as the properties of the Hi-Bi fibre (i.e. its polarisation mode-coupling) and characteristics of the low-coherence light source (multimode laser diode), are also discussed.

5.3.1 Polarisation Maintaining Fibre Optic

A single mode, Hi-Bi fibre is able to transmit two orthogonal polarisation modes (called eigenmodes) with slightly different velocities. The polarisation axis which permits a higher mode velocity is called the "fast axis", while the other is called the "slow" axis. A polarisation maintaining fibre will preserve the linear polarisation of the propagating light when launched in one of the two eigenmodes, and therefore, such a fibre may be used in applications where linearly polarised light is required to be transmitted and its polarisation maintained in the fibre. However, the fabrication difficulties and the small core diameter required makes launching and coupling between optical elements difficult. The high index of refraction difference between the core and the cladding also makes the construction of such low-loss fibre more complex. The "beat length" of a fibre provides a measure of its polarisation-holding ability, and the shorter the beat length, the better the polarisation-maintaining properties [19]. The beat length is defined as the

length, L_B, of fibre corresponding to a phase shift between the two orthogonally polarised modes of 2π. It is given by

$$L_B = \lambda/B \qquad\qquad (5.1)$$

Where λ is the wavelength of the light source, and B is the fibre birefringence.

Table 5.1 Characteristic of single mode Hi-Bi fibres products (York)

Fibre type:	HB 600	HB 750	HB 800	HB 1250
Operating wavelengths,λ_{op}(nm)	633	780	830	1300
Cut-Off wavelengths(nm)	<600	<750	<800	<1250
Attenuation (dB/Km)	<12	<8	<2	<2

Other specifications:

Polarisation cross-coupling (or extinction ratio)	-20dB over 1 km (typical)
Beat length at 633 nm	typical 1.3 mm, max. 2mm
Coating diameter:	220 μm (nominal)
Coating type	mode stripping acrylate
Core diameter	2-8μm depending on wavelength
Fibre diameter	
all types	125 μm $\pm$ 3 μm
HB 800 also available with	80 μm $\pm$ 3 μm
Core refractive index difference	0.01 nominal

There are a number of approaches to making Hi-Bi fibre by controlling the geometry of the fibre or incorporating stress elements in the fabrication process. Several types of single mode Hi-Bi fibres have been manufactured, as illustrated in Figure 1.17. In this work, three types of Hi-Bi fibres, bow-tie, E-series and D-series are used in the sensor system investigated.
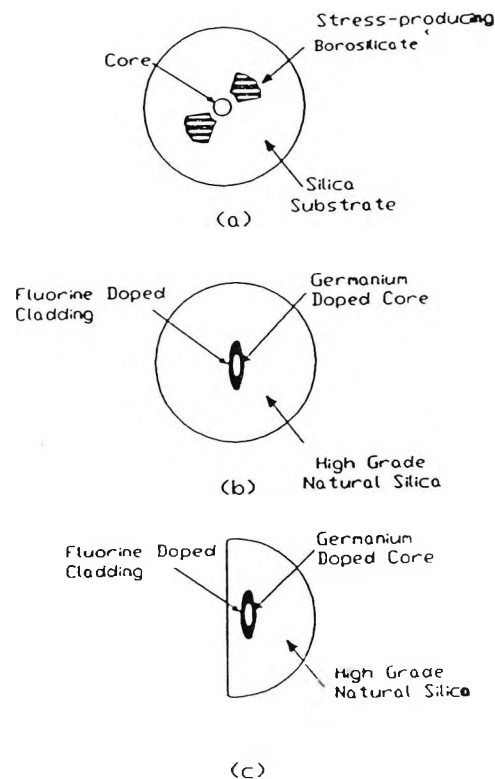
Figure 5.1 Cross-sectional structure of polarisation preserving single mode optical fibres: (a) Bow-tie, (b) E-series, (c) D-series.

5.3.1.1 *Bow-tie*

The Bow-tie fibre used was type HB800 manufactured by York. Its characteristics and those of other related York fibres, for comparison, are illustrated in Table 5.1 [20], and its cross-section illustrated in Figure 5.1(a). Its main advantage is that it offers a large birefringence which is of use in

certain applications [21] such as polarimetric sensors, velocimetry, and coherent communications, where a stable polarisation state is required. However, its thermal instability has often limited the use in such applications. This problem will be discussed in subsequent work in this chapter.

5.3.1.2 *E-series*

An illustration of the (Andrew) E-fibre [22] used is shown in Figure 5.1(b) and its specification in Table 5.2. The geometric birefringence of this fibre offers many advantages over fibres which achieve their polarisation-holding capability in other ways. E-fibres exhibit very stable characteristics under adverse conditions of bending and twisting, and wide temperature variations which can seriously degrade the performance of stress-induced birefringent fibres. Also the large index differential, together with elliptically shaped core, is an advantage when coupling light from lasers where high power densities are required, along with polarisation holding.

5.3.1.3 *D-series*

D-fibres (manufactured by The Andrew Corporation) [22] possess the same precise core centrallity as E-fibres (see Table 5.2), but, in this configuration, the flat side of the "D" lies within a few microns of the elliptical core and is parallel to its major axis, providing easy access to the guiding region without grinding and polishing (see Figure 5.1(c)). These features simplify attachment to other structures by allowing accurate location of the guiding region and alignment of the plane of polarisation. In addition to retaining all of the same optical performance characteristics of E-fibres, the D-fibres

exhibit a strong coupling ability and, because of their small minimum bending radius, are especially suited to coiling.

Table 5.2 Specfications of single mode Hi-Bi fibre products

(Andrew Corp.)

Type Number

E-Series fibre	48280
D-Series fibre	205170

Operating wavelength   514 nm-1550 nm

Composition   Natural silica

Diameter(850 nm fibre)

Fibre   80 μm and 125 μm

Over plastic jacket   200 μm and 500μm

Core Size(850 nm fibre)   1.3x2.6 μm ellipse

Core Centrality   ±0.5% of fibre diameter

Mnimum Bending Radius   0.5 cm

Normalized Birefringence(B) 1.5×10^{-4}

Core/Cladding Index Difference   0.03 to 0.04

Numerical Aperture   0.30 to 0.34

Attenuation

At 850 nm   9 dB/km

At 1300 nm   < 3 dB/km

Polarisation Holding(h)   50 dB.m (20 dB.km)

5.3.2 Polarisation Mode-Coupling

When light propagates in a single mode Hi-Bi fibre, coupling between the two propagation modes may be observed. This effect may be used as a means of distributed sensing as will be described. This effect differs from reflectometric techniques in that the scheme is based on transmission, rather than backscattered signals. The basic principle of operation for the case involving the use of orthogonal polarisation modes and their coupling effects has been reviewed by Chen [15].

When one mode of polarised light is launched from a low-coherence light source into a Hi-Bi fibre, the mode coupling effect at a coupling point, p, due to an external perturbation such as force/pressure, can be observed. This effect results in mode coupling, and a fraction of the light in the input mode is coupled into the orthogonal mode. This result may be observed by placing only a single detector and polariser at the far end of the fibre. However, location information on the coupling point can be derived utilising a recovery interferometer. This effect offers some applications in a sensor system, of which details will be discussed. One example of using this application was described by Chen [15], where the fast axis was the launch axis and the output polariser was aligned at 45^0 to the input polariser.

Generally, the alignment of the output polariser may be considered as falling into one of three cases such as being induced at 0^0, 45^0 and 90^0 (i.e. crossed) to the axis of the input polarised light.

When no coupling point is applied to the Hi-Bi fibre, the output light may be considered in terms of two different cases, according to the position of an output polariser. First, if the output polariser is aligned at 0^0 to the launch

axis (in a parallel position), a large fringe visibility is observed using a balanced Michelson interferometer as a recovery interferometer. Second, no interferometer output signal is detected at the balanced position, when the output polariser is aligned in the crossed position.

To avoid the effect of overlapping between the output fringes and the required signals, which may give rise to measurement uncertainty in this work, the output polariser was aligned in the crossed position.
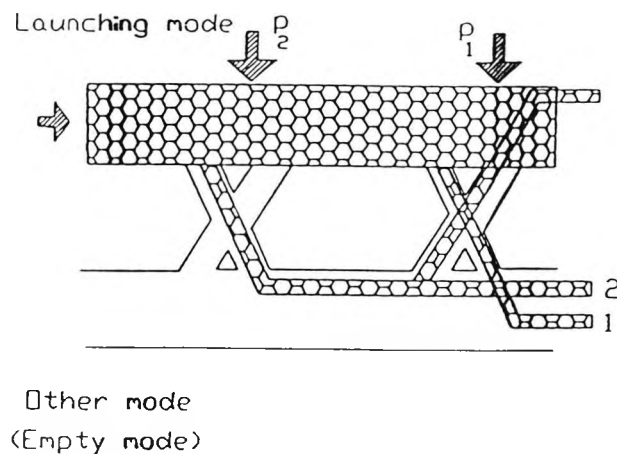
Figure 5.2 Illustration of the mode-coupling of light propagating in a Hi-Bi fibre when 2 coupling points (p_1, p_2) are applied to it.

When one coupling point is applied at p_1, as shown in Figure 5.2, when the output polariser is crossed, the interferometer output is observed at position 1 i.e. at the balanced position. The other case to be considered is when two coupling points, p_1 and p_2, are applied to the sensing fibre. Then the interferometer output gives fringes at two different positions at 1 and 2 along the optical axis. One of these corresponds to the balanced position, the other will be found at a particular optical path difference corresponding to the optical path difference of the light in the fibre. The peaks of the interferometer output corresponding to the two coupling points (i.e. p_1 and

p_2) are illustrated in Figure 5.3. The relationship between the coupling point position or its coupled power may be related to the required measurand, i.e. distance between these two points or coupling force, as will be described later in the chapter.
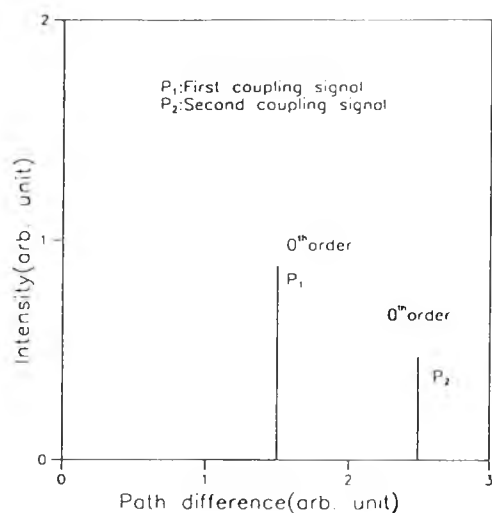
Figure 5.3 Illustration of the 0th order peak of the interferometer output when two coupling points are applied to the fibre, with light launched into one mode of a Hi-Bi fibre and with the
polariser crossed.

5.3.3 Quasi-Distributed Sensor

A distributed sensor is a system that enables the making of continuous measurements along the length of an unbroken optical fibre, i.e. a continuous length of fibre. In the simplest quasi-distributed fibre optic sensor concept, a modified fibre optic waveguide consists of sections that are spliced together into a long fibre. The quasi-distributed fibre optic sensor possesses the capability of sensing the measurand at a number of discrete, pre-determined points. This technique can be used to sense a variety of measurands such as temperature [23], force [8], and displacement [24].

The quasi-distributed sensing approach is different from the fully distributed sensor only in that the measurand can now be determined at a finite number of locations, not continuously along the fibre path. However, the approach has the advantage over distributed sensing of increasing the capability of the sensor system at various locations (i.e. a number of sensor heads can be applied to the same length of fibre).
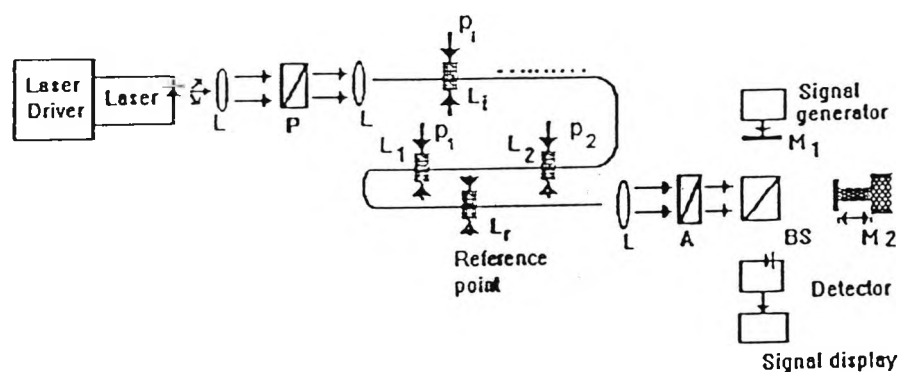
Figure 5.4 Illustration of the general sensing system arrangement when i coupling points are applied on the sensing unit: Ls Lenses, P Polariser, A Output polariser, BS Beamsplitter, Ms Mirrors,
ps Coupling points.

5.3.4 Applications

5.3.4.1 *Force Sensitivity*

When linear polarised light is launched into one mode of a Hi-Bi fibre, its output remains in the same polarisation state. The intensity transmitted by a crossed polariser at the output will be minimum, while it will be maximum at a parallel position. As discussed in the previous section, if the output polariser is aligned at 0^0 (parallel) to the launch axis (with no coupling

point), the interferometer output will present a fringe visibility characteristic of the light source, such as that discussed in Chapter 3.

When a coupling force/pressure is applied to the fibre by placing it in the coupling device, a certain amount of optical energy is coupled between the two polarisation modes of the Hi-Bi fibre is observed. The coupling device consists of a pair of wedges each of width w, the applied fibre will be sandwiched between them. If force or pressure is applied at the ith coupling point along the optical fibre, as shown in Figure 5.4, then the coupling ratio at each coupling point, i, is given by [15]

$$k_i = G[\sin 2\varphi \, \sin(\pi Bw/\lambda)]^2 \, f^2 \qquad (5.2)$$

where G is a constant, φ is the angle between the direction of applied force and the fast axis of the fibre, λ is the light source wavelength, w is the width of the coupling region (i.e. the coupling tooth width), and f is the force per unit length. From equation (5.2), the maximum coupling term can be obtained when the applied force angle is

$$\varphi = (2n+1)\pi/4 \qquad (5.3)$$

and the width of the coupling teeth,

$$w = (2n+1)L_B/2, \qquad (5.4)$$

where $n = 0,1,2.....$ This means that the first maximum of output intensity can be detected when $\varphi = 45^0$ and $w = L_B/2$. The other parameters in equation (5.2) can be arranged to be constant, and so the coupling term, i.e. the coupled intensity will vary with the applied force, F, (i.e. $f = (F/w)$).

For measurement of force via this coupled power relationship, one coupling point is required in the sensing system. The output signal is observed at the balanced position of a recovery interferometer when the output polariser is crossed. A series of calibrated masses may be applied to the sensing fibre by loading on the coupling device.

Further, the position of the coupling points along the fibre can be located when at least two coupling points are applied to the fibre. One acts as a reference, and the position of the other may be found relative to it. One important property is that the distance between any pair of coupling points must be large enough for the optical path difference between the modes of the fibre to be outside the light source coherence length. This will be discussed in the next section.

5.3.4.2 *Position Sensitivity*

As shown in Figure 5.4, the position of the sensing unit is marked by a coupling point, i, which introduces a certain degree of power coupling between the two polarisation modes. The different refractive indices associated with the eigenmodes imply that there is an optical path difference, OPD, between the light in the two modes emerging from the end of the fibre. Considering a simple case where two coupling points are applied to the fibre, the optical path difference, OPD, is related to the fibre birefringence, B, and is given by

$$OPD = B(L_r - L_i) \tag{5.5}$$

where L_i and L_r are the length of the fibre from the end of the fibre to the ith and reference coupling points. The interferometer output signals can then be detected, corresponding to this optical path difference by adjusting the position of one arm in the recovery interferometer. However, this OPD must be greater than that the coherence length of the light source. Thus the relation between the displacement along the fibre and the OPD in the recovery interferometer provides the required measurand.

As an example, a typical case may have a fibre birefringence B $=4\times10^{-4}$ and $(L_r - L_i)$ $= L = 10$ cm, the OPD between the light is 40 μm. For the two coupling points case, the interference signal may be illustrated by Figure 5.3 with peaks at p_1 and p_2 repectively. The position of the reference corresponds to the position when the interferometer is balanced (p_1), whereas the signal due to the moving coupling point, a distance L from the reference position gives rise to a second peak (p_2).

By adjusting the length of one arm in a Michelson interferometer (by moving the mirror M_2 as shown in Figure 5.4), then the maximum of interference signal can be observed when the OPD in the Michelson interferometer matches that in the fibre, as given by equation (5.5).

This system can be used to locate many sensing element distributed along the fibre in the same way, providing that the distances between their coupling points are arranged to be sufficiently large, so that their corresponding signal peaks will not overlap with each other in the output fringe visibility. This means that the separation between coupling points must be greater than the minimum separation distance, $(L_r- L_i)_{min}$, which using equation (5.5), can be expressed as

$$(L_r - L_i)_{min} = L_c/B \qquad (5.6)$$

where L_c is the coherence length of the optical light source.

5.3.4.3 *Birefringence*

From equation (5.5), the fibre birefringence is a constant term, relating the optical path difference and fibre length. Therefore, for each Hi-Bi fibre type, the birefringence can be deduced from this relation. When light propagates along a fibre of length, L, the phase difference, $\Delta\phi$, between light propagating in the two eigenmodes can be related to the OPD, by

$$\Delta\phi = (2\pi/\lambda) \text{ OPD} \qquad (5.7)$$

and from equation (5.5), yields

$$\Delta\phi = (2\pi/\lambda) \text{ BL} \qquad (5.8)$$

where $L = (L_r - L_i)$.

5.4 Experimental Arrangements

A quasi-distributed fibre optic sensor and its applications are demonstrated in this section, using three different types of Hi-Bi fibres with a low-coherence light source, incorporating a Michelson interferometer as a recovery interferometer. The system was used to measure force/pressure and locate the position of a coupling point along the fibre.
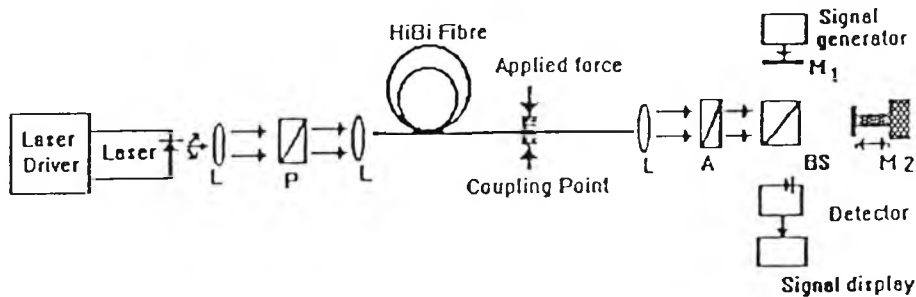
Figure 5.5 Illustration of the experimental arrangement when one coupling point is applied on the sensing unit: Ls Lenses, P Polariser, A Output polariser, BS Beamsplitter, Ms Mirrors.

5.4.1 Force Measurement

The measurement of coupled power and applied force relationship could be observed by placing a detector directly beyond the output polariser in the sensor system. However, this system utilised a recovery interferometer for the investigation of the characteristic of the light source used. In this scheme as shown in Figure 5.5, the light source used was a low-coherence light source, a multimode laser diode manufactured by Sharp (type LT023MD) [25] with an output of 3 mW, operating at a wavelength of 780 nm. Its output interferogramme was shown in Figure 1.13(b). The output light was collimated by a x10 objective lens with NA = 0.25, which then passed through a polariser (P). It was then focussed into a Hi-Bi fibre via a x10 objective lens (see Table 5.1 for fibre specifications). A short length of the fibre constituted the sensing unit where force was applied. The light output from the fibre was collimated and passed through a polariser (A) to allow selection of the light polarisation emerging from the fibre. Light was

launched via one of the two modes into the fibre by controlling the polariser P. The analyser was rotated and the extinction ratio length product measured to be ~ 30 dB.m. The polariser A was aligned in the crossed position throughout the experimental measurements.

The angle of applied force (with respect to fibre axes) could be controlled by rotating the fibre at the sensing unit as illustrated in Figure 5.6. Force was applied on the coupling point, by a series of calibrated masses. When such a force was applied, the amount of cross-coupling power from one mode to other could be observed and read from the signal display device, when the recovery interferometer was at the balanced position.
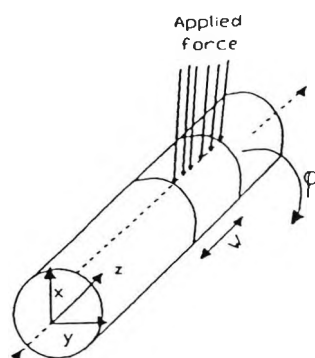
Figure 5.6 A coupling point unit.

The fibre was generally rotated through 2π to investigate the coupling efficiency and also to determine the optimum angle experimentally. The coupled power can be described by parameters such as the magnitude of the force, its angle with the respect to fast axis, φ, and coupling tooth width, w, as discussed earlier (see equation (5.2)). The procedure of force measurements were repeated when each of the fibre types was configured into the sensor system.

5.4.2 Position Detection

In the second system, shown in Figure 5.7, light was again launched into one mode. In this case, two coupling points, p_1 and p_2 were applied to the fibre, at a fixed angle (ideally at 45^0 to the fast axis). The sensing unit is as shown in Figure 5.8. A constant force of 2N was applied at each coupling point, and for each coupling point the fibre was rotated through 2π to experimentally determine the orientation to maximise the coupled power. The coupled power was input to the recovery interferometer. Signals obtained represented the corresponding positions in the interferometer where the OPDs balanced.
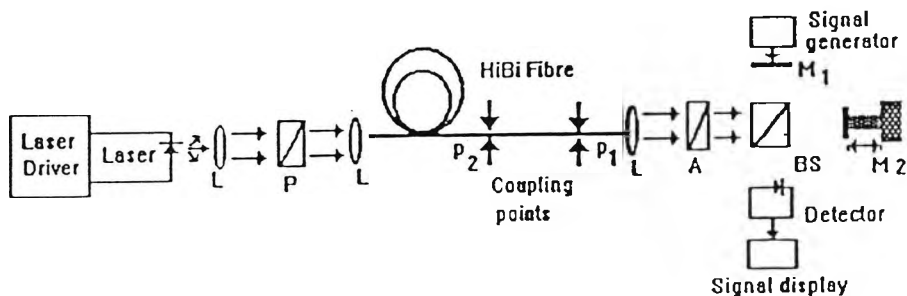
Figure 5.7 The experimental arrangement when two coupling points are applied on the sensing unit: Ls Lenses, P Polariser, A Output polariser, BS Beamsplitter, Ms Mirrors, ps Coupling points.

One of the coupling points i.e. the "moving" point, was moved along the sensing fibre while the other was fixed as the "reference" point. The displacement of the moving point along the sensing fibre was obtained corresponding to the interferometer output signal position, i.e. the OPD, in

the Michelson interferometer. This configuration was also placed in a temperature controlled environment, in order that its thermal properties might be observed. A temperature range of 20^0C to 100^0C was applied to the system.
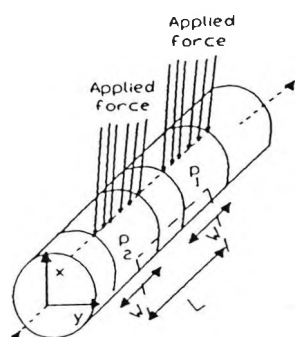
Figure 5.8 The sensing unit for the system used in Figure 5.7.

5.5 Results and Discussion

The results reported in this section are the characteristics of the three types of single-mode Hi-Bi fibres, the bow-tie, E-series and D-series. All of these fibres were used for force and position (displacement) measurements, and the associated temperature effects were also investigated.

5.5.1 Force Sensor

The sensor system as shown in Figure 5.5 was employed in this measurement. The results reported here were each obtained from the Bow-tie, E-series and D-series Hi-Bi fibres, the total length of each fibre employed was 1.5 m, (see Tables 5.1 and 5.2 for their characteristics). The

first fibre used was the Bow-tie fibre. A coupling point (as shown in Figure 5.6) was fixed to the rotating device (i.e. such a device allows the adjustment of the applied force angle with respect to the fibre fast axis). The widths of the coupling teeth used were 0.5 mm and 2.5 mm, and the applied force was varied by loading a series of calibrated masses on the sensing unit (i.e. the coupling point). The applied force angle was adjusted and fixed for each set of measurements. The same procedures were repeated when each of the fibre types was used in the sensor system.

(a)

(b)

(c)
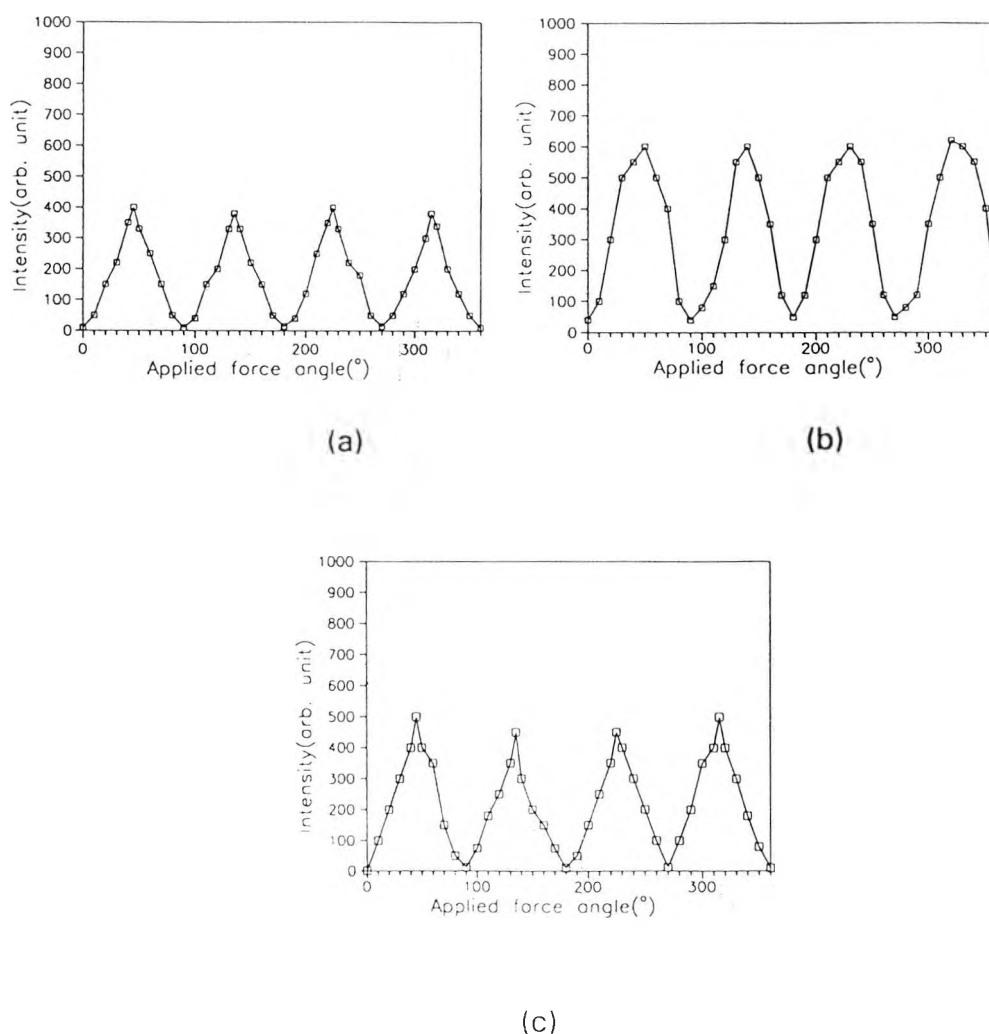
Figure 5.9 Plot of signal amplitude against applied force angle using: (a) Bow-tie, (b) E-series, and (c) D-series fibres.

Figures 5.9 (a) to (c) show the relation between applied force angle and output amplitude for Bow-tie, E and D-series fibres repectively, using a coupling tooth width of 2.5 mm and constant force of 2N. These results show that at $\varphi = 45^0$, i.e. applied force angles of 45^0, 135^0, 225^0 and 315^0, then maximum coupling of power can be obtained. An uncertainty in rotation angle of 1^0 is assigned in this system.
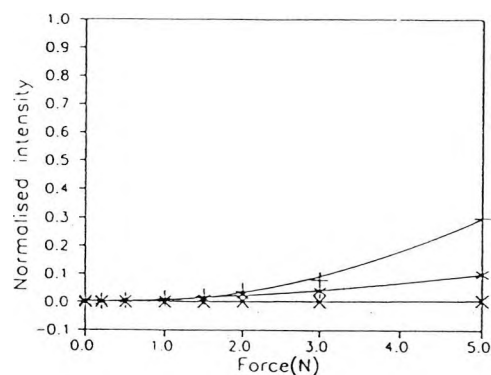
(a)
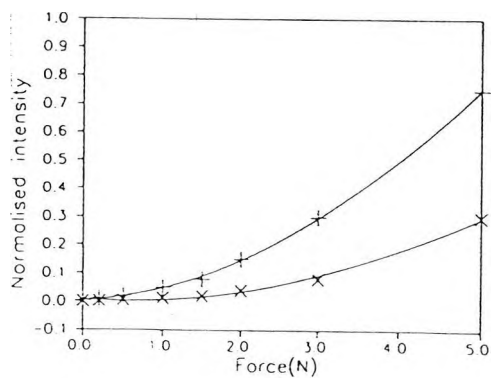
(b)

Figure 5.10 Plot of normalised intensity against applied force using Bow-tie fibre: (a) at applied force angle of 0^0(x), 22.5^0(*) and 45^0 (+), coupling tooth width of 2.5 mm, (b) at applied force angle of 45^0, coupling tooth widths of 2.5 mm(x) and 0.5mm (+).

Results in Figures 5.10 show the relation between the normalised intensity (the ratio of the output amplitude to the intensity propagating in the launch mode) and applied force, using Bow-tie fibre. Maximum coupling power was

obtained with the applied force at an angle of 45^0, while the signal disappeared in noise at 0^0. That a small output may be obtained at all arises from the uncertainty in the angle of 1^0 (This is the assigned resolution of the angle adjustment device) and intrinsic cross-coupling in the fibre itself. An increase in normalised intensity to 30% was noted when an applied force of 5 N was applied at 45^0, with a tooth width of 2.5 mm. Maximum coupling power of 30% and 75% were noted using coupling tooth widths of 2.5 mm and 0.5 mm respectively, with a force of 5N at 45^0, as shown in Figure 5.10(b). Above a loading of 5 N, with a tooth width 0.5 mm, the sensing fibre was susceptible to fracture.

(a)
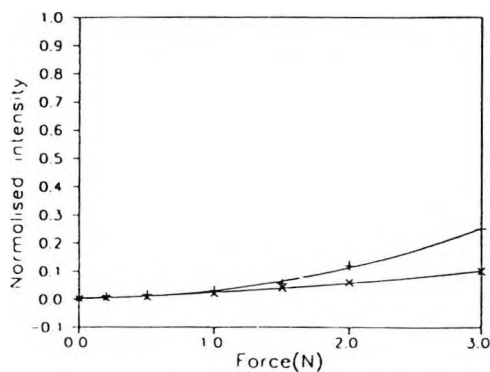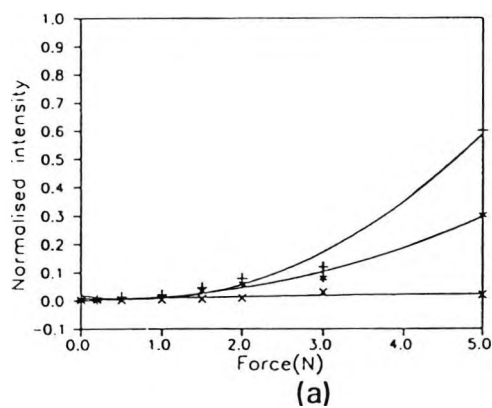
(b)
Figure 5.11 Plot of normalised intensity against applied force using E-series fibre: (a) at applied force angle of 0^0(x), 22.5^0(*) and 45^0 (+), coupling tooth width of 2.5 mm, (b) at applied force angle of 45^0, coupling tooth widths of 2.5 mm(x) and 0.5mm (+).

In the same arrangement, using E-fibre, a coupling tooth width of 2.5 mm was used, all at room temperature ($\sim 20^0$C). Results of measurements with varying applied force angle have shown that a maximum coupled power (i.e. nomalised intensity) of 60% could be observed at 45^0 with an applied force of 5 N, as shown in Figure 5.11(a). The comparison of the output power obtained from two different tooth widths is shown in Figure 5.11(b). The maximum force that could be applied before the fibre broke, when a coupling tooth width of 0.5 mm was used, was 3 N.
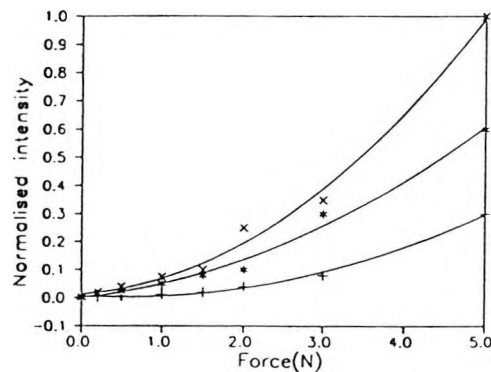
(a)
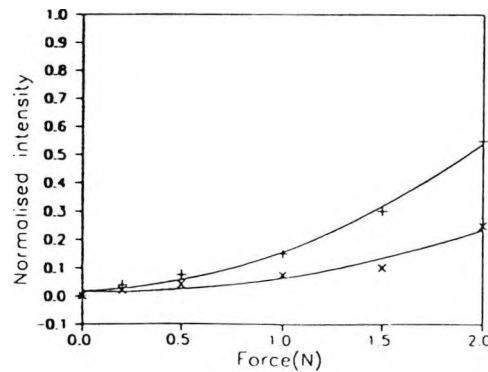
(b)

Figure 5.12 Plot of normalised intensity against applied force using D-series fibre: (a) at applied force angle of 0^0(x), 22.5^0(*) and 45^0 (+), coupling tooth width of 2.5 mm, (b) at applied force angle of 45^0, coupling tooth widths of 2.5 mm(x) and 0.5mm (+).

Figure 5.12(a) illustrates a plot of normalised coupled intensity against applied force for a range of angles, and tooth width of 2.5 mm using D-series Hi-Bi fibre. Results have shown that a greater coupling power than was experienced with the previous two fibres could be obtained from this configuration. A maximum power coupling of 100% could be achieved with an applied force of 5 N, as shown in Figure 5.12(a). An applied force larger than 5 N was found to damage the fibre. Figure 5.12(b) shows the comparison of coupled power when using two different tooth widths. A narrow tooth width of 0.5 mm produced the bigger effect, but in practice, its smaller dimension gave rise to problems in that the fibre could be easily damaged or broken.
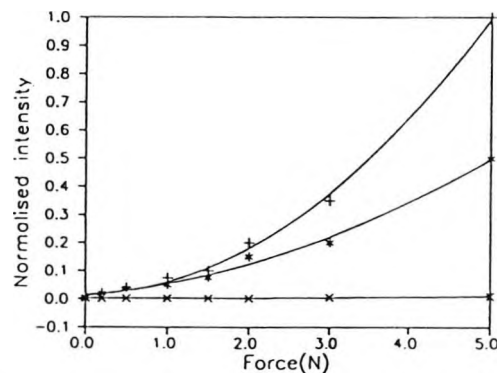
Figure 5.13 Plot of normalised intensity against applied force using: Bow-tie(+), E(*) and D-series(x) fibres with tooth width of 2.5 mm at applied force angle 45^0.

Figure 5.13 shows the comparison of three different Hi-Bi fibres, Bow-tie, E-series and D-series, plotting normalised intensity against applied force, with an applied force angle of 45^0 to the fibre fast axis with a tooth width 2.5 mm. These results were taken under the same experimental conditions for each of the fibres (i.e. applied force angle, tooth width and at room temperature). It illustrates that D-series fibre shows more rapid increase in coupled intensity than with the others, and it is found to be between 1.5

127

and 3 times that of E-series and Bow-tie fibres respectively, when the applied force was 5N. Further, the results obtained have shown that the smaller applied tooth width, corresponding to a half of fibre beat length, gave the best coupled power as shown in Figures 5.10(b), 5.11(b) and 5.12(b) for each of the fibres used.

5.5.2 Displacement Sensor

The system employed in this measurement is as shown in Figure 5.7. Figures 5.14(a) and 5.14(b) show the relation between the change in the OPD of the recovery Michelson interferometer and the position of the second fibre coupling point (i.e. moving point) along the fibre, using Bow-tie fibre. This coupling point applied a constant force of 2 N, at an angle of 45^0 and 22.5^0. The cross-coupling power was controlled by rotating the sensing fibre to allow the applied force angle to be adjusted, with respect to the fast axis of the fibre. The position of the sensing point was varied by moving one of the two coupling points along the length of the fibre used.

The reference and moving coupling point were fixed at a distance L_r and L_i respectively from the far end of the sensing fibre. The first coupling point (at L_r) was called the "zero" position (i.e. a reference position with no displacement). The displacement from the zero position to the moving point could be located along the fibre length with respect to this reference position. The minimum distance between the reference and the moving points was limited by the light source coherence length, and in this case, the light source coherence length of ~40 μm, gave the minimum distance between the coupling points (i.e. L_r- L_i) along the Bow-tie fibre length of 10 cm.
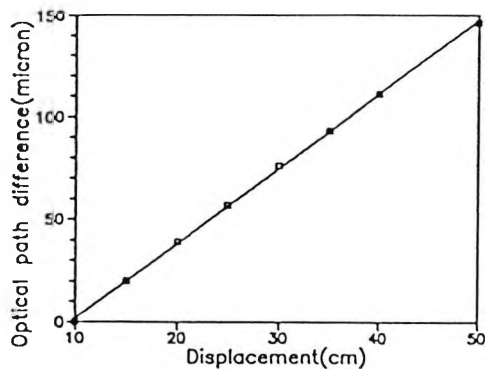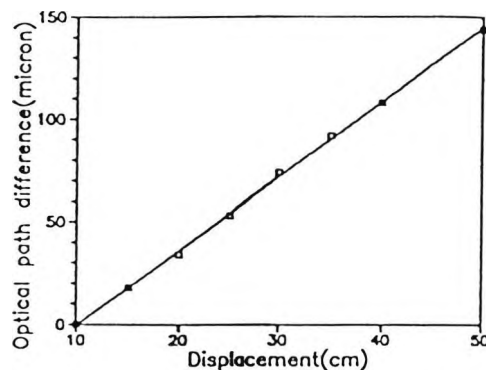
(a)   (b)
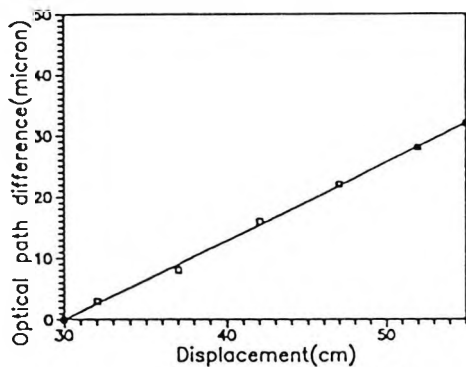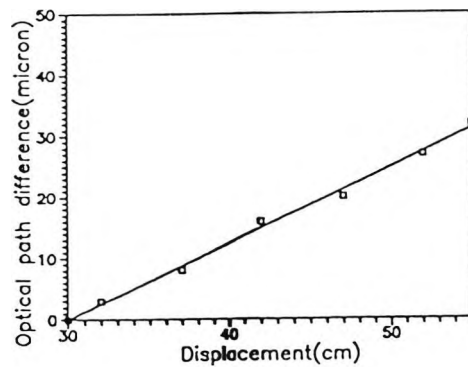
(c)   (d)
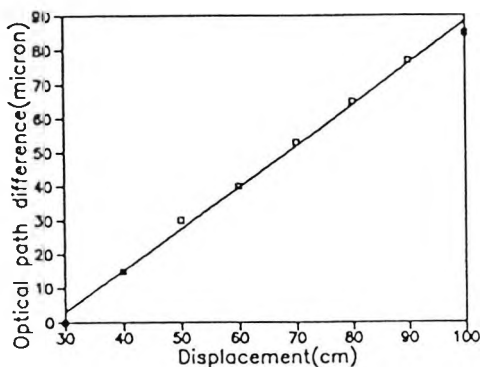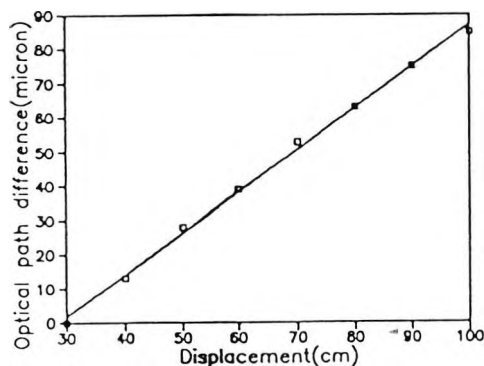
(e)   (f)

Figure 5.14 Plot of the change in optical path difference against
displacement, using: (a) Bow-tie at 45^0, (b) at 22.5^0
, (c) E-series at 45^0 , (d) at 22.5^0, (e) D-series at 45^0 , (f) at 22.5^0 .

129

The interference signal arising from each coupling points could be located using a Michelson interferometer. Scanning one arm of the recovery interferometer from the reference position (i.e. the zero position) the 2nd interference maximum was observed; then a reading of the OPD at this fringe-maxima position from the micrometer adjustment gave the required measurand. The sensor sensitivities of 3.64×10^{-4} and 3.63×10^{-4} at the applied force angle of 45^0 and 22.5^0 were noted respectively. The slight difference of sensitivity with different force angles is most likely to have arisen from the fringe-maxima position uncertainty, rather than a change in properties of the fibres.

Figures 5.14(c) and 5.14(d) show the relation of OPD and displacement of the E-series fibre at the applied force angle of 45^0 and 22.5^0. The gradients, i.e. fibre birefringences, of 1.28×10^{-4} and 1.25×10^{-4} were noted. In this case, a minimum fibre length between the reference and signal coupling points of 30 cm was required to obtain the interference signal outside the coherence region. Figure 5.14(e) and 5.14(f) presents the relation between the OPD and displacement of the D-shaped fibre, and a gradient of 1.22×10^{-4} was noted, to be the same at 45^0 and 22.5^0. In this case the value of this constant (i.e. the fibre birefringence, B) is slightly smaller than that observed for the E-series fibre.

5.5.3 Birefringence Measurement

The fibre birefringence measurement can be obtained from the gradient of each graph of OPD-displacement relations as follow. From equation (5.5), OPD $= B (L_r - L_i)$, where B in this equation is an average birefringence of the fibre used. The birefringence, B, of the Bow-tie, E-series and D-series fibres have been found to be 3.64×10^{-4}, 1.28×10^{-4} and 1.22×10^{-4},

respectively. Fibre beat lengths were also calculated by using the relation expressed in equation (5.1).   From this relation, and the fibre birefringences, the beat lengths of bow-tie, E and D-series fibres were found to be 2 ± 0.2 mm, 5 ± 0.2 mm and 5.5 ± 0.2 mm, respectively. For the smaller beat length, the smaller tooth width is required at the coupling point to provide efficient coupling of power as shown in equation (5.4), the first maximum of output intensity obtained when w is equal to $L_B/2$.

(a)   (b)

(c)
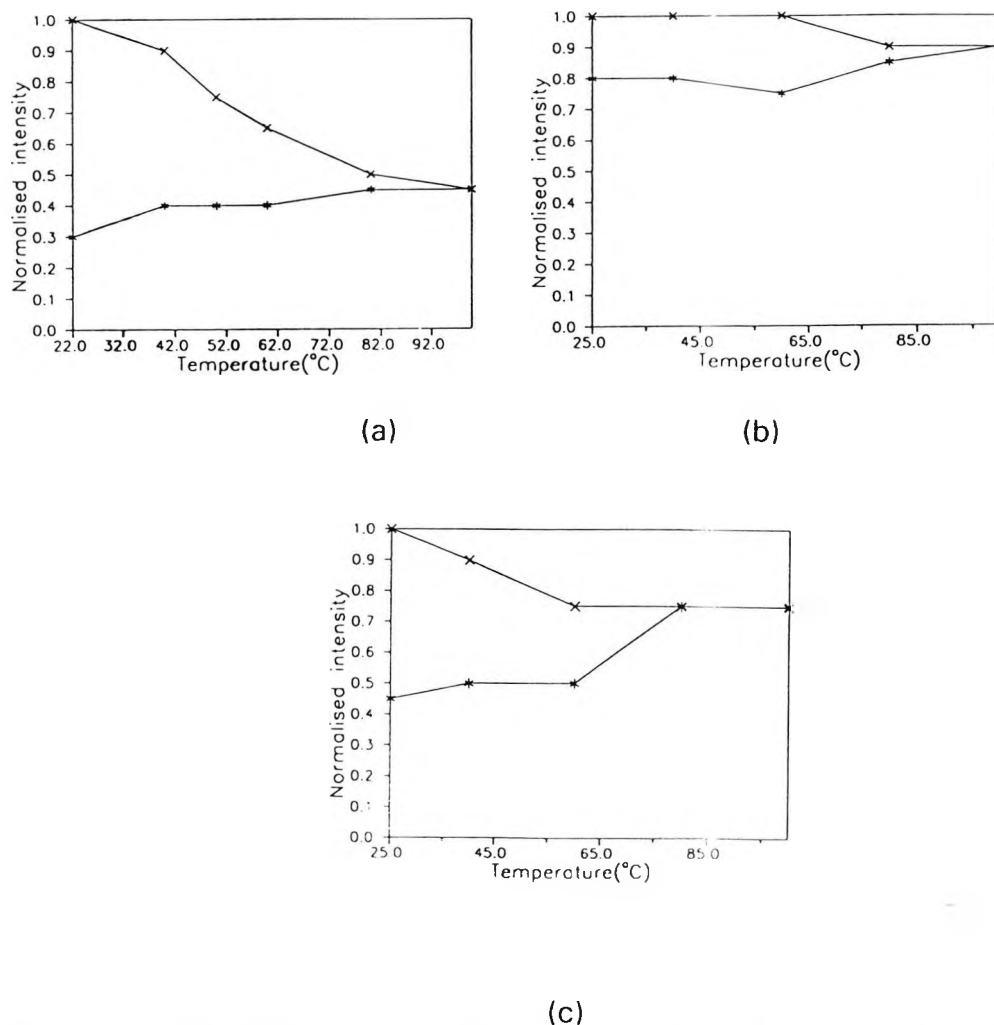
Figure 5.15 Plot of normalised intensity against temperature using three different Hi-Bi fibres, Heating up(x) and cooling down(*) : (a) Bow-tie, (b) E-series, (c) D-series.
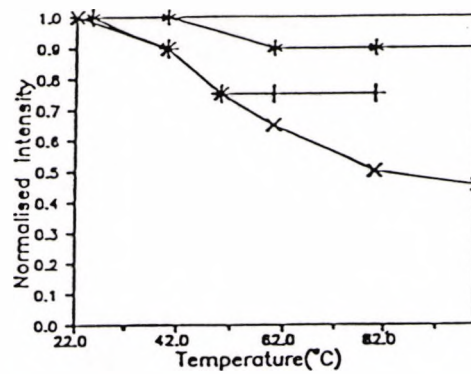
Figure 5.16 Plot of the normalised intensity against temperature using :
Bow-tie(x), E-series(*), and D-series(+), for increasing temperature.
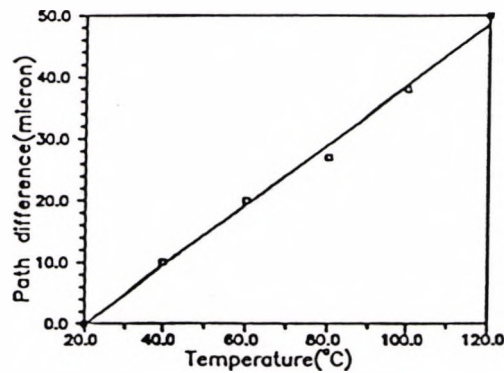
Figure 5.17 Plot of optical path difference against temperature using Bow-tie fibre.

5.5.4 Testing of Temperature Effects

The effect of temperature variations to the coupled power was investigated using the system as shown in Figure 5.5. The sensing unit of each fibre was placed in the temperature controlled environment and tested, with a constant force of 2 N was applied to each coupling point. Figure 5.15 shows the plot of the stability of the coupled power against temperature over a range from room temperature ($\sim 20^0$C) to 100 ^{0}C, using Bow-tie

(Figure 5.15(a)), E-series (Figure 5.15(b)) and D-series (Figure 5.15(c)) fibres. However, after the first heating cycle the initial temperature used was about 25^0C for the other cycles. It appears from the comparison of the stability of the coupling power intensity, as shown in Figure 5.16, that the E-series shows the smallest thermal effect of all the fibres studied.

The temperature sensitivity of each fibre type was also investigated by using the position sensor scheme as shown in Figure 5.7. The distance between two coupling points of 40 cm was fixed throughout the experimental measurements. In each case, a length of fibre used of 60 cm was placed in the temperature controlled system. The change in OPD (the associated change in phase) between the applied coupling points, due to the change in temperature, was observed in a recovery interferometer. The first fibre tested was the Bow-tie fibre, and the plot of temperature sensitivity of the Bow-tie fibre is shown in Figure 5.17, yielding a sensitivity of 4.8 $rad/^0C/m$ which was noted. The changes in OPD (i.e. phase) with temperature of the E and D-series fibres were also tested, and their estimated senstivities of 1.4 and 2.0 $rad/^0C/m$ respectively for these fibres were noted.

5.5.5 Measurement and Limitation

Results obtained have shown that the minimum range of measurement (i.e. the distance between two coupling points along the sensing fibre) of the position sensor is limited by the coherence length of the light source. For example, an initial minimum fibre length of 10 cm is required when the Bow-tie fibre is employed in the sensor system where for the other two fibres it is 30 cm. The temperature effect of the fibre investigated has also limited the use such fibres in sensor applications. In this study, it was found

that the Bow-tie fibre was more sensitive to temperature than the other two fibres, which limits its suitability in such sensor applications. The other limit of this measurement is the resolution of the mechanical scanning movement of the Michelson interferometer which in this configuration was estimated to be about $\pm$ 2 μm.

5.6 Conclusion and Summary

A "quasi-distributed" fibre optic sensors for measuring modal conversion (coupled power) along a polarisation-maintaining fibre was presented. Mode coupling effects in three Hi-Bi fibres, having different birefringence and structures, have been investigated experimentally using an interferometric method. The sensors were used to measure the force-induced coupling power of the fibre employed, which is observed using an interferometer, and with a specially designed optical fibre sensing unit. By mean of this method, the magnitudes and locations of mode couplings caused by transverse force/pressure were evaluated quantitatively. An optical path difference accuracy of $\pm$ 2 μm and minimum fibre lengths of 10 and 30 cm (associated with the light source coherence length of ~40 μm) at a wavelength of 780 nm were required for the Bow-tie, E and D-series fibres used repectively to obtain the required measurand.

A study of polarisation maintaining fibre characteristics has been undertaken for use in quasi-distributed force and displacement sensors, and their applications to beat length and birefringence measurements investigated. The results obtained show that this sensing system may be suitable as a displacement sensor, where the response of the device is linear. Pressure sensor may also be applied using the force sensor system, where pressure measurement may be obtained when force is applied on the

known area, however, the non-linearity in device sensitivity may not be suitable as a realistic sensor. Experimental results of temperature testing using these fibres have also been presented showing the difference for each fibre, indicating the different aspect of potential applications. A summary of the sensing performances of each fibre is shown in Table 5.3, from which the choice of fibre to be used for particular applications may be made. For examples, a temperature sensor may be required with high sensitivity, therefore, the Bow-tie fibre may be best employed in such a sensor scheme, while the E-series fibre may be suitable in such work that a small change in coupled power to temperature variations may be required.

Table 5.3 The comparison of the three Hi-Bi fibres used

Characteristics relation	Fibre types		
	Bow-tie	E-series	D-series
Intensity-force (Normalised intensity %, Force = 5N, Tooth width = 2.5mm, force angle = 45^0)	30	50	100
OPD-Displacement (Sensitivity(or B), OPD/Coupling point displacement, x 10^{-4})	3.64	1.28	1.22
Thermal Effects (Sensitivity, rad/^{0}C/m)	4.8	~1.4	~2.0

References

[1] NODA, J. OKAMOTO, K. and SASAKI, Y. (1986). Polarisation-maintaining fibres and their applications. <u>Journal of Lightwave Technology</u> <u>4</u> (8) : 1071-1089.

[2] TSAI, K.H. KIM, K.S. and MORSE, T.F. (1991). General solutions for stress-induced polarisation in optical fibres. <u>Journal of Lightwave Technology</u> <u>9</u> (1): 7-17.

[3] SAKAI, I. PARRY, G. and YOUNGQUIST, R.C. (1986). Multiplexing fibre-optic sensors by frequency modulation : cross-term considerations. <u>Optics Letters</u> <u>183</u> (3): 183-185.

[4] YOSHINO, T. HASHIMOTO, T. NARA, M. and KUROSAWA, K. (1992). Common path heterodyne optical fiber sensors. <u>Journal of Lightwave Technology</u> <u>10</u> (4): 503-513.

[5] OURMAZD, A. VARNHAM, M.P. BIRCH, R.D. and PAYNE, D.N. (1983). Thermal properties of highly birefringent optical fibres and performs. <u>Applied Optics</u> <u>22</u> (15): 2374-2379.

[6] BOUCOUVALAS, A.C. RAYIT, N.S. and GREAVES, M. (1986). Special shaped fibres for distributed sensors. Paper presented at Institute of Electrical Engineer Colloquium on Distributed Optical Fibre Sensing, London, Digest No: 1986/74, 1986.

[7] TSUBOKAWA, M. HIGASHI, T. and SASAKI, Y. (1989). Measurements of mode coupling and extinction ratios in polarisation-maintaining fibres. <u>Journal of Lightwave Technology</u> <u>7</u> (7): 45-50.

[8] TSUBOKAWA, M. HIGASHI, T. and NEGISHI, Y. (1988). Mode couplings due to external forces distributed along a polarisation-maintaining fibres: an evaluation. <u>Applied Optics</u> <u>27</u> (1) : 166-173.

[9] DUNPHY, J.R. MELTZ, G. and ELKOW, R.M. (1987). Distributed strain sensing with a twin-core fibre-optic sensor. <u>ISA Transactions</u> <u>26</u> (1):7-10.

[10] KOTROTSIOS, G. and PARRIAUX, O. (1989). White light interferometry for distributed sensing on dual mode fibres. <u>In</u>: Springer Proceedings in Physics <u>44</u>, Ed. by H.J. Arditty, J.P. Dakin and R. Th. Kersten. (Berlin: Springer-Verlag).

[11] DAKIN, J.P. (1987). Multiplexed and distributed optical sensor systems. <u>Journal of Physics E: Scientific Instruments</u> <u>20</u> (8): 954-967.

[12] HARTOG, A.H. (1983). Distributed temperature sensor based on liquid core optical fibres. <u>Journal of Lightwave Technology</u> <u>1</u> (3) : 498-509.

[13] ROGERS, A.J. (1988). Distributed optical-fibre sensors for the measurement of pressure, strain and temperature. <u>Physics Reports</u> <u>169</u> (2): 99-143.

[14] ROGERS, A.J. (1991). Distributed optical-fibre sensing. <u>In:</u> <u>HOLOGRAPHIC OPTICS III CONFERENCE, 1991. Proceedings</u>. SPIE <u>1507</u>, pp. 2-24.

[15] CHEN, S. (1990). Optical interferometry for novel optical fibre sensor systems. Ph.D. thesis : King's College, University of London, Department of Electronic and Electrical Engineering.

[16] FRANKS, R.B. TORRUELAS, W. and YOUNGQUIST, R.C. (1985). Birefringent stress location sensor. <u>In:</u> <u>FIBRE OPTIC SENSORS CONFERENCE, Cannes 1985. Proceedings</u>. SPIE <u>586</u>, pp. 84-89.

[17] KUROSAWA, K. and HATTORI, S. (1987). Distributed fibre-optic sensor using forward travelling light in polarisation maintaining fibre. In:<u>FIBRE OPTIC SENSORS II CONFERENCE, 1987, Proceedings</u>. SPIE <u>798</u>, pp. 36-41.

[18] DAKIN, J.P. PEARCE, D.A.J. STRONG, A.P. and WADE, C.A. (1987). A novel distributed fibre sensing system enabling location of disturbances in a sagnac loop interferometer. <u>Journal of Optical Sensors</u> <u>2</u> (6): 403-406.

[19] CARRARA, S.L.A. KIM, B.Y. and SHAW, H.J. (1986). Elasto-optic alignment of birefringent axes in polarisation hold optical fibre. <u>Optics Letter</u> <u>11</u> (7): 470-472.

[20] Polarisation preserving fibre, Data sheet, p. 7/86, Available from York V.S.O.P., York House, School Lane, Chandler's Ford, Hampshire SO5 3DG, U.K.

[21] Applications of Hi-Bi fibers, Data sheet, p. 9/86, Available from York V.S.O.P., York House, School Lane, Chandler's Ford, Hampshire SO5 3DG, U.K.

[22] Polarisation maintaining optical fibres, The Andrew Corporation, Bulletin 1295D, Available from Andrew Antenna, Weybridge, Surrey, U.K.

[23] LECOY, P. GROSS, M. and GUENADEZ, L. (1987). New fibre-optic distributed temperature sensor. <u>In:</u> <u>FIBRE OPTIC SENSORS II CONFERENCE, 1987, Proceedings</u>. SPIE <u>798</u>, pp.131-136.

[24] GUSMEROLI, V. VAVASSORI, P. and MONITORING, M. (1989). Quasi-distributed single-length polarimetric sensor. <u>Optics Letter</u> <u>14</u> (23):1330-1332.

[25] SHARP laser diodes, Laser diode user's manual, Available from Access Pacific Ltd., Kymbrook School House, Kimbolton Road, Keysoe, Bedford MK44 2HH, U.K.

Chapter 6

Conclusions

6.1 Summary

From the historical point of view, pressure has been one of the most important variables to be measured, for industrial purposes, and many general methods of pressure measurements are found in references [1- 3]. An interferometric technique incorporating a fibre optic is also one of those techniques which offers a number of advantages [4]: e.g. high precision measurement, small size, light weight, and it can be used in high voltage, electrically noisy, high temperature environments. This technique has matured to the point that an optical fibre sensor has been the subject of increased development because of its specific advantages, with the combination of its potential for high sensitivity.

There is a need to focus on the development of new sensor schemes which may lead to on offer a more acceptable device for certain industrial applications. The work presented in this thesis has described the study, development and application of optical pressure sensors; both intrinsic and extrinsic fibre optic devices. The work discussed in this thesis offers further information on the wide choice of schemes for sensor use, employing optical technology. Techniques using polarimetry have been recognised as offering a temperature compensation technique, where a simple Michelson interferometer is used, and this has been applied sucessfully in this subject area [5, 6]. However, problems of output signal ambiguity and temperature dependence of sensor sensitivity still exist to some extent and are areas where the need for continued improvement is recognised. A primary

objective of this work was to investigate a scheme that would reduce these effects, which could be readily implemented as a practical device.

This thesis has described, in general terms, the relevant background to the field of optical sensors, and then concentrated on the area of polarimetric interferometry, photoelastic based sensors and the technique of white light interferometer. Using these techniques it is believed that the problems of thermal effects and interferometer output signal ambiguity could be overcome, at least partially, and in addition an acceptable device sensitivity and dynamic range could be maintained.

In summary, the work discussed by the author was divided into four different sections. The first described in this work was an all fibre, optical interferometer where an ordinary single mode bi-directional coupler was used as a conventional Michelson interferometer. Static force or pressure was measured using either coated or uncoated fibre as an intrinsic sensing element (i.e. sensing arm). The change in phase of the propagating light was found to be linear with the applied force. The sensing unit (i.e. both sensing and reference arms) was placed in a temperature controlled environment to test the variations in sensor sensitivity, with temperature. A range from room temperature of up to 95 ^{0}C was applied to the sensing unit, and the device sensitivity was found to be linear over a range of small ambient temperature changes. Results obtained show that the polarimetric technique could be used to make temperature independent measurements. An increase in sensor sensitivity by using an uncoating sensing fibre of 18 % over that achieved with a coated sensing fibre was noted. However, the problems of signal ambiguity in both dynamic range and direction, interferometric noise [7], and also the force distribution on the sensing

device still remained to some degree and represent an area for possible future work for refinement of the technique.

The study using "low-coherence" interferometry [8] showed that the operating range (dynamic range) of the interferometer output could be increased by using a low-coherence technique. A minimum value of measured optical path difference of 25 μm (or equivalence to a change in phase of 64 π rad) was noted. The direct application of force to the sensing element could reduce the force distribution problem, and so a photoelastic material was configured for use in the scheme to produce an extrinsic sensor. The technique has been demonstrated, and preliminary investigations have found that different sensing materials investigated were suitable for different ranges of measurement. Linearity of sensor sensitivity was obtained within the material elastic limits, and the temperature effects were seen to be small. However, the problem of the offset signal remained due to the characteristics of the light source (i.e. a signal arising from the case where the optical path difference is less than the light source coherence length). A scheme where this may be overcome by using a biassing device, (e.g. fibre optic (Hi-Bi fibre), or birefringent material) was investigated. An increase in the dynamic range (i.e. in terms of the minimum value of OPD/pressure that could be measured) by 20 % over the unbiassed scheme was noted when using bow-tie Hi-Bi fibre to provide the bias. The smallest value measured was 20 μm in optical path difference (or a change in phase of 51π rad). The accurate measurement of fringe-maxima position and material properties such as stress-relaxation and the elastic limit are the limitations in this system. The investigation of such problems is proposed as subsequent to this thesis investigation.

The use of an LED and two different selected materials in the **pressure** sensor system allowed material properties to be investigated using white light interferometry. Two different materials were considered in **terms** of both force and temperature sensitivities. The improvement of device dynamic range gives rise to a smaller minimum measurement, **and** the fringe-maximum position was also more easily obtained, due to **the** very short coherence length of the light source. The results showed that sensor sensitivity was also linear and stable with temperature. An increase in the dynamic range of 40 % over the unbiassed system was noted, and a smallest possible measurement value of 15 μm or 35 π rad was recorded. However, the limitation due to the material property consideration remained. The wider study of a range of other suitable materials would be required to identify if materials with more suitable material properties were available.

A distributed sensing technique using polarisation maintaining fibre as an intrinsic sensing element offers more promise in light of the consideration of a practical sensor, i.e. in terms of large dynamic range, where the multiplexed sensor (i.e. a number of sensor heads) could be applied. The use of a low-coherence light source and three different Hi-Bi fibres was investigated for pressure sensor applications. Light from the multimode laser diode was polarised and launched into one mode of the Hi-Bi fibre used. The power coupled into the orthogonal empty mode depends on the application of an external force, and this is a function of both its direction and magnitude. Calibrated masses were used and the relationship between the coupled power and applied force measured. The differences in sensor sensitivity and the influence of thermal effects with different Hi-Bi fibres were examined. However, the sensitivity is seen to be non-linear with applied force.

A position/displacement sensor using these Hi-Bi fibres also were investigated. Two coupling points termed "reference" and "moving" points were applied to the fibre, and the positions of the moving "point" may be located with respect to the "reference" point by using a recovery interferometer. The device sensitivity, in terms of the OPD and displacement are linear, and the position along the length of a fibre may be located and thus known with respect to the reference point. The temperature effects of E-series and D-series fibres was found to be less than that of a bow-tie fibre. This may be important to the wider use of these fibres in sensor applications. The particular and schematic comparison of the approaches used in this work is shown in Table 6.1

6.2 Suggestions For Further Work

From the study undertaken, it could appear that the ideal optical pressure sensing device is a combination of a very short coherence length source, a polarisation preserving medium, a high resolution and large dynamic range detector, and a sensitive (i.e. sensitive to parameter of interest) and reliable sensing element, where these features can be integrated into a compact device. Up to now, no clear evidence that such an optical pressure sensor could be constructed at reasonable cost has been found. However, as discussed in the text, there are some indications that considerable advances in related research are being made. There are several directions in to which future research might profitably be channelled to meet this need.

The use of an ordinary single mode fibre, with care being taken over polarisation orientation, force distribution and temperature compensation may still be a valid method for a pressure sensor, where improvement in signal processing may make a more promising device. The development of

the sensing element itself by using a different material and/or more sensitive coating material on the fibre would appear to increase its performance. Alternatively, to overcome two significant problems: temperature effects and polarisation fluctuations, a different arrangement using a section of a polarisation maintaining fibre spliced to the sensing element could be configured as a pressure sensor, and these effects reduced [9].

Using a CCD array as a detector has become a well known technique to improve sensitivity in white light interferometry, as discussed earlier [10]. Its resolution can be significantly improved into the sub-micron range. The use of an LED with a multimode fibre, where reasonable coupling of power can be achieved, in white light interferometry, makes this an attractive technology for industrial applications.

In the future, an investigation may be required into suitable photoelastic materials where the range of measurement may be optimised for a particular application (range of measurement). This might mean an application where high speed is required (short relaxation time) but high sensitivity is less important (i.e. a device which is not sensitive to a small applied force), which then may lead to a more promising sensing device.

Sensing devices using Hi-Bi fibres as the intrinsic sensor, may give rise to more areas of application. If an LED (or SLD) can be used to couple a reasonable level of power into a Hi-Bi fibre [6, 11], with a combination of a CCD array detector or a nano-positioning device [12] in the recovery interferometer, then this system may well be worthy of integration into high quality sensing devices.

Table 6.1 Comparison summary of optical pressure sensor experimental schemes used

Chapter reference	Experimental schemes	Achievements	Problems
2	All Michelson fibre optic	Good linearity, Good temperature stability	Signal ambiguity, Phase direction ambiguity, Force distribution (May arise from method of applying force)
3 & 4	Photoelastic material & White-light interferometry	Linear before reaching material limits, Good temperature stability, Increased dynamic range over an all fibre optic scheme	Determination of Fringe-maxima position, Material limits (elastic limit, relaxation effects)
5	Quasi-distributed pressure sensor	High coupling power needed, May be configured as a position sensor	Non-linear (May be overcome in signal processing)

References

[1] DOEBELIN, E.O. (1983). Measurement system: application and design. 3 rd edit. (Singapore:McGraw-Hill).

[2] BARNLEY, G.C. (1988). Intelligent instrumentation:microprocessor applications in measurement and control. 2 nd edit. (London : Prentice-Hall).

[3] MEDLOCK, R.S. (1986). Review of modulating techniques for fibre optic sensors. Journal of optical Sensors 1(1):43-68.

[4] HOSS, R.J. (1990). Fibre optic communications: design handbook. (Englewood Cliffs : Prentice-Hall).

[5] WEIR, K. GRATTAN, K.T.V. and PALMER, A.W. (1992). Static force measurement using a polarimetric interferometric technique. In: OPTICAL FIBRE SENSOR CONFERENCE, 7th, Sydney 1991, Proceedings. Pub: IREE, Australia, pp. 221-223.

[6] PICHERIT, F. and MINEAU, J. L. (1990). Interferometric-polarimetric force and temperature sensor using high and low birefringence fibres with a short coherence length source. Optics Communications 79 (5): 295-299.

[7] ECONOMOU, G. YOUNGQUIST, R.C. and DAVES, D.E.N. (1986). Limitations and noise in interferometric systems using frequency ramped single-mode diode lasers. Journal of Lightwave Technology 4 (11):1601-1608.

[8] NING, Y. GRATTAN, K.T.V. MEGGITT, B.T. and PALMER, A.W. (1989). Characteristics of laser diodes for interferometric use. Applied Optics 28 (17):3657-3661.

[9] BOCK, W.J. and WOLINSKI, T.R. (1989). High-pressure fibre-optic sensor based on polarisation-rotated reflection. In: Springer Proceeding in Physics 44, Ed. by H. J. Arditty, J.P. Dakin and R. Th. Kersten. (Berlin:Springer-Verlag).

[10] KOCH, A. and ULRICH, R. (1991). Fibre-optic displacement sensor with 0.02 mm resolution by white light interferometry. Sensors and Actuators A 25-27:202-207.

[11] JONES, R. (1992). White-light interferometry-a road to low cost, high performance optical fibre sensors. Paper presented at IEE Colloquium on Fibre Optics Sensor Technology, London, 1992.

[12] System 2000, NanoPositioning User's Guide, Available from Queensgate Instruments Ltd., Silwood Park, Ascort, Berkshire SL5 7PW, U.K.

Appendices

Appendix A: Some Fundamental Measurement Definitions

Accuracy : A British Standard defines the term accuracy as : "the quantity which characterises the ability of the measuring instrument to give an indication equivalent to the true value of quantity measured. The quantitative expression of this concept should be in terms of uncertainty".

Calibration is the process of determining and recording, with appropriate uncertainty, the relationship between the values indicated by a measuring instrument and the true value (or conventional true value) of the measured quantity.

Conventional true value is the value of measurand as indicated by the best available standard measuring instrument.

Error (E) is the difference between the result of measurement Q_M and the true value of the measured quantity Q_T, that is:

$$E = Q_M - Q_T \qquad\qquad (A.1)$$

Error may be expressed as:

(1) *absolute error*: in the specific units of the measurement;

(2) *relative error*: as a percentage of the measured quantity;

(3) *full scale error*: as a percentage of the full scale indication of the measuring instrument.

Measurement is the process of empirical objective assignment of numbers (Q_M) to properties of objects or events in the real world in such a way as to described them: *Measurement* is a description of the properties of an object, not a descrption of the object.

Precision refers to the quality of the instrument and its potential accuracy. Precision is a measure of an instrument's freedom from random errors. Precision is often implied in numerical terms by the number of significant figures used to express a result.

Random errors are errors which are different in repeated measurements of the same value of measured quantities. Random errors are unpredictable and arise through irregular, chance or random causes. Their treatment is by statistical method. Causes of random errors are

(1) intrinsic errors arising from an indeterminated response law and/or

(2) influence errors arising from a short term variation of influence variables.

Repeatability is the ability of an instrument to give identical indications and responses for repeated applications of the same value of the measured quantity under standard conditions of use (same variable, same value, same method, same instrument, same location, same observer, etc.)

Reproduciblity is an expression of closeness of the measurement of the same value of the same variable but under different conditions of use (different method, different instrument, different location, different observer).

Resolution or ***descrimination Resolution*** is a term which defines the ability of an instrument to respond and detect the smallest change in the input measurand.

Standard : A standard, whether material or recipe, provides the primary, secondary or lower order of comparison against which an instrument may be calibrated.(see Figure A.1)

Systemetic errors are errors which are the same in repeated measurements of the same value of the measure quantity. Systematic errors are due to a constant cause and can be taken account of by calibration. In general they are due to

(1) intrinsic errors arising from a determinate false law and/or

(2) influence errors arising from long term variations in the influence variables.

Traceability is a principle whereby the uncertainty of the standard has been measured against a superior standard, allowing the uncertainty of an instrument to be certified. (see Figure A.1)

True value is the actual value assigned to a quantity. The true value (Q_T) of a quantity can never be found and is not known. The value assigned to a quantity will only be known to some uncertainty. In practice true value is replaced by conventional true value.

Uncertainty states the range of values (X) within which the true value (or conventional true value) is estimated to lie.
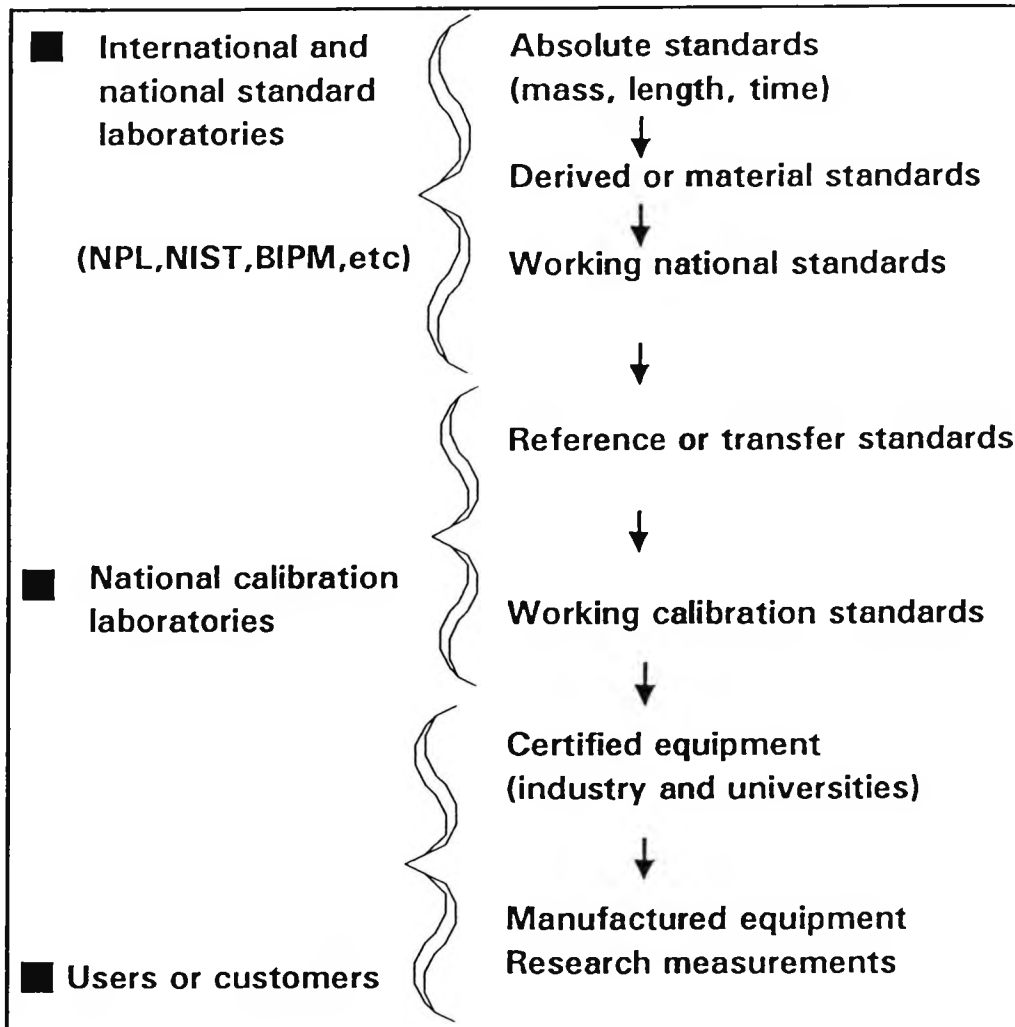
Figure A.1 Calibration, traceability and standards.

Appendix B : List of Publications By The Author Relevant To The Thesis

1. YUPAPIN, P. V. P. WEIR, K. GRATTAN, K. T. V. and PALMER, A. W. (1991). Static force measurement incorporating a reduction in thermal effects. In: Sensors and their Applications V Conference, Edinburgh 1991. Proceedings. Pub. in: Sensors-Technology, System and Applications, Ed. by K. T. V. Grattan. (Bristol: Adam Hilger).

2. YUPAPIN, P. V. P. WEIR, K. GRATTAN, K. T. V. and PALMER, A. W. (1993). An optical pressure sensor using a low-coherence light source with a highly birefringent fibre. In:SYMPOSIUM ON PHOTONIC MEASUREMENT, 14th. Sopron 1992. Proceedings. SPIE, 1712, 1993.

3. YUPAPIN, P. V. P. WEIR, K. GRATTAN, K. T. V. and PALMER, A. W. (1992). A photoelastic interferometric technique using a low-coherence light source for pressure sensor applications. In: INTERNATIONAL CONFERENCE ON ELECTRONIC MEASUREMENT & INSTRUMENTS . Tianiin 1992. Proceedings. Pub. (ICEMI'92).

4. YUPAPIN, P. V. P. WEIR, K. GRATTAN, K. T. V. and PALMER, A. W. (1992). White light interferometer based pressure sensor for qualitative measurements. In: APPLIED OPTICS AND OPTO-ELECTRONICS CONFERENCE, Leeds 1992. Proceedings. IOP Pub., pp. 235-237.

5. YUPAPIN, P. V. P. WEIR, K. GRATTAN, K. T. V. and PALMER, A. W. (1993). A polarimetric interferometry based pressure sensor for qualitative measurements. Journal of Flow Measurement and Instrumentation, in press.

6. YUPAPIN, P. V. P. WEIR, K. GRATTAN, K. T. V. and PALMER, A. W. (1993). An optical pressure sensor using a low-coherence light source with a photoelastic sensing element. Sensors and Actuators 36(2):105-111.

7. YUPAPIN, P. V. P. WEIR, K. GRATTAN, K.T.V and PALMER, A. W. (1993). A study of polarisation maintaining fibre characteristics using an interferometric technique for sensor applications, submitted to IEEE Journal of Lightwave Technology.

8. YUPAPIN, P.V.P. WEIR, K. GRATTAN, K.T.V. and KUSAMRAN, S. (1993). A flap angle control based on fibre optical measurements. In: Sensors and their Applications VI Conference, Manchester 1993. Proceedings. IOP. Pub., 1993.

Appendix C: Brief of Overview of Light Wave Processing

C.1 Coherence Length

As shown in Figure C.2, two light beams from a single source are arranged to travel along two different paths of length L_1 and L_2. The difference in path-length between them on recombining on the detector is the distance $\Delta L = L_1 - L_2$. If one of the paths is oscillated in length, as described in Chapter 3 (and also by Ning et al [1]), so that the relative path-length difference is driven through a distance equal to wavelength of light, then if the two light beams are coherent with respect to each other, an amplitude-modulated signal is observed using a photodetector.

L_1

Detector

Light
Source

L_2
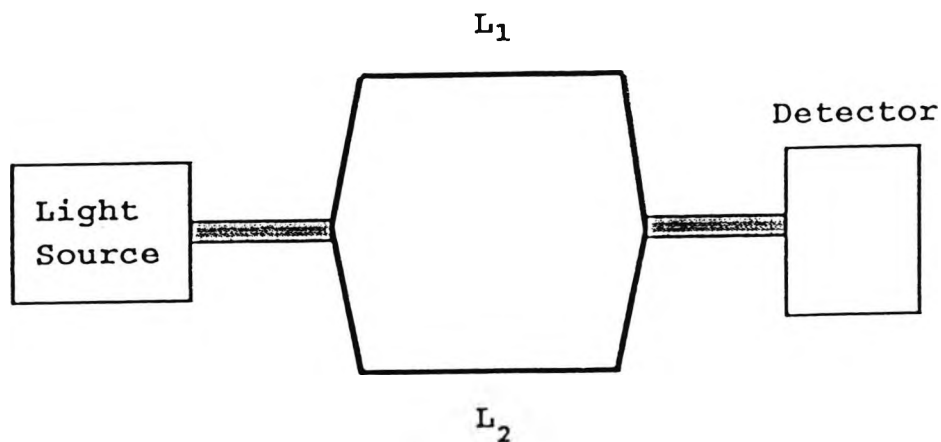
Figure C.1 Diagram illustrating the principle of coherence length.

By using a basic Michelson interferometer, the visibility of the interferometer output signal will be seen to peak for small values of optical path difference (ΔL) and gradually fall off to zero as ΔL increased (i.e. no signal is observed outside the coherence region). The coherence length is defined as the width of the visibility function as shown in Figure C.3. It has a maximum amplitude for $\Delta L = 0$ and then falls off to zero as $|\Delta L|$ increases. It is convenient to define the

152

coherence length as the full-width half-maximum (**FWHM**) of this visibility function.
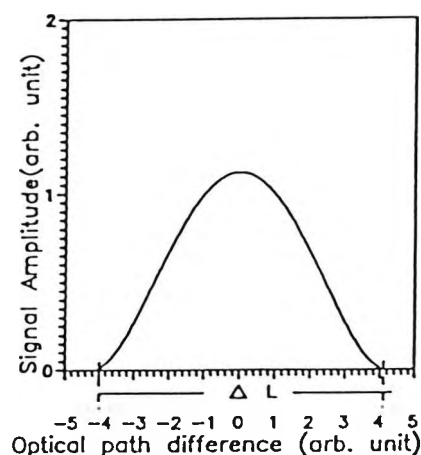
Figure C.2 Illustration of visibility function of an LED.

Generally, the coherence length is defined in terms of a description of the monochromaticity of a source [2]. If the source is totally monochromatic, the output would consist of an electromagnetic field of constant amplitude that oscillates for an infinitely long time with a single output frequency and wavelength. Any deviation in the shortening of the length of time of oscillation results in an increase in the bandwidth of the light source or, alternatively, a decrease in the coherence length of the radiation. The relation between the coherence length, L_c, and the bandwidth is

$$L_c = (c/\Delta v) = (\lambda^2/\Delta\lambda) \qquad (C.1)$$

where c is the speed of light in vacuum, Δv is the frequency bandwidth (spectral linewidth), and $\Delta\lambda$ is the wavelength bandwidth (spectral width) of the light source. The smaller the bandwidth, the more monochromatic the light source.

153

A short-coherence-length light sources provide a useful tool for optical sensors used to measure lengths accurately [3, 4] since interference will occur only when two optical path lengths are closely matched.

Figure C.3 shows the semi-visibility function of a multimode laser diode obtained using a Michelson interferometer. As discussed in Chapter 3, theoretically, each of these peaks (i.e. a group of fringes) has the same width (i.e. optical path difference) ΔL which is equivalent to the coherence length of the light source.
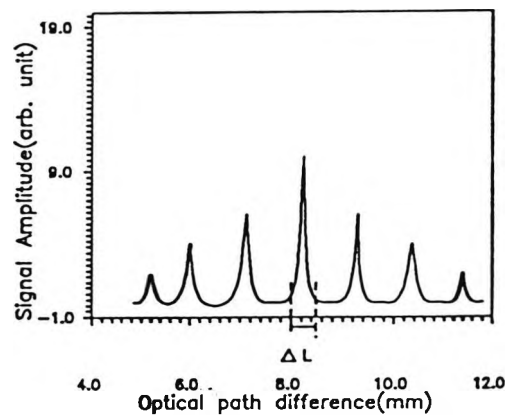
Figure C.3 Illustration of semi-visibility function (a.c. component) of a multimode laser diode.

C.2 A Sandwiched Birefringent Sensing Element

C.2.1 Between Parallel Polarisers

Consider a birefringent sensing element (plate) sandwiched between a pair of polarisers. The plate is oriented so that the "slow" and "fast" axes are at 45^0 with respect to the polariser. Let the birefringence be n_1-n_2, and the plate thickness l. The phase retardation, $\Delta\phi$, is then given by

$$\Delta\phi = (2\pi/\lambda)(n_1-n_2)\, l \qquad\qquad\text{(C.2)}$$

It may be assumed that the intensity of the incident beam is unity and only half of the intensity passes through the polariser. Using Jones vector representation [5] of the electric field vector, the transmitted beam is obtained. When the analyser is orientated parallel to the polariser, the intensity transmitted vertically polarised beams, I, is given by

$$I = (1/2)\cos^2[\pi(n_1-n_2)(l/\lambda)] \qquad\qquad\text{(C.3)}$$

The transmitted intensity is sinusoidal function of the wave number and peaks at $\lambda = (n_1-n_2)l$, $(n_1-n_2)l/2$, $(n_1-n_2)l/3$,..... The wave-number separation between transmission maxima increases with decreasing sensing element thickness. Further, the change in sensing element birefringence, n_1-n_2 is also observed as a change in transmitted intensity.

C.2.2 Between Crossed Polarisers

If the analyser is rotated as shown in Figure C.4 by 90^0, then the input and output polarisers are crossed. The transmitted beam is horizontally polarised with an intensity given by

$$I = (1/2)\sin^2[\pi(n_1-n_2)(l/\lambda)] \qquad\qquad\text{(C.4)}$$

This is again a sinusoidal function of the wave number. The transmission spectrum consists of a series of maxima at $\lambda = 2(n_1-n_2)l$, $2(n_1-n_2)l/3$,..... These wavelengths correspond to phase retardations of π, 3π, 5π,....., that is, when the

wave plate becomes a half-wave plate or an odd integral multiple half-wave plate.
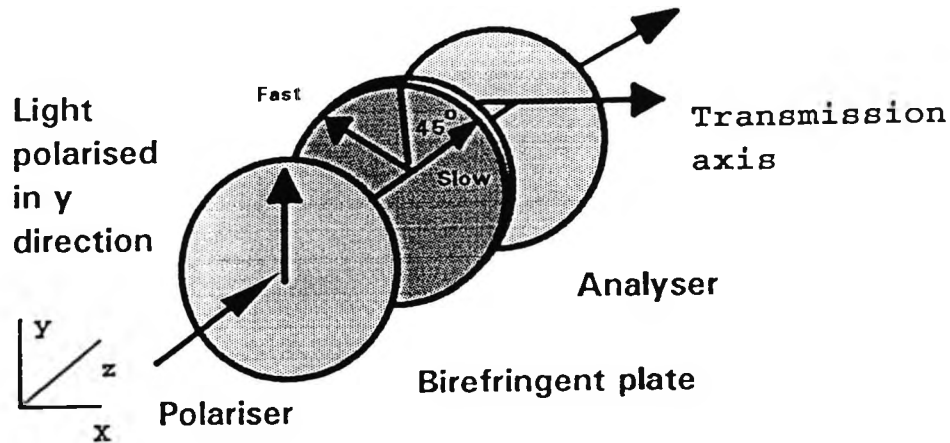
Figure C.4 A birefringent sensing element sandwiched between a pair of polarisers.

C.2.3 Photoelastic Sensors

There are many types of transparent material as dicussed earlier in Chapter 3, whose index of refraction distribution will be changed through the application of stress or pressure. They can be configured to act as stress-dependent sensing element in optical systems. Some basic photoelastic sensor configurations for measurement of stress-induced birefringence are given in Table C.1 along with the transmitted intensity function [6]. A list of some common photoelastic materials and their properties in given in Table D.1 [6, 7] in Appendix D.

C.3 Sensing Elements and Their Thermal Effects

C.3.1 Ordinary Single Mode Fibre

A change in temperature ΔT of a fibre changes the fibre length due to thermal expansion or contraction, and also changes the refractive index. Thus, if the phase of the transmitted light $\phi = (2\pi l n)/\lambda$, the following may be written

$$(\Delta\phi/\Delta T) = (2\pi /\lambda)[n (d l /dT) + l (dn/dT)] \qquad (C.5)$$

where the effects of fibre diameter changes are neglected, and is assumed to be small. For example, using He-Ne laser source $\lambda = 632.8$ nm and fused silica fibre n=1.456 [8], and $(1/l)(dl/dT) = 5\times10^{-7}/^0Cm$, $dn/dT = 10\times10^{-6}/^0C$, then

$$(1/l)(\Delta\phi/\Delta T) = 107 \text{ radians}/^0C.m \qquad (C.6)$$

However, the value in equation (C.6) could be different for other fibre material compositions.

C.3.2 Highly Birefringent Fibre

For a Hi-Bi fibre, the relative phase retardation between the two perpendicularly polarised eigenmodes propagating in a Hi-Bi fibre will be given by

$$\Delta\phi = (2\pi /\lambda)(\Delta n l) \qquad (C.7)$$

and the temperature-induced phase retardation can be expressed as [9]

$$d(\Delta\phi/dT) = (2\pi /\lambda)[(\Delta n \, dl/dT) + l \{d(\Delta n/dT)\}] \qquad (C.8)$$

For example, using light source λ =632.8 nm and Bow-tie Hi-Bi fibre (York) [10], i.e. fused silica fibre n =1.456, and Δn =4x10^{-4}, (1/l) (dl/dT) = 5.5x10^{-7}/^{0}Cm, d(Δn/dT) = 4.2x10^{-7}/^{0} C, then

$$(1/l)[d(\Delta\phi/\Delta T)] = 4.2 \text{ radians}/^0\text{C.m} \tag{C.9}$$

Experimentally, the temperature sensitivity of Hi-Bi fibre is due to an internal mechanical stress or cross-sectional geometry, for examples (as discussed in Chapter 5) Bow-tie (York), E-series and D-series (Andrew) Hi-Bi fibres were estimated at 4.8, 1.4, and 2.0 radians/ ^{0}C.m, respectively.

C.3.3 Photoelastic Sensing Element

When linearly polarised light propagates through a photoelastic sensing element, thickness l. The phase retardation between light emerging from its two eigenmodes may be represented by equation (C.7). Further, the temperature-induced phase retardation may be given by equation (C.8). However, from reference [11], data on the temperature dependence of the photoelastic materials are rare. For most of commonly used photoelastic materials, the thermal effect may be neglected if the temperature variations are limited to $\pm$ 3 ^{0}C [7, 12].

Table C.1 Basic photoelastic sensor configurations

Sensor Configurations	Transmitted Intensity Function
Polariser at $\pi/4$ — Polariser at $-\pi/4$. Unpolarised monochromatic light I_o at λ. Photoelastic material, width l.	$I=(I_o/4)[1-\cos\{(2\pi lC/\lambda)(\sigma_x-\sigma_y)\}]$
Polariser at $\pi/4$ — Bias sensing element — Sensing element — Polariser at $-\pi/4$. Unpolarised monochromatic light I_o at λ. Photoelastic material, width l each, $\lambda/2$.	$I=(I_o/4)[1+\cos\{(2\pi lC/\lambda)(\sigma_x-\sigma_y)\}]$
L, P, B — Photoelastic sensing element, stressed along x-axis — L, P	$I=(I_o/4)[1+\cos(2\pi\sigma lC/\lambda)]$ $\sigma=(\lambda/2\pi l)\cos^{-1}[(4I/I_o)-1]$
L, P, Q — Photoelastic sensing element, stressed along x-axis — L, P	$I=(I_o/4)[1+\sin(2\pi\sigma lC/\lambda)]$ $\sigma=(2\lambda I/\pi lI_o)-(\lambda/2\pi l)$
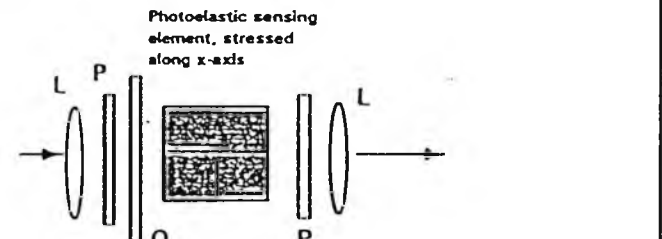
L:Lens , P:Polariser at $\pi/4$, B and Q : Optical retarder(bias) and Quarter wave retarder with fast axis at 0, $\lambda/2$: Half-wave plate.

Appendix D : Table of Some Material Constants

Table D.1 Properties of common photoelastic materials [6, 7]

Materials	Density (Kg/m^3)	Young's modulus (MPa)	Poisson's ratio	Stress-optic coefficient ($\lambda = 589$ nm)
Gelatin	~ 1000	0.08	0.5	0.002
PSM-4 (Polyurethane)	1300	~ 3	0.5	0.18
PSM-1 (Polycarbonate)	1190	2300	0.4	7
Glass	2500-4500	6900	0.4	175-350
Homolite 100	-	3860	0.35	-
Epoxy	-	3275	0.36	-
Urethane rubber	860-2000	3	0.46	

References

[1] NING, Y. GRATTAN, K. T. V. MEGGITT, B. T. and PALMER, A. W. (1989). Characteristics of laser diodes for interferometric use. Applied Optics 28 (17): 3657-3661.

[2] Projects in fibre optics: applications handbook. (1986). Newport Corporation, U.S.A.

[3] YUPAPIN, P. V. P. WEIR, K. GRATTAN, K. T. V. and PALMER, A.W. (1992). White light interferometer based pressure sensor for qualitative measurements. In : APPLIED OPTICS AND OPTO-ELECTRONICS CONFERENCE, Leeds 1992. Proceedings. IOP Pub., pp. 235-236.

[4] JONES, R. (1992). New concepts in white light interferometric sensing. In: APPLIED OPTICS AND OPTO-ELECTRONICS CONFERENCE. Leeds 1992. Proceedings. IOP Pub., pp. 77-78.

[5] YARIV, A. and YEH, P. (1984). Optical waves in crystals: propagation and control of laser radiation. (Toronto:John Wiley & Sons).

[6] UDD, E. (1991). Fibre optic sensors: an introduction for engineers and scientists. (Toronto:John Wiley & Sons).

[7] DALLY, J. W. and RILEY, W. F. (1991). Experimental stress analysis. 3 rd edit. (New York:McGraw-Hill).

[8] HOCKER, G. B. (1979). Fibre-optic sensing of pressure and temperature. Applied Optics 18 (9): 1445-1448.

[9] BOCK, W. J. WOLINSKI, T. R. and BARWICZ, A. (1990). Development of a polarimetric optical fibre sensor for electronic measurement of high pressure. Instrumentation and Measurement 39(5):715-721.

[10] CHEN, S. (1990). Optical interferometry for novel optical fibre sensor systems. Ph.D. thesis: King's College, University of London, Department of Electronic and Electrical Engineering.

[11] MARTENS, G. (1992). Fibre optic photoelastic sensor. International Journal of Optoelectronics 17(3):385-407.

[12] AYUB, M. SPOONCER, R. C. and JONES, B. E. (1990). Measurement of temperature dependence of stress-optic coefficient of photoelastic materials. Paper presented at International Conference on New Materials and their Applications, University of Warwrick, 1990.